SINGLE-SITE OLEFIN POLYMERIZATION CATALYSTS VIA THE MOLECULAR DESIGN OF POROUS SILICA

A Dissertation
Presented to
The Academic Faculty

By

Michael W. McKittrick

In Partial Fulfillment
Of the Requirements for the Degree
Doctor of Philosophy in
Chemical and Biomolecular Engineering

Georgia Institute of Technology

March, 2005

SINGLE-SITE OLEFIN POLYMERIZATION CATALYSTS VIA THE MOLECULAR DESIGN OF POROUS SILICA

Approved by:

Dr. Christopher W. Jones, Advisor
School of Chemical & Biomolecular Engineering
Georgia Institute of Technology

Dr. Pradeep K. Agrawal
School of Chemical & Biomolecular Engineering
Georgia Institute of Technology

Dr. William J. Koros
School of Chemical & Biomolecular Engineering
Georgia Institute of Technology

Dr. Marcus Weck
School of Chemistry & Biochemistry
Georgia Institute of Technology

Dr. Angus P. Wilkinson
School of Chemistry & Biochemistry
Georgia Institute of Technology

Date Approved: March 21, 2005

…If you can fill the unforgiving minute
With sixty seconds' worth of distance run,
Yours is the Earth and everything that's in it,
And--which is more--you'll be a Man, my son!

"If"- Rudyard Kipling

ACKNOWLEDGEMENTS

First, I would thank my advisor, Chris Jones. My development as a scientist is a direct result of his support and guidance. I appreciate the opportunities given to me in the Jones Group. Thanks to my committee members, Dr. Pradeep Agrawal, Dr. Bill Koros, Dr. Marcus Weck, and Dr. Angus Wilkinson for their advice, encouragement, and time. Thanks also to Dr. Kunquan Yu for his contributions to the metallation method study and Dr. Johannes Leisen for his assistance with solid-state NMR experiments. I would also like to thank the members of the Jones Group, past and present.

I also would like to acknowledge my friends, without whom my tenure at Georgia Tech may have been a little more productive, but not nearly as much fun: Amy Meyers for countless lunch discussions about work, sports, and research; Bryan White and Cody Berger for their friendship on and off the golf course; Beckie Jones, for her friendship and multiple Thanksgiving dinners. I would especially like to thank Jason Hicks, Benn Wilson, and Rebecca Shiels. Not only were they my colleagues in the Jones Group and sources of endless humor, they helped me keep my sanity while driving me crazy at the same time.

I would like to thank my parents. I cannot imagine a person having more supportive parents than mine. Words cannot adequately describe my appreciation for them, but the world would be an amazing place if everyone had parents like mine. I would also like to thank my sister Karen and my grandmother, both gave little touches of home when I needed them most.

Finally, I would like to thank Alexis Hillock. Whether it was listening to me rant about research problems or celebrate with me on a job well done, you were always there for me. I especially appreciate your understanding during this final stage of my work.

TABLE OF CONTENTS

LIST OF TABLES

LIST OF FIGURES

LIST OF SCHEMES

LIST OF ABBREVIATIONS

CGC – constrained geometry catalyst

Cp - cyclopentadienyl

Cp' - tetramethylcyclopentadienyl

CP-MAS – cross polarization magic angle spinning

DP-MAS – decoupling magic angle spinning

DSC – differential scanning calorimetry

GPC – gel permeation chromatography

HMDS - hexamethyldisilazane

MAO – methalumoxane

NMR – nuclear magnetic resonance

PDI – polydispersity index

PE – polyethylene

PNB – polynorbornene

PP – polypropylene

TEOS – tetraethylorthosilicate

TGA – thermogravimetric analysis

TIBA – triisobutylalminum

TMA – trimethylaluminum

UV-Vis – ultraviolet-visible

SUMMARY

The major goals of this thesis work were to: 1) Develop a new methodology for the preparation of site-isolated catalytic sites on a silica surface, 2) Prepare the first truly single-site supported metallocene/CGC polymerization catalyst, 3) Develop structure-reactivity relationships for these new systems.

To synthesize these novel catalysts, the approach taken was to develop a protocol which allows for the synthesis of an aminosilica material with isolated, uniform amine sites. This patterned aminosilica was then used as a scaffold to support a constrained geometry catalyst. These functionalizations occurred at essentially a quantitative level, in stark contrast to previous literature reports. The patterned catalysts were evaluated in the polymerization of ethylene and compared to densely loaded literature materials. Overall, it was found the patterned materials were 5-10 times more active than traditional immobilized CGC catalysts.

The patterned catalysts were also found to be effective catalysts for the copolymerization of norbornenes (including functionalized norbornenes) and ethylene, which was the first reported use of a tethered CGC for the production of ethylene-norbornene copolymers. The control materials were inactive in these polymerizations, providing further evidence that the patterning protocol allows for the synthesis of unique highly active, isolated catalytic sites.

Additional work was done in comparing two metallation strategies commonly used in the synthesis of CGCs. Using the same aminosilica scaffolds, the Royo and Jordan methods for metallation were compared using various characterization techniques

and polymerization studies. These studies showed that the Royo metallation yielded a more active titanium site than the amine elimination metallation. Both metallation routes showed improved performance of the immobilized complexes when the patterned aminosilica scaffold was used compared to the densely loaded aminosilica scaffold.

Various structural components of the immobilized CGC developed in this work were then tested for their impact on the catalyst synthesis and reactivity in ethylene polymerizations. The results showed the patterned materials in general behaved according to the trends seen in homogeneous CGC polymerizations. These results, while congruent with similar homogeneous CGC studies, are in direct conflict with previous work on supported CGCs reported in the literature. This discrepancy is likely the result of the difference between the isolated, possibly single-site patterned catalysts developed in the course of this work and the multi-sited catalysts prepared by traditional supporting protocols. This also further illustrates the difficulty in developing structure-reactivity relationships when ill-defined solid catalysts are used.

CHAPTER 1

INTRODUCTION

1.1 Polyolefins

Polyolefins, for example polyethylene and polypropylene, are among the world's most widely used synthetic commodity polymers due to their extreme versatility. They possess a combination of properties including flexibility, strength, lightness, stability, impermeability and easy processability. Polyethylene and polypropylene are also well-suited to recycling and re-use.

Polyethylene with a density of 0.910 to 0.930 g/cm^3 is classified as low-density and high density between 0.931-0.970 g/cm^3. In 2002, annual production of polyethylene was approximately 55 million metric tons which represented about $35 billion in sales[1]. Growth expectations were approximately 5 percent a year, reaching over 85 million metric tons in 2010[1]. Polypropylene production was approximately 34 metric million tons in 2002. Projected growth estimates production in 2010 to nearly 60 million[1]. Propylene made by metallocenes account for less than 1% of all polypropylene (PP) made.

Demand for metallocene-based polyethylene represents only a small percentage of the market. However, analysts forecast growth of about 30 percent a year, from 1 million tons in 2000 to 17 million tons in 2010, as superior metallocene polyethylene products displace those made from other plastics or from glass, paper and metal. By decade's end, metallocene-based polyethylene is expected to represent more than one-fifth of the total polyethylene market.

1.2 Ziegler-Natta Catalysis

Since the 1950s, polyolefins have been produced using Ziegler-Natta catalysts[2]. These are based on the works of Karl Ziegler and Guilio Natta, which jointly won them the Noble Prize for Chemistry in 1963. Federal courts have since determined Robert L. Banks and J. Paul Hogan were in fact the first to discover these catalysts[3]. These catalyst systems allowed for the production of specialized polyolefins, such as linear unbranched polyethylene and isotactic polypropylene. Free radical vinyl polymerizations can only produce branched polyethylene and cannot be used in the production of propylene.

Ziegler-Natta catalyst systems are typically based on a titanium chloride complex, for example titanium trichloride ($TiCl_3$) or titanium tetrachloride ($TiCl_4$), and an alkyl aluminum species, such as triethylaluminum. One of the major difficulties of these systems is the determination of the true active species. It does appear certain the active catalytic sites are not simple coordination adducts formed from the titanium halide and the alkylaluminum. An "activation" period, in which the titanium and aluminum species are mixed together before the addition of monomer, is often needed before the system reaches its highest activity. Several complex reactions are proposed to occur during this activation period, which result in the formation of a highly active species. Among these reactions include an exchange of substituent groups between the two metals to form titanium-carbon bonds such as shown in Equations 1 and 2. The organotitanium complexes formed in this step are unstable and can undergo further reductive decomposition processes, as shown in Equations 3 and 4. Radicals formed during these processes may be removed by combination, disproportionation, or reaction with solvent.

$$AlR_3 + TiCl_4 \rightleftharpoons R_2AlCl + RTiCl_3 \quad (1)$$

$$R_2AlCl + TiCl_4 \rightleftharpoons RAlCl_2 + RTiCl_3 \quad (2)$$

$$RTiCl_3 \rightleftharpoons R^{\bullet} + TiCl_3 \quad (3)$$

$$R_2TiCl_2 \rightleftharpoons R^{\bullet} + RTiCl_2 \quad (4)$$

It is believed that Ziegler-Natta catalysts function by the formation of a transient π-complex between the olefin and a low-valence transition metal species. These types of complexes are well known in the literature[4]. The overlap of the d-orbitals of the transition metal with the π-orbitals of the olefin hold the complex together. This can occur several ways, most notably the d_{xy} orbital of the metal can overlap with the π-antibonding orbitals of the olefin (Figure 1.1a). Overlap can also occur between one lobe of a $d_{x^2-y^2}$ orbital and an olefin π-orbital (Figure 1.1b). As discussed above, the reduction

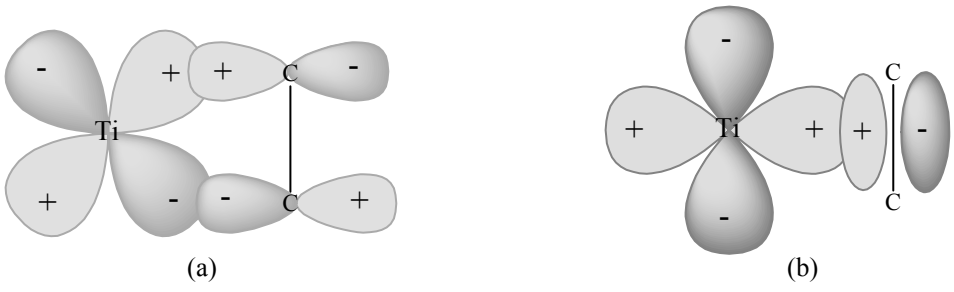

Figure 1.1: Orbital overlap scheme for the formation of a π-type interaction between an olefin and a transition metal: (a) use of the π-antibonding orbitals of the olefin; (b) overlap of one lobe of a $d_{x^2-y^2}$ orbital from the metal with a π-bonding orbital of the olefin.

of the transition metal is critical, as π-complex formation could not occur as the titanium occupied its highest valence state (by having all coordination sites occupied by strongly bound ligands). The exact mechanism for olefin addition is still not fully understood. Two general mechanisms have been proposed, one which involves the coordination of the olefin to a vacant site on the transition metal and the other suggests a participation by both the transition metal and the aluminum species.

The proposed monometallic mechanism is shown in Scheme 1.1. The olefin coordinates to the vacant site on the titanium. An organic group, R, is then transferred from the metal to the olefin. An incoming olefin molecule then coordinates to the new vacant site and can be inserted into the Ti-alkyl bond. The insertion mode is dependent on the geometry of the complex and the location of the vacant coordination site. There is

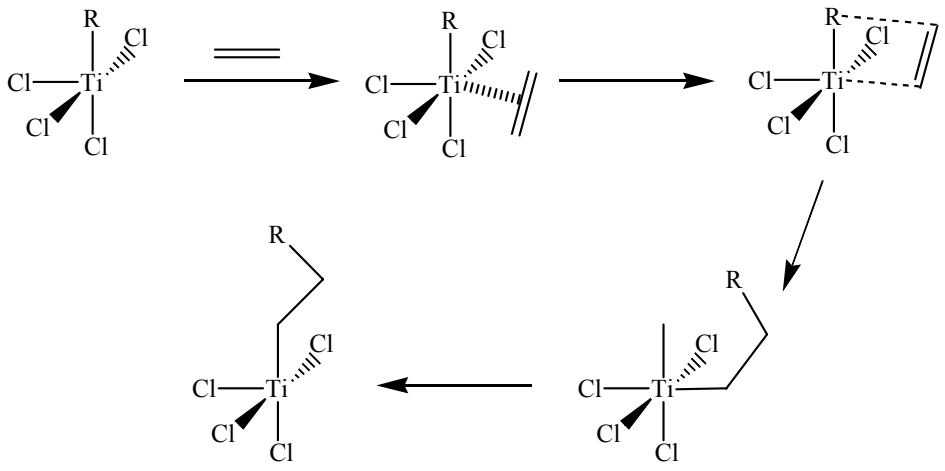

Scheme 1.1. Monometallic Ziegler-Natta Polymerization Mechanism

evidence it is this step of the polymerization mechanism which can direct stereospecificity. The side groups on the olefin sterically determine the coordination and insertion geometries.

The bimetallic mechanism is shown in Scheme 1.2. The alkyl groups from the aluminum species are believed to function as a bridging unit. This is documented in the literature[4]. The initial π-coordination of the olefin is followed by insertion of the olefin into the Ti-C bond to form a new bridged species. After rearrangement, the coordination and insertion of addition olefin molecules can take place via the same pathway.

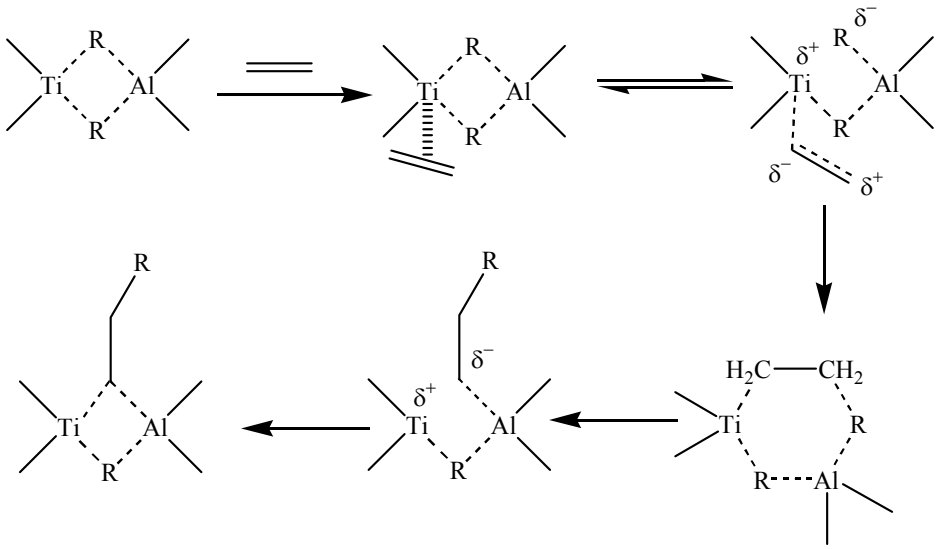

Scheme 1.2. Bimetallic Ziegler-Natta Polymerization Mechanism

A problem of the early Ziegler-Natta systems was their low productivity. Large amounts of catalyst were required to reach acceptable yields of polymer. It was found by impregnating a solid support (such as $MgCl_2$ or MgO), the activities of the system were

dramatically enhanced. The exact mechanism for this enhancement is not entirely clear. It is presumed the support maximizes the number of active sites on the surface. Researchers have shown that increasing the number of surface defects in the magnesium support increases the activity of the resulting catalyst[4]. It has been suggested the active titanium chloride species "sits" in small crevices and cracks in the surface, whereas inactive species are more likely bound by the surface[4].

The evolution of Ziegler-Natta catalysts can be categorized into four major generations, which can be seen in Table 1.1. As shown, a large increase in productivity can be seen in evolution of Generation III, supporting the catalysts on a support. The optimization of supporting protocols have led to a largely empirical understanding of these systems. Additionally, the materials developed have multiple types of titanium sites, yielding ill-defined materials. The mechanisms for structure-property relationships are not well understood. In addition, these systems are not able to polymerize functional monomers[4].

Table 1.1. Development of Ziegler-Natta catalyst systems

Generation	Time Frame	Catalyst	Productivity (kg PP/g Ti)	Isotacticity
I	1950-1970	$TiCl_3/AlEt_2Cl$	5	90
II	1950-1970	$TiCl_3$/isoamyl ether/$AlCl_3/AlEt_2Cl$	15	95
III	1970-1990	$MgCl_2$/ester/$TiCl_4/AlEt_3$/ester	300	92
IV	1990-	$MgCl_2$/ester/$TiCl_4/AlEt_3/PhSi(OEt)_3$	600	98

1.3 Metallocene Polymerization Catalysts

Metallocene catalysts (for example, see Scheme 1.3). offer higher versatility and flexibility due to their single-sited nature for both the synthesis and the control of structure of polyolefins, compared to conventional multi-site Ziegler-Natta catalysts[5]. In addition to being able to produce polyolefins with a desired stereoregularity and tacticity, metallocenes are able to polymerize olefins with high activities. Polymers with high molecular weights, low molecular weight distributions (typically about 2), and homogeneous composition can be synthesized using metallocenes[6]. This unique class of compounds can also be used to produce high-density polyethylene (HDPE), polypropylene with various tacticities (atactic, isotactic, syndiotactic, etc.), co-polymers of ethylene with α-olefins, and novel elastomers[5].

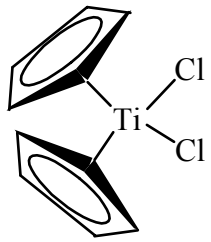

Scheme 1.3 Titanocene Dichloride

Metallocenes were the first homogeneous polymerization catalysts reported. In 1957, Natta and co-workers reported that bis-(cyclopentadienyl) titanium dichloride, when complexed with an alkyl aluminum, catalyzed the polymerization of ethylene[7]. However, the polymers produced were of low molecular weight and the activities of these

systems were poor. Natta's results show the titanium-aluminum complex produced 8.4 g polyethylene in presence of 0.6 g of Ti-Al complex after 20 hours (40 atm, 95 °C). Therefore they were not suitable replacements for heterogeneous Ziegler-Natta catalysts, which typically can have activities of 3 kg polymer/g M h)[8].

An important discovery by Natta and confirmed by Breslow, was the complete inactivity of bis-(cyclopentadienyl) titanium dichloride alone for the polymerization of ethylene[9]. The alkyl aluminum species served an important role as a co-catalyst. In 1980, it was found that using partially hydrolyzed trimethyl aluminum, or methyl alumoxane (MAO), as a co-catalyst greatly improved the polymerization activity of metallocenes[10]. As a result, interest in using metallocenes as olefin polymerization catalysts increased. Methyl alumoxane is an ill-defined oligomer; the general structure can be seen in Figure 1.2. MAO as a metallocene co-catalyst serves several roles. The active species of group IV metallocene systems is generally assumed to be a 14 electron species. The catalytic cycle for a propylene polymerization can be seen in Figure 1.3. First, MAO alkylates the metallocene, displacing the chlorine ligands. Another part of

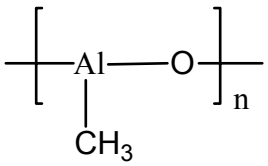

Figure 1.2. Methyl Alumoxane

the MAO then abstracts one of the methyl groups, which creates a cationic metal center and a weakly coordinated anion. It is this species which is the active species for

polymerization. The bis-(cyclopentadienyl) zirconium dichloride (1.3a) has an electron count of 16. The active species (1.3c) has 14 d electrons. There may be some interaction between the metal and the hydrogen on the remaining methyl, called an α-agostic interaction[4]. This interaction helps stabilize the active species. Upon addition of monomer, shown as propylene in Figure 1.3d, a four member transition state forms (1.3e). The strained four-membered ring allows for the breaking of the Zr-methyl bond, and a bond between Zr and the β carbon on the monomer forms. Again, a fourteen electron species is created (1.3), allowing for the addition of another monomer.

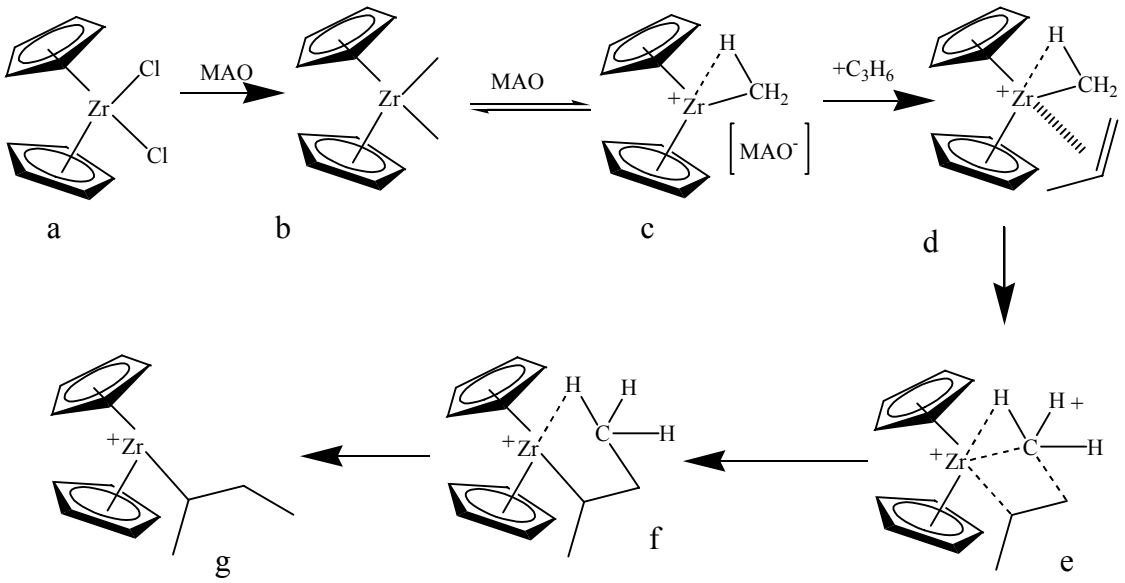

Figure 1.3. Metallocene Catalytic Cycle

The main-chain termination pathway is β-hydrogen elimination (Figure 1.4) [11]. This process produces long chain olefins, which can reincorporate as long chain branches. β-hydrogen elimination can be catalyzed by the presence of a second

metallocene center, therefore supported metallocenes typically produce polymers with increased molecular weight, as the metal centers are not free in solution[12].

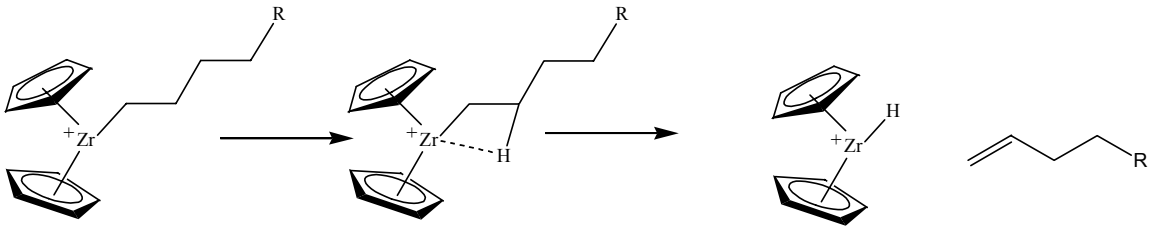

Figure 1.4. β-hydrogen Transfer

Other termination mechanisms include chain-transfer to aluminum (Figure 1.5) and β-methyl transfer (Figure 1.6)[11]. While the β-hydrogen elimination is usually the dominant mode of chain transfer, β-methyl transfer becomes more important in sterically crowded systems, for example bis-$\eta^5C_5Me_5$-metallocenes. It has been suggested the reason for this is the orientation of the polymer. The migrating methyl group lies

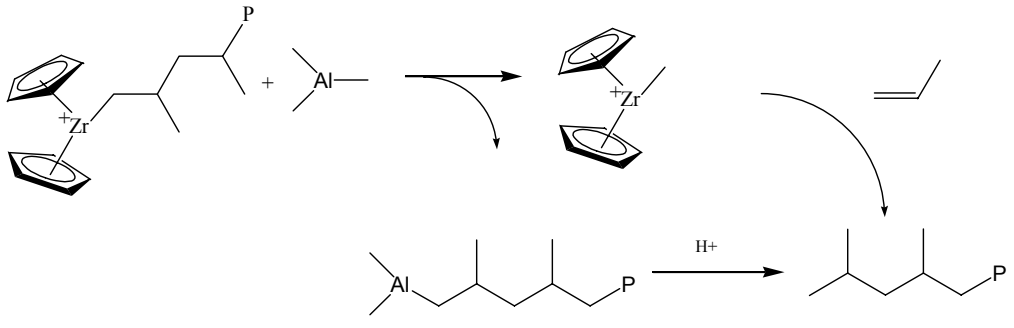

Figure 1.5. Chain-Transfer to Aluminum

between the Cp* rings, and can migrate to the Lowest Unoccupied Molecular Orbital (LUMO) of the metal, while the β-hydrogen cannot[13].

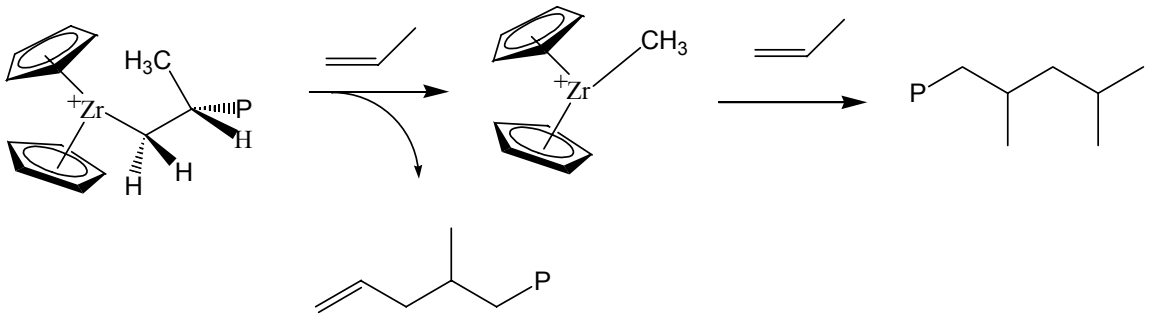

Figure 1.6. β-Methyl Transfer

The ligands and the growing polymer chain both influence the stereochemistry of the polymerization. Since the polymer chain remains bound to the metal center, the stereogenic center from the last monomer added will have an effect on the stereochemistry of the next monomer addition. If this is the dominant mode of stereochemical control, the mechanism is referred to as "chain-end control." However, if the chirality of the ligand has the dominant role in determining stereochemistry, the mechanism is called "enantiomorphic-site control"[14]. The effect of catalyst symmetry on polymer stereoselectivity can be seen in Figure 1.7.

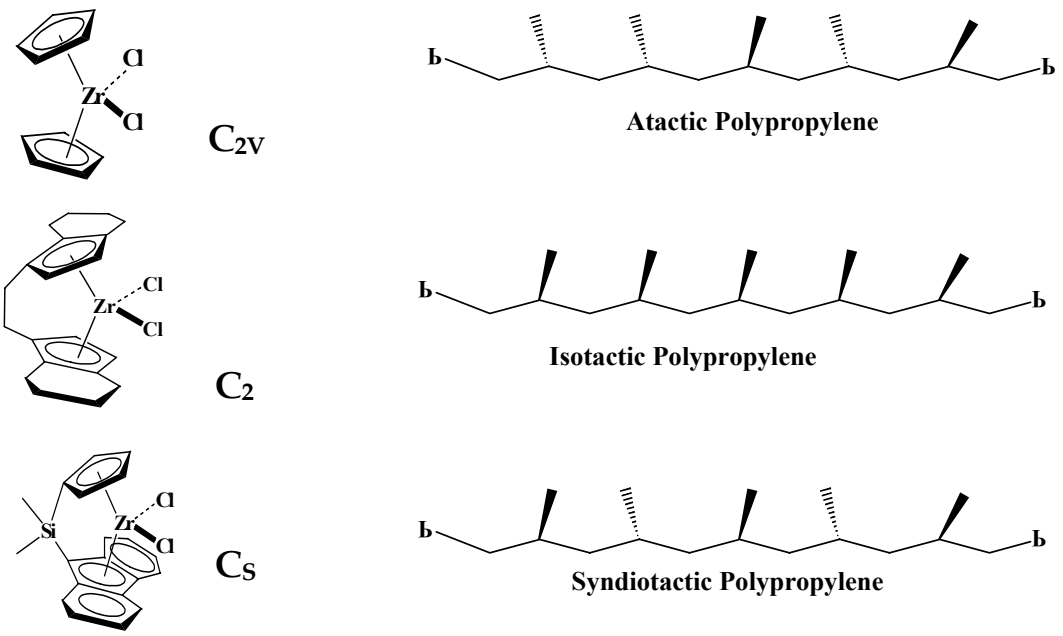

Figure 1.7. Symmetry Effects on Stereoselectivity

Catalysts with C_{2v} symmetry typically produce atactic polypropylene. C_2 symmetric catalysts produce isotactic polymers by a site-control mechanism. This can be seen in Figure 1.8. The chirality of the ligand is relayed to the incoming monomer through the β-carbon of the growing polymer chain[14]. Catalysts with C_s most often produce syndiotactic polymers, which is controlled by the polymer chain-end.

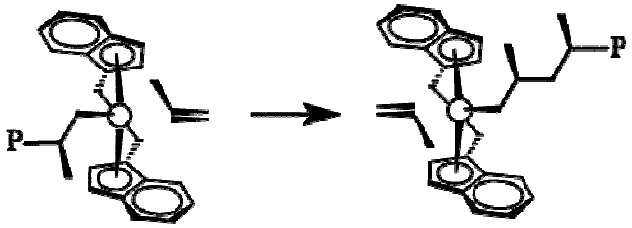

Figure 1.8. Isotactic Polypropylene via Catalyst with C_2 Symmetry[7]

In Figure 1.9, the mechanism for propylene polymerization with a C_s symmetric catalyst is shown. The last incorporated monomer directs the addition of the next propylene molecule. As a result, there is regular alternating insertion of the monomer at the active site. It is this ability to control the properties of the polymers produced by controlling the symmetry of the active site that differentiates single-site catalysts, like metallocenes, from traditional, multi-sited Ziegler-Natta catalysts.

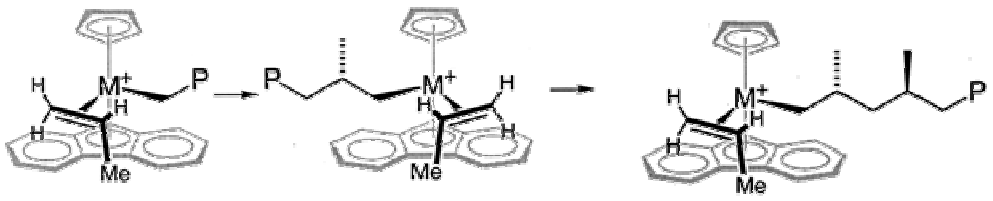

Figure 1.9. Syndiotactic Polypropylene Mechanism

1.4 Constrained Geometry Catalysts

Constrained Geometry Catalysts (CGCs: which are related to metallocenes), are among the most important single-site catalysts for olefin polymerization. The first CGC was reported by Bercaw and is shown in Figure 1.10A[15, 16]. These scandocene derivatives were found to undergo olefin insertion and β-H and β-alkyl elimination, all present in olefin polymerization catalysis. The Group III constrained geometry catalysts require no co-catalyst, however generally they have a low olefin polymerization activity[17]. Shortly after Bercaw and co-workers reported the Group III constrained

geometry catalyst, corresponding Group IV catalysts were developed industrially. Dow Chemical Company

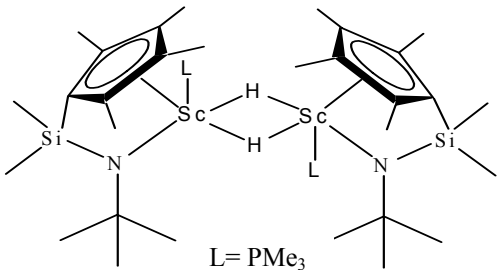

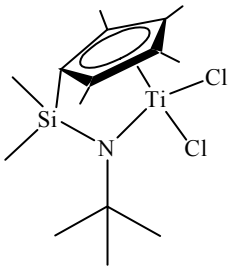

Figure 1.10 A. Group III CGC B. Group IV CGC

commercialized the technology, the Insite® catalyst from Dow is shown in Figure 1.10B. The reactive center is less sterically hindered than most other olefin polymerization catalysts due to the lack of a second Cp ligand. The reduction of steric bulk, in addition to the weaker π- donating character of the bifunctional ligand, $\{[(C_5Me_4)SiMe_2(N\text{-}t\text{-}Bu)]^{2-}\}$[18], increases the Lewis acidity of the metal. The amido group also makes the metal even more electron deficient than typical metallocenes, as the amido group does not donate as many electrons to the metal center as a η^5-cyclopentadienyl ligand. The open nature of the active site, increased Lewis acidity, and increased electron deficiency promote olefin insertion, increase the activity of these constrained geometry catalysts. These highly active homogeneous catalysts, typically showing an activity of 1500 g polymer/mmol M h bar[17], have many unique properties including the ability to produce very high molecular weight atactic polypropylene, long chain branched polyethylene, and short chain branched polyethylene[19].

Polymer branching is facilitated through the open nature of the active site, which can easily accommodate the incorporation of co-monomers, such as 1-hexene and 1-octene[17]. By modulating the quantity and the nature of olefin monomers, it is possible to synthesize novel long-chain branched polyethylenes by design to give novel polymers with unique properties. CGCs apparently have a lower tendency to undergo chain transfer, which allows very high molecular weight polymers to be produced (including co-polymers with ethylene and α-olefins)[12]. Constrained geometry catalysts typically do not have steric control over the polymerization of α-olefins as the open nature of the active site generally leads to atactic polymers[20]. The molecular weight distribution of polymers produced by constrained geometry catalysts are similar to those made by conventional metallocene systems (~ 2)[17]. The activities of homogeneous constrained geometry catalysts widely vary as small changes in ligand structure and coordination environment can have a large effect on catalyst activity. Therefore, subtle differences in supported CGC structure may also substantially impact the catalysts' performance.

1.5 Supporting Olefin Polymerization Catalysts

As a result of these properties, there is considerable interest in supporting constrained-geometry-catalysts, as well as metallocenes. Although these catalysts develop their novel properties from their homogeneous single-site nature, there is a substantial driving force to develop heterogeneous analogues. Most polyolefin plants were developed for use with heterogeneous catalysts (e.g. Ziegler Natta catalysts - $TiCl_4$ supported on $MgCl_2$; or Phillips catalysts - Cr_xO_y supported on SiO_2) in slurry or gas phase polymerizations [6]. Thus, in many cases, to use a homogeneous catalyst, new plants

or significant retrofitting of older plants would be required [21]. Furthermore, when using homogeneous catalysts, reactor fouling is a major concern [21]. Supporting the catalyst on a solid alleviates both of these problems. The most common support used is silica, due to its low cost and ease of functionalization [6].

There are three major ways that metallocenes or other single-site catalysts have been immobilized on silica supports. The first approach, commonly used commercially, is to contact the support material with a co-catalyst (either methyaluminoxane or a combination of a borane and alkyl aluminum). The organometallic precatalyst is then added to the support/co-catalyst combination. While this often leads to an effective catalyst, it gives a material that is extremely difficult to characterize and understand on the molecular level, as the activator is typically methylaluminoxane (MAO), an ill-defined oligomeric species [6, 22]. In addition, a 100-1000 fold excess of aluminum (relative to the transition metal) is routinely used, making molecular characterization of the small number of supported metallocene active sites exceedingly difficult. Thus, to generate a model system that has the potential to be well-characterized on the molecular level, other methods must be developed.

A second method used to support single-site catalysts is to physisorb a complex such as a metallocene or CGC onto the support's surface [23-39]. Alternately, a pre-formed complex that is designed to form covalent bonds between the ligand and the support could also be used (Scheme 1.4) [12, 40-46]. The difficulty with both of these methods stems from the potential reactivity of the pre-formed complex with the surface silanols [27, 37, 47]. When a reaction between the silanols on the surface and the metal center occurs, multiple types of sites are often formed, removing the "single-sited" nature of the system.

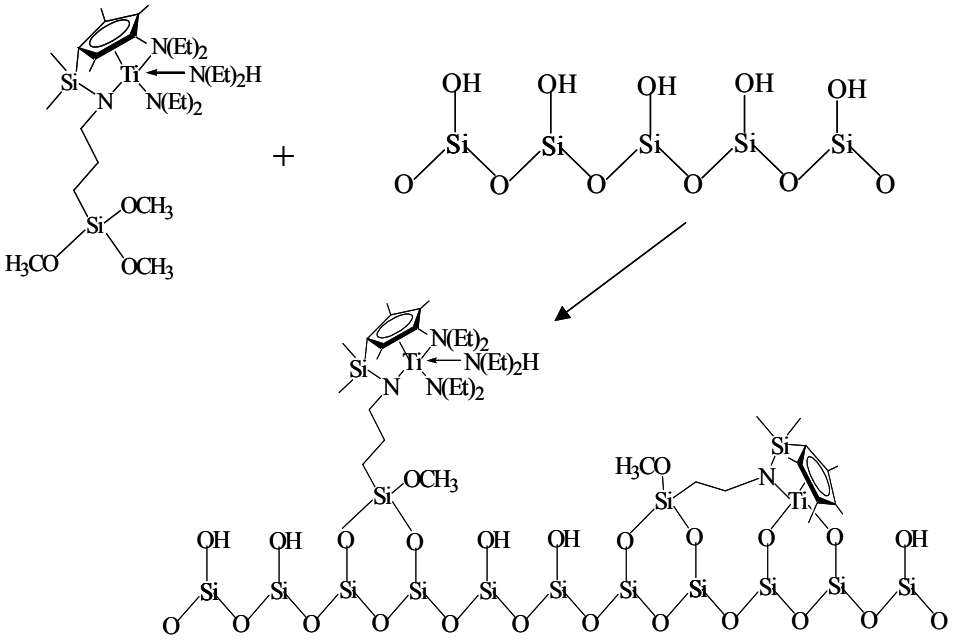

Scheme 1.4 Preformed Complex Addition to Silica Surface

A third method is to immobilize the complex via a covalent linkage between the ligand and the support using a multi-step grafting approach [48-65]. For instance, cyclopentadienyl ligands have been immobilized on oxide and polymer supports and subsequently metallated to form immobilized metal complexes [66-79]. For immobilizing a CGC, an amine functionalized support is often used in place of the cyclopentadienyl-functionalized support (Scheme 1.5). Two major difficulties result from this approach if a truly single-site catalyst is desired. First, quite often the procedure used in preparation

of the homogeneous complex is simply applied to the supported amine. For example, an alkyl lithium reagent has been used to deprotonate the amines for further

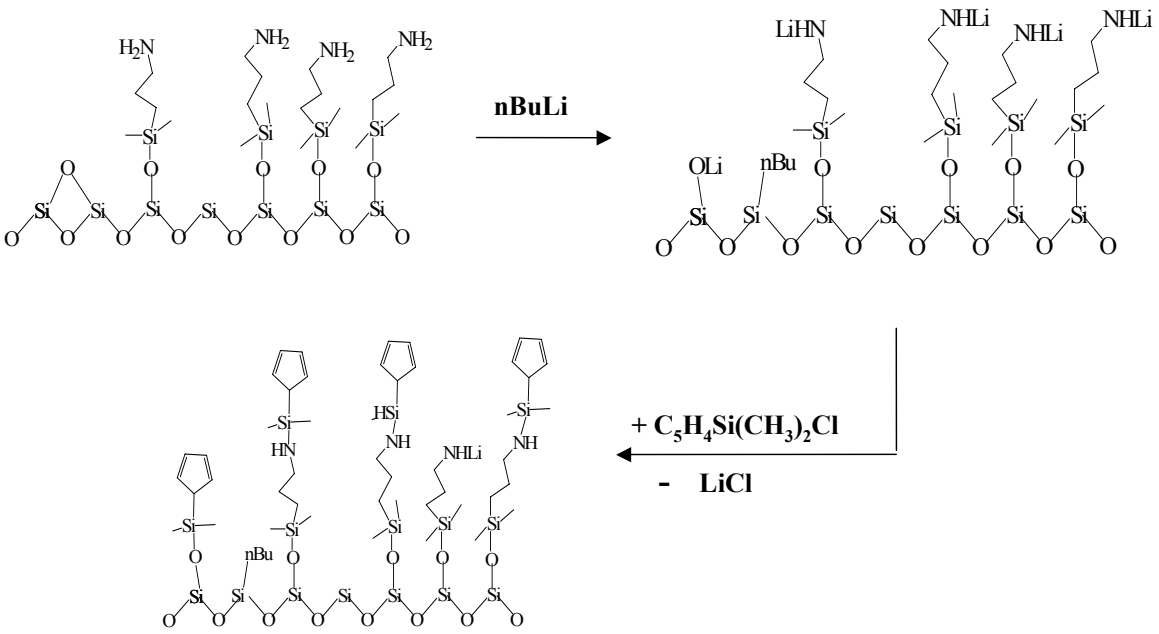

Scheme 1.5 Multi-step Grafting Method

functionalization [60-62, 80, 81]. However, such reagents are extremely harsh towards the silica support and can alkylate the surface, allowing for the formation of multiple types of sites[82]. Furthermore, the steric crowding of the amines on the surface as well as interactions between the amines and the surface can create multiple types of anchoring sites[83].

Thus, to build a truly single-site CGC on an amino-silica surface via a multi-step grafting technique, a well-defined aminosilica (ideally with uniform, isolated sites) is required as a starting material. Here we report the detailed description of the supported patterned organometallic complex and demonstrate its applicability in the catalytic

polymerization of ethylene using both methylaluminoxane (MAO) and borane/trialkyl aluminum co-catalysts.

1.6 Summary of Supported Metallocenes

As discussed previously, Ziegler-Natta systems are ill-defined solids with multiple types of titanium species present on the support surface. The lack of a well-defined site limits researchers to a largely empirical understanding of the catalytic system. This results in it being very difficult to rationally design the catalyst to achieve a desired polymer property.

Metallocenes offer a significant advantage in this area, largely the result of their single-site nature. As discussed previously, simple defined changes in catalyst symmetry can result in polymers with various stereochemistries. However, as metallocenes are homogeneous, significant retrofitting of existing plants or building new polymer plants would be necessary to implement these systems on a larger scale.

Supporting metallocenes on a solid would limit massive capital expenditures while allowing for the production of commodity polymers in existing polyolefin plants. However, current immobilization methods result in ill-defined, multi-sited materials. As with the Ziegler-Natta systems, this has led an empirically-driven development of supported metallocenes. A significant disadvantage of current industrial supporting protocols is the inability to characterize the catalyst on a molecular-level.

The hypothesis of this work is that molecular level structure-property relationships for supported metallocene catalysts do not exist due to the difficulty in preparing well-defined catalysts with a single type of site that are amenable to structural characterization. As such, the approach undertaken is as follows: Develop a new

synthetic protocol for making supported catalysts that have: 1) isolated sites; 2) uniform sites; 3) structures that are amenable to detailed characterization. This approach will yield a model system that is well-defined and characterizable.

1.7 Major Goals of Work

The major goals of this thesis work are to:

1. Develop a new methodology for the preparation of site-isolated catalytic sites on a silica surface.
2. Prepare the first truly single-site supported metallocene/CGC polymerization catalyst.
3. Develop structure-reactivity relationships for these new systems.

The development and testing of a well-defined supported constrained geometry catalyst complex will be addressed in the following chapters. The first major goal of the work was the development, synthesis, and testing of an amine-functionalized support for the olefin polymerization catalyst which is presented in Chapter 2. This support would ideally have uniform, isolated amine functionalities which would serve as a scaffold for further functionalization. The synthetic protocol for immobilizing a constrained geometry type catalyst on the well-defined aminosilica is discussed in Chapter 3. Also, material characterization and ethylene polymerization behavior of the catalyst is examined and compared to various supported materials synthesized by literature protocols. In Chapter 4, various metallation routes are used to immobilize a Ti-CGC on patterned aminosilica, as well as densely functionalized aminosilica. The ethylene

polymerization behavior of these materials is examined to determine the effect of synthetic protocol on material properties. The ability of these novel supported catalysts to polymerize various norbornene monomers and the copolymerization of norbornenes/ethylene is the subject of Chapter 5. A number of structurally different (i.e. various ligands and metals) were synthesized using the method. These structural variations allow for the preliminary development structure-reactivity relationships. The development and testing of these various structural variations is discussed in Chapter 6. Summary of the work and future outlook is presented in Chapter 7.

1.8 References

1. Tullo, A. H., *Chem. Eng. News* 2003, *81*, 26-27.

2. Natta, G.; Ziegler, K. 2,691,647, 1954.

3. Banks, R. L.; Hogan, J. P. 2,642,467, 1953.

4. Stevens, M. P., *Polymer Chemistry: An Introduction*. 3rd ed.; Oxford University: Oxford, 1999.

5. Ribeiro, M. R.; Deffieux, A.; Portela, M. F., *Ind. Eng. Chem. Res.* 1997, *36*, 1224-1237.

6. Hlatky, G. G., *Chem. Rev.* 2000, *100*, 1347-1376.

7. Natta, G.; Pino, P.; Mazzanti, G.; Giannini, U., *J. Am. Chem. Soc.* 1957, *79*, 2975-2976.

8. Pino, P.; Mulhaupt, R., *Angew. Chem. Int. Edit.* 1980, *19*, 857-875.

9. Breslow, D. S.; Newburg, N. R., *J. Am. Chem. Soc.* 1957, *79*, 5072-5073.

10. Sinn, H.; Kaminsky, W.; Vollmer, H. J.; Woldt, R., *Angew. Chem. Int. Edit.* 1980, *19*, 390-392.

11. Resconi, L.; Cavallo, L.; Fait, A.; Piemontesi, F., *Chem. Rev.* 2000, *100*, 1253-1345.

12. Galan-Fereres, M.; Koch, T.; Hey-Hawkins, E.; Eisen, M. S., *J. Organomet. Chem.* 1999, *580*, 145-155.

13. Lin, M.; Spivak, G. J.; Baird, M. C., *Organometallics* 2002, *21*, 2350-2352.

14. Coates, G. W., *Chem. Rev.* 2000, *100*, 1223-1252.

15. Shapiro, P. J.; Bunel, E.; Schaefer, W. P.; Bercaw, J. E., *Organometallics* 1990, *9*, 867-869.

16. Shapiro, P. J.; Cotter, W. D.; Schaefer, W. P.; Labinger, J. A.; Bercaw, J. E., *J. Am. Chem. Soc.* 1994, *116*, 4623-4640.

17. Britovsek, G. J. P.; Gibson, V. C.; Wass, D. F., *Angew. Chem. Int. Edit.* 1999, *38*, 428-447.

18. Carpenetti, D. W.; Kloppenburg, L.; Kupec, J. T.; Petersen, J. L., *Organometallics* 1996, *15*, 1572-1581.

19. McKnight, A. L.; Waymouth, R. M., *Chem. Rev.* 1998, *98*, 2587-2598.

20. Chen, Y. X.; Marks, T. J., *Organometallics* 1997, *16*, 3649-3657.

21. Xie, T. Y.; Mcauley, K. B.; Hsu, J. C. C.; Bacon, D. W., *Ind. Eng. Chem. Res.* 1994, *33*, 449-479.

22. Pedeutour, J. N.; Radhakrishnan, K.; Cramail, H.; Deffieux, A., *Macromol. Rapid Commun.* 2001, *22*, 1095-1123.

23. Soga, K.; Park, J. R.; Shiono, T., *Polym. Commun.* 1991, *32*, 310-313.

24. Soga, K.; Shiono, T.; Kim, H. J., *Makromol. Chem.* 1993, *194*, 3499-3504.

25. Kaminsky, W.; Renner, F., *Makromol. Chem. Rapid. Commun.* 1993, *14*, 239-243.

26. Semikolenova, N. V.; Zakharov, V. A., *Macromol. Chem. Phys.* 1997, *198*, 2889-2897.

27. Dufrenne, N. G.; Blitz, J. P.; Meverden, C. C., *Microchem. J.* 1997, *55*, 192-199.

28. Quijada, R.; Rojas, R.; Alzamora, L.; Retuert, J.; Rabagliati, F. M., *Cat. Lett.* 1997, *46*, 107-112.

29. Dupuy, J.; Spitz, R., *J. Appl. Polym. Sci.* 1997, *65*, 2281-2288.

30. Xu, J. T.; Zhao, J.; Fan, Z. Q.; Feng, L. X., *Macromol. Rapid Commun.* 1997, *18*, 875-882.

31. Roscoe, S. B.; Frechet, J. M. J.; Walzer, J. F.; Dias, A. J., *Science* 1998, *280*, 270-273.

32. Moroz, B. L.; Semikolenova, N. V.; Nosov, A. V.; Zakharov, V. A.; Nagy, S.; O'Reilly, N. J., *J. Mol. Catal. A* 1998, *130*, 121-129.

33. dos Santos, J. H. Z.; Da Rosa, M. B.; Krug, C.; Stedile, F. C.; Haag, M. C.; Dupont, J.; Forte, M. D., *J. Polym. Sci. Pol. Chem.* 1999, *37*, 1987-1996.

34. dos Santos, J. H. Z.; Larentis, A.; da Rosa, M. B.; Krug, C.; Baumvol, I. J. B.; Dupont, J.; Stedile, F. C.; Forte, M. D., *Macromol. Chem. Phys.* 1999, *200*, 751-757.

35. dos Santos, J. H. Z.; Krug, C.; da Rosa, M. B.; Stedile, F. C.; Dupont, J.; Forte, M. D., *J. Mol. Catal. A* 1999, *139*, 199-207.

36. Roscoe, S. B.; Gong, C. G.; Frechet, J. M. J.; Walzer, J. F., *J. Polym. Sci. Pol. Chem.* 2000, *38*, 2979-2992.

37. Jezequel, M.; Dufaud, V.; Ruiz-Garcia, M. J.; Carrillo-Hermosilla, F.; Neugebauer, U.; Niccolai, G. P.; Lefebvre, F.; Bayard, F.; Corker, J.; Fiddy, S.; Evans, J.; Broyer, J. P.; Malinge, J.; Basset, J. M., *J. Am. Chem. Soc.* 2001, *123*, 3520-3540.

38. Musikabhumma, K.; Spaniol, T. P.; Okuda, J., *J. Polym. Sci. Pol. Chem.* 2003, *41*, 528-544.

39. Sacchi, M. C.; Zucchi, D.; Tritto, I.; Locatelli, P.; Dallocco, T., *Macromol. Rapid Commun.* 1995, *16*, 581-590.

40. Lee, D. H.; Yoon, K. B.; Noh, S. K., *Macromol. Rapid Commun.* 1997, *18*, 427-431.

41. Chan, M. C. W.; Chew, K. C.; Dalby, C. I.; Gibson, V. C.; Kohlmann, A.; Little, I. R.; Reed, W., *Chem. Commun.* 1998, 1673-1674.

42. Suzuki, N.; Asami, H.; Nakamura, T.; Huhn, T.; Fukuoka, A.; Ichikawa, M.; Saburi, M.; Wakatsuki, Y., *Chem. Lett.* 1999, 341-342.

43. Lee, B. Y.; Oh, J. S., *Macromolecules* 2000, *33*, 3194-3195.

44. Tian, J.; Soo-Ko, Y.; Metcalfe, R.; Feng, Y. D.; Collins, S., *Macromolecules* 2001, *34*, 3120-3122.

45. Suzuki, N.; Yu, J.; Shioda, N.; Asami, H.; Nakamura, T.; Huhn, T.; Fukuoka, A.; Ichikawa, M.; Saburi, M.; Wakatsuki, Y., *Appl. Catal. A* 2002, *224*, 63-75.

46. Zhang, Y. H.; Sita, L. R., *Chem. Commun.* 2003, 2358-2359.

47. Toscano, P. J.; Marks, T. J., *Langmuir* 1986, *2*, 820-823.

48. Soga, K.; Kim, H. J.; Shiono, T., *Macromol. Chem. Phys.* 1994, *195*, 3347-3360.

49. Soga, K.; Kim, H. J.; Shiono, T., *Macromol. Rapid Commun.* 1994, *15*, 139-143.

50. Soga, K., *Macromol. Symp.* 1995, *89*, 249-258.

51. Soga, K.; Arai, T.; Hoang, B. T.; Uozumi, T., *Macromol. Rapid Commun.* 1995, *16*, 905-911.

52. Jin, J. H.; Uozumi, T.; Soga, K., *Macromol. Rapid Comm.* 1995, *16*, 317-322.

53. Soga, K.; Ban, H. T.; Arai, T.; Uozumi, T., *Macromol. Chem. Phys.* 1997, *198*, 2779-2787.

54. Arai, T.; Ban, H. T.; Uozumi, T.; Soga, K., *Macromol. Chem. Phys.* 1997, *198*, 229-237.

55. Hong, S. C.; Ban, H. T.; Kishi, N.; Jin, J. Z.; Uozumi, T.; Soga, K., *Macromol. Chem. Phys.* 1998, *199*, 1393-1397.

56. Hong, S. C.; Teranishi, T.; Soga, K., *Polymer* 1998, *39*, 7153-7157.

57. Arai, T.; Ban, H. T.; Uozumi, T.; Soga, K., *J. Polym. Sci. Pol. Chem.* 1998, *36*, 421-428.

58. Lee, D. H.; Lee, H. B.; Noh, S. K.; Song, B. K.; Hong, S. M., *J. Appl. Polym. Sci.* 1999, *71*, 1071-1080.

59. Ban, H. T.; Uozumi, T.; Sano, T.; Soga, K., *Macromol. Chem. Phys.* 1999, *200*, 1897-1902.

60. Juvaste, H.; Pakkanen, T. T.; Iiskola, E. I., *Organometallics* 2000, *19*, 4834-4839.

61. Juvaste, H.; Pakkanen, T. T.; Iiskola, E. I., *Organometallics* 2000, *19*, 1729-1733.

62. Juvaste, H.; Pakkanen, T. T.; Iiskola, E. I., *J. Organomet. Chem.* 2000, *606*, 169-175.

63. Schneider, H.; Puchta, G. T.; Kaul, F. A. R.; Raudaschl-Sieber, G.; Lefebvre, F.; Saggio, G.; Mihalios, D.; Herrmann, W. A.; Basset, J. M., *J. Mol. Catal. A* 2001, *170*, 127-141.

64. Medard, N.; Soutif, J. C.; Lado, I.; Esteyries, C.; Poncin-Epaillard, F., *Macromol. Chem. Phys.* 2001, *202*, 3606-3616.

65. Alt, H. G.; Schertl, P.; Koppl, A., *J. Organomet. Chem.* 1998, *568*, 263-269.

66. Grubbs, R. H.; Gibbons, C.; Kroll, L. C.; Bonds, W. D.; Brubaker, C. H., *J. Am. Chem. Soc.* 1973, *95*, 2373-2375.

67. Bonds, W. D.; Brubaker, C. H.; Chandrasekaran, E. S.; Gibbons, C.; Grubbs, R. H.; Kroll, L. C., *J. Am. Chem. Soc.* 1975, *97*, 2128-2132.

68. Reissova, A.; Bastl, Z.; Capka, M., *Collect. Czech. Chem. C.* 1986, *51*, 1430-1438.

69. Iiskola, E. I.; Timonen, S.; Pakkanen, T. T.; Harkki, O.; Lehmus, P.; Seppala, J. V., *Macromolecules* 1997, *30*, 2853-2859.

70. Kitagawa, T.; Uozumi, T.; Soga, K.; Takata, T., *Polymer* 1997, *38*, 615-620.

71. Barrett, A. G. M.; de Miguel, Y. R., *Chem. Commun.* 1998, 2079-2080.

72. Timonen, S.; Pakkanen, T. T.; Iiskola, E. I., *J. Organomet. Chem.* 1999, *582*, 273-278.

73. Stork, M.; Koch, M.; Klapper, M.; Mullen, K.; Gregorius, H.; Rief, U., *Macromol. Rapid Commun.* 1999, *20*, 210-213.

74. Alt, H. G., *J. Chem. Soc. Dalton* 1999, 1703-1709.

75. Timonen, S.; Pakkanen, T. T.; Iiskola, E. I., *J. Mol. Catal. A* 1999, *148*, 235-244.

76. Uusitalo, A. M.; Pakkanen, T. T.; Iiskola, E. I., *J. Mol. Catal. A* 2000, *156*, 181-193.

77. Koch, M.; Stork, M.; Klapper, M.; Mullen, K.; Gregorius, H., *Macromolecules* 2000, *33*, 7713-7717.

78. Uusitalo, A. M.; Pakkanen, T. T.; Iskola, E. I., *J. Mol. Catal. A* 2002, *177*, 179-194.

79. Barrett, A. G. M.; de Miguel, Y. R., *Tetrahedron* 2002, *58*, 3785-3792.

80. Juvaste, H.; Iiskola, E. I.; Pakkanen, T. T., *J. Organomet. Chem.* 1999, *587*, 38-45.

81. Juvaste, H.; Iiskola, E. I.; Pakkanen, T. T., *J. Mol. Catal. A* 1999, *150*, 1-9.

82. Tao, T.; Maciel, G. E., *J. Am. Chem. Soc.* 2000, *122*, 3118-3126.

83. McKittrick, M. W.; Jones, C. W., *Chem. Mater.* 2003, *15*, 1132-1139.

CHAPTER 2

PREPARATION OF AMINE-FUNCTIONALIZED SURFACES EXHIBITING SITE-ISOLATED BEHAVIOR[†]

2.1 Introduction

Amine-functionalized silica has been synthesized for a number of years for use in catalysis[1-3], adsorption[4-6], and separations[7-9]. Despite this widespread use, the preparation of well-defined aminosilica surfaces is not straightforward due to the myriad ways that the primary amine can interact with its environment (Scheme 2.1). In particular, the weakly basic amine site can interact with the weakly acidic silica surface; the amine sites can also hydrogen bond with adjacent amine groups; or they can be relatively non-interacting if the amines are isolated.

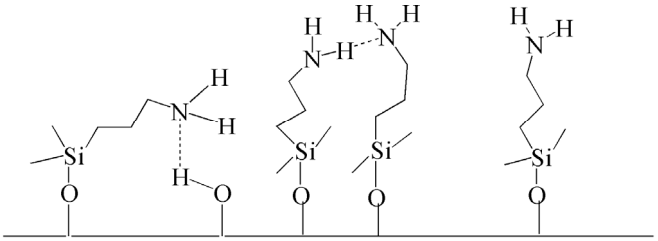

Scheme 2.1 Immobilized Aminosilica Interactions

There are two common methods used to prepare amine-functionalized silicas. The first is to contact a silica material with an alkoxyaminosilane solution, hereby grafting the silane onto the silica surface[10]. The second approach involves the co-condensation of an

[†] This work has been published in Chemistry of Materials, 2003, 15, 1132-1139.

alkoxyaminosilane with tetraethyl orthosilicate (TEOS), a direct synthesis method[11]. These methods generally result in a continuous or semicontinuous loading of amine groups immobilized on the silica surface with a distribution of types of sites present (vide supra). This can be advantageous when the goal is to maximize the number of amines on the surface. However, it can be a major disadvantage in many applications as well. In catalysis, molecular scale structure-property relationships cannot be developed when multi-sited solids are used. For instance, one may wish to know if a specific reaction catalyzed by amines requires a single amine site or if multiple amines in close proximity are needed. In this case, a solid with a random distribution of amine groups will not be useful, as there will be isolated amines present as well as amines hydrogen-bonded to other amines or the silica surface. In another example, if the amine is used as an anchor for further functionalization of the surface, the immediate environment around each amine site can be critically important. As mentioned above, the amine ligands may be close enough to hydrogen bond, creating multiple types of amines, with potentially different chemical reactivities, present on the surface. Second, when attempting to functionalize the surface-immobilized ligands, the steric hindrance that results from the closeness of the amines to each other can prevent high conversion[12-14]. An example of this phenomenon is depicted in Scheme 2.2 and is described in the literature, where incomplete conversion is observed when functionalizing aminopropylsilica with silyl-cyclopentadienyl groups[12-14]. Another difficulty in working with amine ligands immobilized on a silica surface is the possible interaction of the amine with surface silanols[15]. As shown in Scheme 2.1, since the alkyl chain is flexible, the basic amine

group could fold toward the surface and hydrogen-bond with the mildly acidic surface silanols, making it less likely to participate in further surface-functionalization reactions.

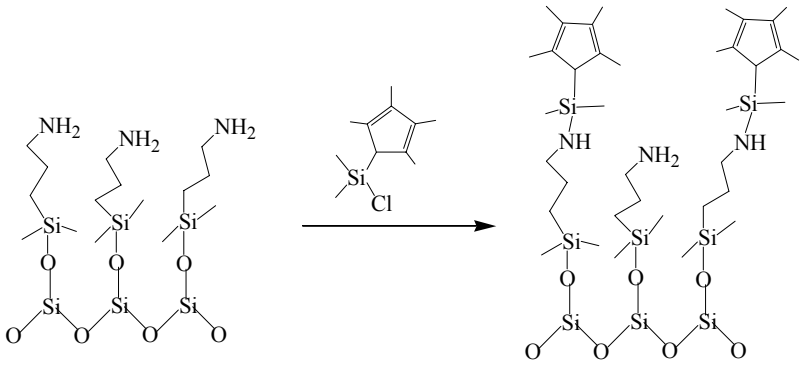

Scheme 2.2 Steric Hinderance on Typical Aminosilicas

Clearly, for some applications, a well-defined amine surface with site-isolated amine groups on the surface is desired. Previously, Wulff et al. demonstrated that it is possible to position two amines a specific distance from each other by connecting them via a hydrolysable linkage and utilizing a grafting technique[16, 17]. Sasaki and co-workers utilized a similar technique to position three amines on a silica surface[18, 19]. Subsequently, Katz and coworkers immobilized up to three amines a specific distance from each other via direct synthesis of imprinted silica[20]. In all of these cases it was possible to position amines a specific distance from each other, but only at low loadings. Wulff et al. reported loadings of 0.09-0.2 mmol of amine/g of solid; Katz and co-workers reported 0.07-0.23 mmol of amine/g of solid. At higher loadings, there is nothing that prevents the amines from becoming closer than the distance prescribed by the imprinting or patterning technique that was utilized (see Scheme 2.3A). Here, we report a molecular patterning

technique that allows for the preparation of well-defined, isolated amines on a silica surface in relatively high loading (see Scheme 2.3B). This method eliminates the

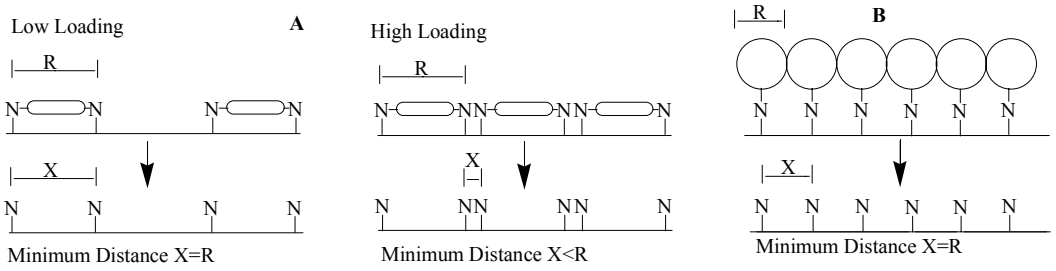

Scheme 2.3 Amine Patterning Cartoon

common problems described above that limit amine reactivity such as amine-silanol interactions, amine-amine interactions, and steric constraints.

After the completion and publication of the patterning protocol discussed in this work, a similar patterning protocol developed by V.N. Zaitsev was brought to our attention[21]. In his work, Zaitsev and coworkers used a trityl patterning agent, with an amide linkage instead of a Schiff base linkage. The entirety of his work was published in Russian journals, however extensive literature searches did not find any of Zaitsev's references due to translation error; "Aminosilica" was translated to "Aminosilicon". Dr. Zaitsev is aware of the work we have done in this area and of the fact it was done without knowledge of his work. Despite this independence, it is important to acknowledge his work in this area.

2.2 Experimental Section

General Considerations. The following chemicals were commercially available and used as received: 3,3,3-Triphenylpropionic acid (Acros), 1.0 M $LiAlH_4$ in tetrahydrofuran (THF) (Aldrich), pyridinium dichromate (Acros), 2,6 di-tert-butylpyridine (Acros), dichlorodimethylsilane (Acros), TEOS (Aldrich), 3-aminopropyltrimethoxysilane (Aldrich), hexamethyldisilazane (Aldrich), terephthaloyl chloride (Acros), anhydrous toluene (Acros), and n-butyllithium in hexanes (Aldrich). Anhydrous ether, anhydrous THF, anhydrous dichloromethane, and anhydrous hexanes were obtained from a packed bed solvent purification system utilizing columns of copper oxide catalyst and alumina (ether, hexanes) or dual alumina columns (tetrahydrofuran, dichloromethane)[22]. Tetramethylcyclopentadiene (Aldrich) was distilled over sodium metal prior to use. Anhydrous methanol (Acros) was further dried over 4-Å molecular sieves prior to use. All air- and moisture-sensitive compounds were manipulated using standard vacuum line, Schlenk, or cannula techniques under dry, deoxygenated argon or in a drybox under a deoxygenated nitrogen atmosphere.

Synthesis of Tritylimine Patterning Agent ([3-(Trimethoxysilanyl)propyl]-(3,3,3-triphenylpropylidene)amine) (1).

3,3,3-Triphenylpropanal was synthesized from 3,3,3-triphenyl propionic acid under argon using standard Schlenk techniques[23]. Triphenylpropionic acid (4.373 g, 14.46 mmol) was added to a flask with THF. The flask was then cooled in an ice-water bath and 8.97 g of pre-cooled 1.0 M $LiAlH_4$ in THF was added dropwise. After the evolution of hydrogen

completed, the mixture was stirred at room temperature for 30 min. The solution was then added to a suspension of pyridinium dichromate (6.00 g, 15.95 mmol) in methylene chloride and allowed to stir for 6 h. The reaction mixture was subsequently diluted with diethyl ether and filtered through a silica column, which was washed with several portions of diethyl ether. The filtrate was collected, and through rotary evaporation, the aldehyde was isolated in 60% yield. ^{1}H NMR (300 MHz, $CDCl_3$): δ 3.6 (d, 2H), 7.1-7.3 (multi, 15 H), 9.5 (t, 1H).

The aldehyde (1.0 g, 3.5 mmol) was then refluxed with 3-aminopropyltrimethoxysilane (0.501, 2.8 mmol) in dry methanol for 24 h. The methanol was removed in vacuo. The imine product was then recrystallized from methanol (38% yield). NMR data: ^{1}H NMR (300 MHz, CD_3OD): δ 0.4 (2 H), 1.51 (2H), 3.14 (2 H), 3.49 (9 H), 3.61 (2 H), 7.22 (15 H), 7.42 (1 H)[24].

Synthesis of SBA-15.

SBA-15 was synthesized by literature methods[25, 26]. The as-prepared material was calcined using the following temperature program: (1) increasing the temperature (1.2 °C/min) to 200 °C, (2) heating at 200 °C for 1 h, (3) increasing at 1.2 °C/min to 550 °C, and (4) holding at 550 °C for 6 h. Prior to functionalization, the SBA-15 was dried under vacuum at 150 °C for 3 h and stored in a drybox.

Synthesis of SBA-15 Functionalized with Patterning Agent (2).

Patterning agent **1** (0.5 g/1.12 mmol) was added to 2 g of SBA-15 with anhydrous toluene and stirred at room temperature under argon for 24 h. The resulting solid was

filtered and washed with toluene in a drybox, dried under vacuum at room temperature overnight, and then stored in a drybox. TGA showed 0.39 mmol/g SiO2 of patterning agent was immobilized on the SBA-15.

Silanol Capping Reaction (3).

The synthesis of **3** was carried out by contacting a large excess of hexamethyldisilazane with **2** in anhydrous toluene at room temperature under argon for 24 h. The resulting solid was filtered and washed with toluene and hexanes in a drybox, dried under vacuum at room temperature overnight, and then stored in a drybox.

Hydrolysis (4).

3 (0.5 g) was added to 50 g of a 2:2:1 solution of H_2O/MeOH/HCl (38 wt %). The mixture was stirred in air at room temperature for 5 h. The solid was collected via filtration, washed with water, methanol, and THF, and then dried under vacuum at room temperature overnight.

Second Silanol Capping (5).

4 was reacted with HMDS using the same procedure as in preparing **3**.

Synthesis of Densely Loaded APTMS-Functionalized SBA-15 (6)-Control Sample. Excess 3-aminopropyltrimethoxysilane (0.5 g, 2.79 mmol; APTMS) was added to 1 g of SBA-15 in anhydrous toluene. The mixture was allowed to stir for 24 h at room temperature under argon. The resulting solid was filtered, washed with toluene, dried under vacuum at room temperature overnight, and then stored in a drybox. TGA showed 1.15 mmol/g SiO_2 of APTMS was immobilized on the SBA-15.

Synthesis of Chlorodimethyl(2,3,4,5-tetramethyl-2,4-cyclopentadien-1-yl)silane. Tetramethylcyclopentadiene (6.02g, 0.049 mol) was added to a Schlenk flask with

anhydrous diethyl ether (150 mL). The mixture was cooled to 0 °C. n-Butyllithium (32 mL of 1.6M solution in hexanes) was slowly added to the Schlenk flask. After addition of the n-BuLi, additional ether (200 mL) was added to the flask. The mixture was allowed to stir overnight. The deprotonated cyclopentadiene ($LiCpMe_4$) was collected via filtration and washed with ether and hexanes in a drybox. Next, excess dichlorodimethylsilane (7.075 g, 0.0548 mol) was added to a flask with anhydrous THF (70 g). The mixture was cooled, and then $LiCpMe_4$ (1.484 g, 0.0116 mol) was slowly added over 75 min in the drybox. The contents were subsequently stirred overnight. The excess, unreacted dichlorodimethylsilane and THF were removed via vacuum. Hexanes were then added to dissolve the product and precipitate lithium chloride, which was removed via filtration in the drybox. The hexanes were then removed in vacuo, allowing for the collection of a pale yellow oil product in 83% yield. ^1H NMR (300 MHz, C_6D_6): δ 0.10 (s, 6 H), 1.67 (s, 6 H), 1.88 (s, 6 H), 2.85(s, 1 H).

Reaction of Chlorodimethyl(2,3,4,5-tetramethyl-2,4-cyclopentadien-1-yl)silane with Silica Materials.

Chlorodimethyl-(2,3,4,5-tetramethyl-2,4-cyclopentadien-1-yl)-silane (excess) was added to a mixture of amine-functionalized silica with hexanes in a drybox. 2,6-Di-tert-butylpyridine (excess) was added as a proton sponge. The mixture was allowed to react while stirring for 24 h. The solid was filtered and washed with hexanes and THF in the drybox. The solid was then contacted with another aliquot of chlorodimethyl-(2,3,4,5-tetramethyl-2,4-cyclopentadien-1-yl)silane and the procedure was repeated.

Synthesis of 7 and 8 from 5 and 6, respectively.

In a typical reaction of the amine-functionalized solids 5 and 6 with terephthaloyl chloride, 0.10 g of 5 (0.037 mmol NH2) was added to a flask with terephthaloyl chloride (2.36 mg, 0.013 mmol) in dichloromethane. The mixture was allowed to stir at room temperature for 24-36 h in a drybox. The resulting solid was removed from the drybox and then filtered and washed with water, methanol, dichloromethane, and hexanes. The solid was then dried under vacuum at room temperature overnight.

Characterization.

Cross-polarization magic angle spinning (CP-MAS) NMR spectra were collected on a Bruker DSX 300-MHz instrument. Samples were spun in 7-mm zirconia rotors at 5 kHz. Typical ^{13}C CP-MAS parameters were 10000 scans, a 90° pulse length of 4 μs, and a delay of 4 s between scans. Typical ^{29}Si CP-MAS parameters were 2000 scans, a 90° pulse length of 5 μs, and a delay of 10 s between scans. FT-Raman spectra were obtained on a Bruker FRA-106. At least 256 scans were collected for each spectrum, with a resolution of 2-4 cm^{-1}. Thermogravimetic analysis (TGA) was performed on a Netzsch STA409. Samples were heated under air from 30 to 1000 °C at a rate of 5 °C/min. The organic loading was measured by determining the weight loss from 200 to 650 °C. Nitrogen physisorption measurements were conducted on a Micromeritics ASAP 2010 at 77 K. Samples were pretreated by heating under vacuum at 150 °C for 8 h.

2.3 Results and Discussion

To synthesize the well-defined, isolated amine functionalities on silica, a bulky tritylimine ([3-(trimethoxysilanyl)propyl]-(3,3,3-triphenylpropylidene)amine) was employed as a patterning agent as shown in Scheme 2.4. A trityl group was chosen as the pattern due to its large size and overall symmetry. The patterning agent was synthesized via condensation of 3,3,3-triphenylpropanal and 3-aminopropyltrimethoxysilane, using techniques adapted from literature[23]. The trityl group not only limits the overall organic loading on the surface but also can ensure site isolation by spacing the amines a minimum distance apart. The imine patterning agent was contacted with mesoporous silica SBA-15 with an average pore diameter of 50 Å.

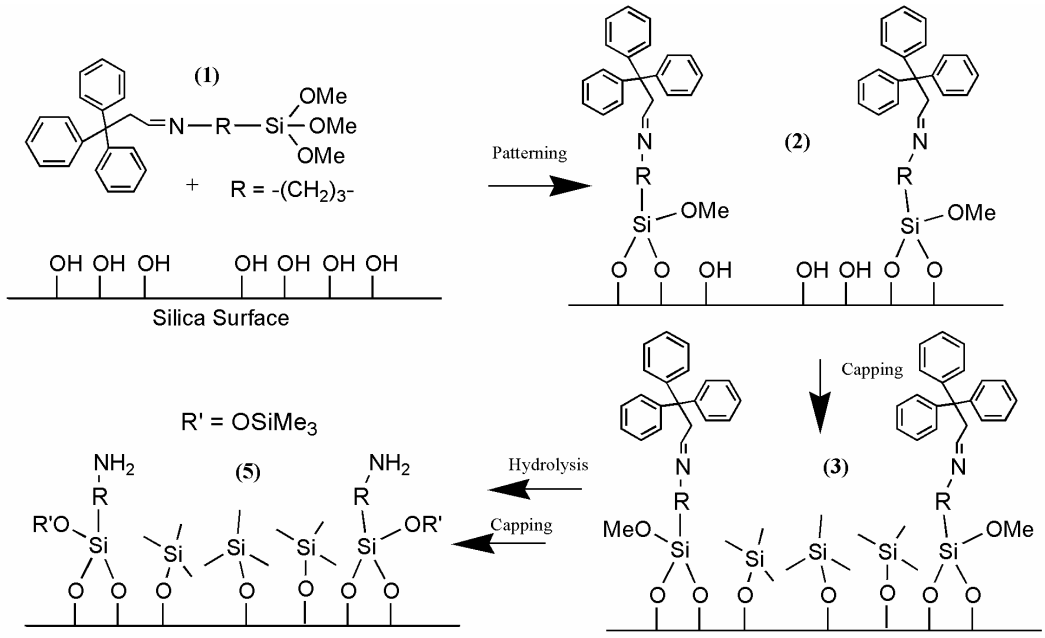

Scheme 2.4 Patterning Protocol

The imine-functionalized solid was then reacted with hexamethyldisilazane (HMDS) to cap excess surface silanols. This prevents the silanols from participating in later stages of the synthesis and prevents silanol-amine interactions after hydrolysis. After capping, the tritylimine was then hydrolyzed, removing the bulky trityl group. All steps up to the hydrolysis were carried out under rigorously dry conditions to facilitate only functionalization of the silica surface and prevent the formation of silane layers via the direct linkage of silanes to each other. After hydrolysis, the amine-functionalized solid was reacted with another aliquot of HMDS to cap any surface silanols formed as a result of the acid treatment. The organic loading was quantified by thermogravimetric analysis (TGA). The loading of the patterning agent was determined to be 0.39 mmol/g of solid. After the initial hydrolysis, TGA showed 0.345 mmol of amine/g of solid; 89% of the imine patterning agent is hydrolyzed to the amine. This hydrolysis treatment routinely hydrolyzes 89-93% of the imine. A second hydrolysis treatment can be used to remove additional imine, resulting in 93-95% total hydrolysis.

^{29}Si CP-MAS NMR experiments were used to characterize the silica framework of the materials. Figure 2.1 shows the spectra of the materials at various stages of the synthesis. The spectrum of calcined, unfunctionalized SBA-15 (Figure 2.1A) shows three overlapping peaks at -92, -100, and -107 ppm. These peaks correspond to the Q_2, Q_3, and Q_4 silicon resonances, respectively[27]. The signals for these resonances can also be seen in the functionalized samples (Figure 2.1B-D). The alkyl linkages to the surface can be characterized by the Si-C bond resonances at -46, -56, and -67 ppm, which correspond to the reaction of 1, 2, and 3 methoxy groups with the silanols on the surface[28]. As the predominant resonance is at -56 ppm, the initial reaction of the patterning agent with the

surface appears to be through mostly two linkages (Figure 2.1B). Hence, on a single patterning agent molecule, two methoxy groups react with the surface, evolving methanol, and the third methoxy group remains intact on average. Figure 2.1C shows the

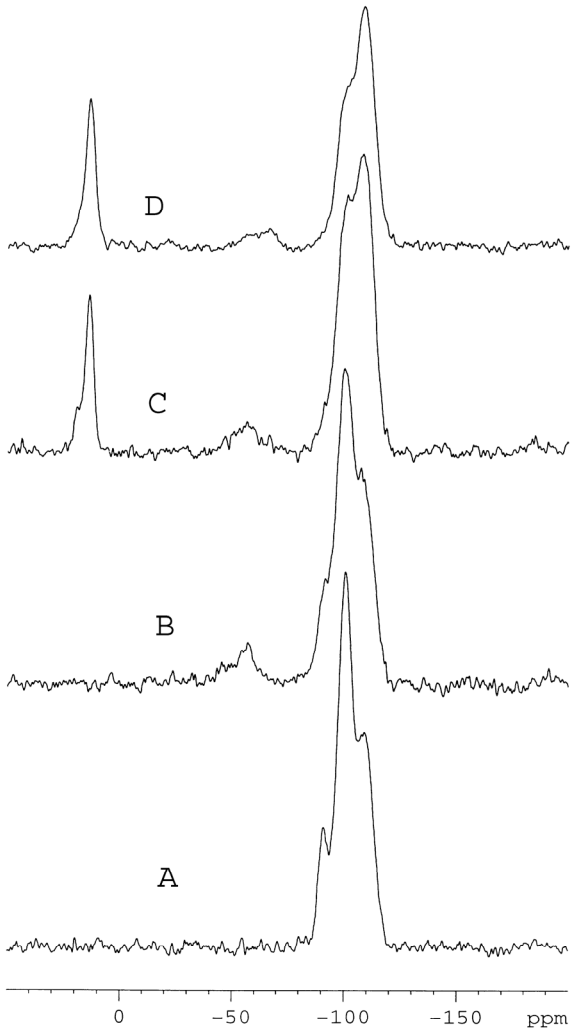

Figure 2.1 ^{29}Si CP-MAS NMR spectra of (A) calcined SBA-15. (B) SBA-15 functionalized with trityl imine patterning agent (**2**)**,** (C) material after silanol capping reaction (**3**), and (D) after hydrolysis (**4**)

spectra of the material after the capping reaction. The ^{29}Si resonance characteristic of the capping agent can be seen at 13.6 ppm. After hydrolysis (Figure 2.1D), the ^{29}Si spectra show evidence of mostly double and triple surface-silane linkages, with no visible single linkages. The signal at 13.6 ppm remains strong. Also noteworthy is that, during the functionalization of the silica with silanes, the intensity of the Q_2 and Q_3 peaks decreases, and the Q_4 peak increases in accordance with some silanols being consumed during the grafting reactions.

Figure 2.2A shows the ^{13}C CP-MAS NMR spectrum for the tritylimine patterning agent supported on SBA-15. The characteristic signals of the immobilized patterning agent are noted in Table 2.1A. Figure 2.2B shows the spectrum after reaction of the supported imine with HMDS. The methyl carbons on the capping agent are seen at -0.4 ppm. This signal is very large, indicating many free silanols are still present after the patterning agent is reacted with the silica, and therefore only a small fraction of the

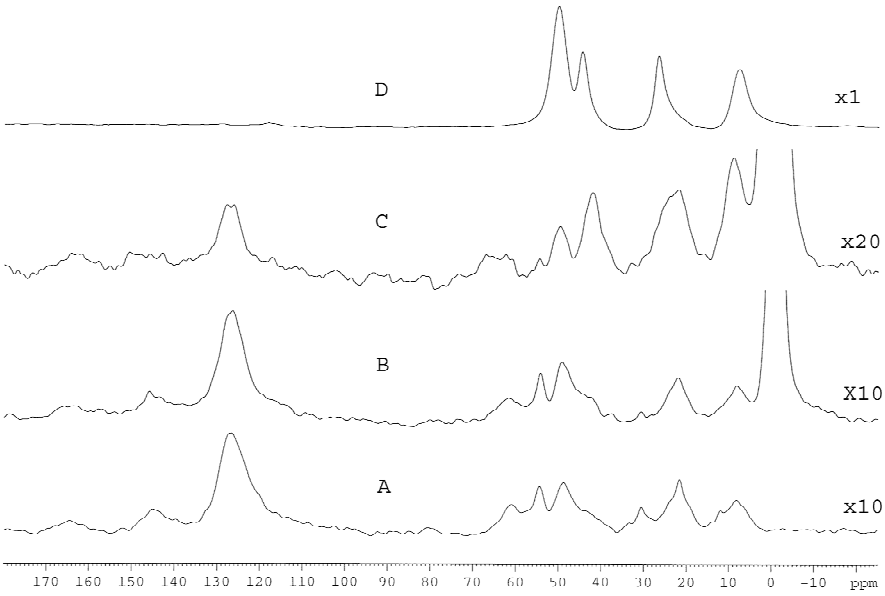

Figure 2.2 ^{13}C CP-MAS NMR spectra of (A) SBA-15 functionalized with supported patt. agent (**2**)**,** (B) material after silanol capping reaction (**3**), (C) material after hydrolysis (**4**), and (D) densely loaded APTMS-functionalized SBA-15 control material (**6)**

Table 2.1 ^{13}C CP-MAS NMR Assignments

A

Assignments	Resonance (ppm)
-**C**H=N-	165
-CH_2-**C**-$(Ph)_3$	145
Aromatic Carbons	128
-N=CH-**C**H_2-	54
-Si-O**C**H_3	49
-CH_2-**C**H_2-N=	31
-Si-CH_2-**C**H2-CH_2	22
-Si-**C**H_2-	8

B

Assignments	Resonance (ppm)
-Si-O**C**H_3	49
-CH_2-**C**H_2-NH_2	42
-Si-CH_2-**C**H_2-CH_2	22
-Si-**C**H_2-	9

available silanol groups reacted with the patterning agent, in contrast to when aminopropyltrimethoxysilane is used as the reactant. The ^{13}C spectrum of the hydrolyzed sample is depicted in Figure 2.2C. Table 2.1B shows the peak assignments[29]. The major change upon hydrolysis is the appearance of the carbon adjacent to the amine group, which can be seen at 42 ppm. For complete hydrolysis, the peaks associated with the patterning agent (164, 145, and 126 ppm) should no longer be present. Despite the strong peak that corresponds to the formation of an amine, a small peak can still be seen at 126 ppm (corresponding to the aromatic carbon resonances). This agrees with the TGA results that there is a small fraction of the trityl groups present, likely due to the presence of some nonhydrolyzed patterning agent. Figure 2.2D illustrates the ^{13}C spectra of densely loaded aminopropylsilica (6) control material prepared using traditional grafting

techniques (g mmol/g of SiO_2). The resonances characteristic of the amine (7.6, 26.6, 42; 50 ppm is due to methoxy groups) agree with those seen in the hydrolyzed sample and in previous works[29]. It is important to note that because these are CP-MAS spectra, they are not quantitative and the relative abundance of the various carbons is only loosely correlated with the peak area.

Figure 2.3 shows the FT-Raman spectra for the supported imine (A), hydrolyzed solid (B), and a densely functionalized aminosilica control material (C). The peak at 3062 cm^{-1} corresponds to the ν_{C-H} bands in the aromatic rings, whereas the region from 3000 to 2800 cm-1 is characteristic of aliphatic ν_{C-H} bands. The imine can be characterized by the C=N stretching band, which appears at 1595 cm^{-1}. Upon hydrolysis, the peaks associated with the aromatic patterning agent and the imine linkage show a large decrease in intensity. The previously sharp band at 1595 cm^{-1} is reduced to nearly the level of background noise. The peak assigned to the aromatic C-H bands is reduced but is still present. The presence of these peaks confirms the results of the TGA and ^{13}C NMR experiments-some trityl groups remain. Although very little of the trityl groups are still present, the characteristic band (ν_{C-H} aromatic) is a strong Raman signal, which accounts for its high visibility[30]. Amines are typically characterized by the ν_{N-H} band present between 3500 and 3200 cm^{-1}. This peak is not visible in Figure 2.3B as it is routinely difficult to see the amine band in Raman spectra. This is likely the result of the relatively low amine loading on the solid. The spectrum for the amine-functionalized control material (densely loaded sample) is shown in Figure 2.3C. The broad peak at 3300 cm^{-1} in this spectrum corresponds to the ν_{N-H} band. Only with the higher loading (~1 mmol of NH_2/g of SiO_2) of the densely functionalized material can the amine peak be seen in the

Raman spectra. Despite the absence of a ν_{N-H} band in the FT-Raman spectrum of the patterned aminosilica, it is known that amine is present based on the ^{13}C NMR results.

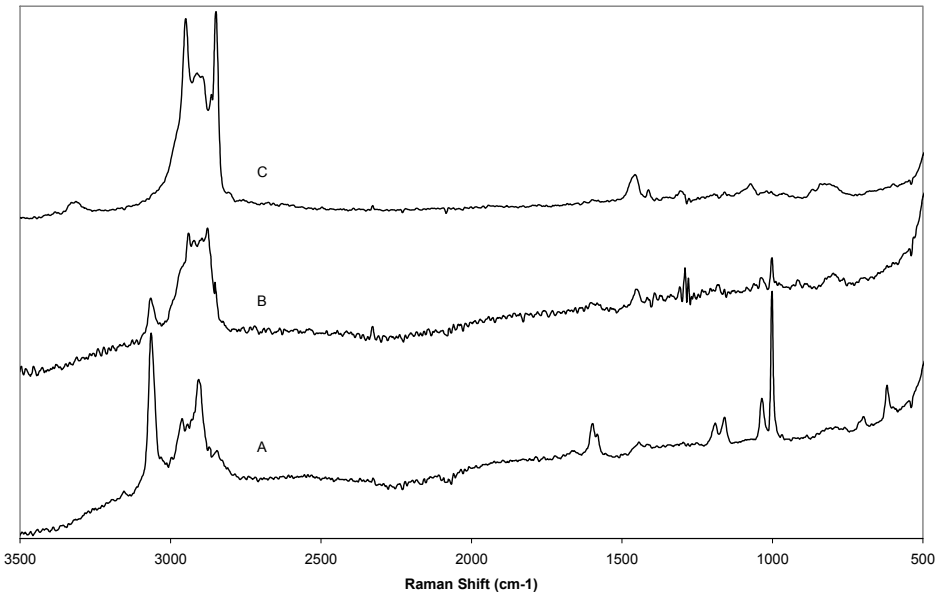

Figure 2.3 FT-Raman spectra of (A) SBA-15 functionalized with supported patterning agent (**2**)**,** (B) material after hydrolysis (**4**), and (C) densely loaded APTMS-functionalized SBA-15 control material (**6)**

N_2 physisorption was also used to characterize the silica material throughout the synthesis; the results are listed in Table 2.2. As expected, the surface area and pore size decreased after the patterning agent was immobilized and then decreased again after the silica was reacted with the capping agent. Upon hydrolysis, both of the parameters increased almost back to the values for pure SBA-15. This suggests there is not a dense loading of amine groups on the surface, nor is there substantial pore blockage. As evidenced by TGA, ^{13}C CP-MAS NMR, and FT-Raman spectroscopy, the hydrolysis step does not completely remove the trityl groups from the porous structure. The hydrolysis was repeated several times, each time only marginally removing more trityl groups. However, the silica was degraded upon repeated exposure to acidic hydrolysis conditions.

Using harsher conditions (i.e., higher acid concentration) in the hydrolysis resulted in the removal of the amine ligand from the surface, while also having an effect on the silica

Table 2.2 Nitrogen Physisorption Results

Sample	BET surface area (m^2/g of SiO_2)	Average pore diameter[a] (Å)
SBA-15	736	50
2	649	40
3	436	35
4	697	49

a Average pore size determined from desorption isotherm

structure. Hence, the functionalized materials are subjected to the hydrolysis treatment at most twice, resulting in 93-95% removal of trityl groups by TGA.

One drawback of aminosilica materials prepared by traditional methods is the nonuniform reactivity imparted by the variety of types of amine sites on the surface. To probe the reactivity of the patterned amine surface, a control reaction was undertaken. Chlorodimethyl-(2,3,4,5-tetramethyl-2,4-cyclopentadien-1-yl)silane (Cp-silane) was reacted with the amine-functionalized surface to give the amidosilyl group shown in Scheme 2.5. This reaction was chosen because it has been previously studied on amine-functionalized silicas[12-14]. TGA shows the hydrolyzed amine functionalities react with the silane, giving nearly a quantitative yield (>99%). As reaction of Cp-silane with capped, amine-free SBA-15 results in no surface functionalization, it can be concluded that this functionalization occurs at the amine site as described in Scheme 2.5. It is important to note that this reaction results in substantially less than quantitative conversion when a traditional, densely loaded amine-functionalized silica is used (~66%

yield)[12-14]. This may be attributed to either steric crowding of the amine groups or to the presence of some amines interacting with silanols on the surface. Hence, unlike traditional materials, the patterned amine material behaves as if it has a single type of amine site.

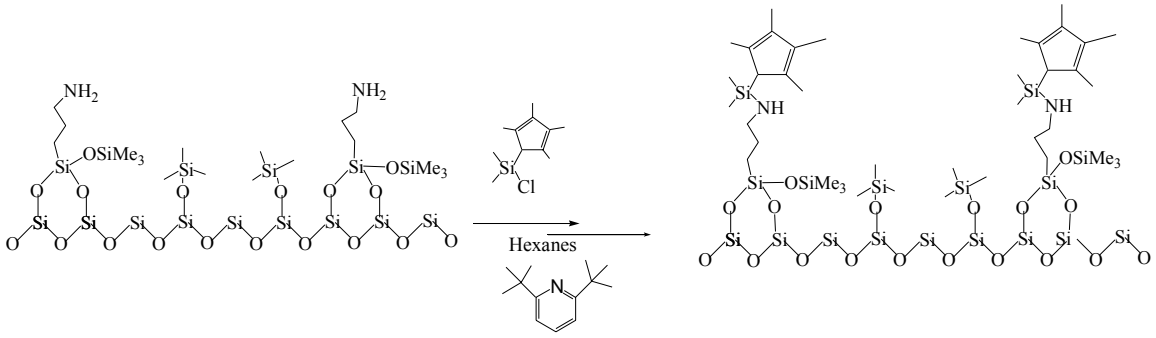

Scheme 2.5 Cp-silane Reaction with Aminosilica

Site isolation was probed by contacting the amine-functionalized materials with a diacid chloride, terephthaloylchloride. The acid chloride functionality readily reacts with an immobilized amine ligand to form an amide. If the amine functionalities are not sufficiently isolated, both acid chloride functionalities on the probe molecule can react to make two amide bonds (Scheme 2.6A). In contrast, for isolated amines only one acid chloride functionality should react, leaving one acid chloride functionality and making one amide bond (Scheme 2.6B). Both solids 5 and 6 were contacted with 0.35 equiv of terephthaloyl chloride in dichloromethane. Only 0.35 equiv was used, as opposed to a full equivalent or excess, so that it is theoretically possible to consume all the acid

chloride groups if the amines are densely loaded[20]. The resulting materials were characterized by FT-Raman spectroscopy. Figure 2.4 shows the important region of the Raman spectrum of solid 7 (2.4A) and solid 8 (2.4B) after reaction with the diacid

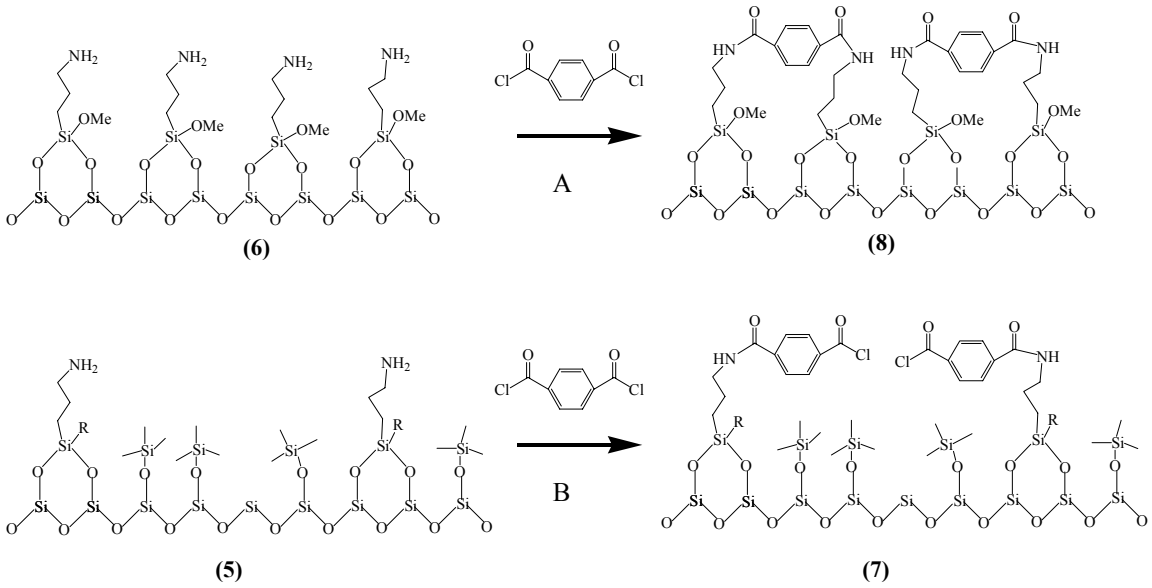

Scheme 2.6. Isolation Probing Reaction

chloride (1550-1750cm^{-1}). The peak corresponding to the amide $\nu_{C=O}$ vibration is seen at 1610 cm^{-1} [20]. The vibration from the acid $\nu_{C=O}$ vibration is seen at 1710 cm^{-1} [20]. As seen in the spectra, the reaction of the diacid chloride with the nonpatterned, amine-functionalized solid results in the complete loss of the acid chloride functionality. This suggests that both functionalities on the probe molecule react with surface amine ligands. As such, the amine ligands are relatively densely packed and nonisolated. However, the presence of the acid and the amide in solid suggests the amine ligands are on average sufficiently spaced on the surface so that the probe molecule cannot react with more than one ligand. While this does not prove that all the amines are isolated, it clearly shows

that the patterned material is substantially different from traditional aminosilicas and suggests that the amine ligands may be isolated by a minimum distance of 7-8 Å.

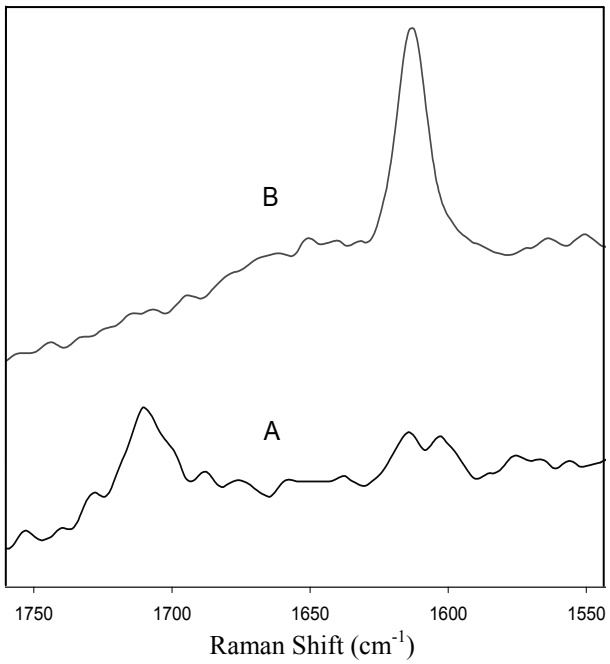

Figure 2.4 FT-Raman spectra of (A) patterned amine-functionalized SBA-15 contacted with the di-acid chloride probe molecule (**7**) and (B) densely loaded APTMS-functionalized SBA-15 reacted with di-acid chloride probe molecule (**8)**

2.4 Summary

All of these results, when taken together, support the presence of a well-defined, amine-functionalized surface with site-isolated amine groups. The evolution of the organic functional groups can be easily tracked using ^{13}C NMR and Raman spectroscopy and all of the relevant groups can be identified by one or both of the techniques. Reactivity studies with the Cp-silane and diacid chloride probe molecules illustrate that the

amines are effective foundations for subsequent synthesis on the solid surface and that the amine groups behave as if they are isolated compared to aminosilica materials prepared by traditional methods. The method appears to be versatile in that the minimum spacing between the amines can theoretically be controlled by proper design of the patterning molecule. For instance, one can imagine using other patterning molecules such as one derived from 3,3,3-trifluorenylpropanal (instead of 3,3,3-triphenylpropanal) to increase the spacing. It is expected that these new materials will allow for the synthesis of well-defined, single-site organometallics and other catalysts with nanostructured active sites previously unattainable using current synthetic methods.

2.5 References

1. Fey, T.; Fischer, H.; Bachmann, S.; Albert, K.; Bolm, C., *J. Org. Chem.* **2001,** *66*, 8154-8159.

2. Muller, C. A.; Schneider, M.; Mallat, T.; Baiker, A., *Appl. Catal. A* **2000,** *201*, 253-261.

3. Wight, A. P.; Davis, M. E., *Chem. Rev.* **2002,** *102*, 3589-3613.

4. Kramer, J.; Garcia, A. R.; Driessen, W. L.; Reedijk, J., *Chem. Commun.* **2001**, 2420-2421.

5. Evans, J.; Zaki, A. B.; El-Sheikh, M. Y.; El-Safty, S. A., *J. Phys. Chem. B* **2000,** *104*, 10271-10281.

6. Walcarius, A.; Etienne, M.; Bessiere, J., *Chem. Mater.* **2002,** *14*, 2757-2766.

7. Basiuk, V. A.; Chuiko, A. A., *J.Chromatogr.* **1990,** *521*, 29-42.

8. Patton, E. V.; Wonnacott, D. M., *J. Chromatogr.* **1987,** *389*, 115-125.

9. Porsch, B.; Kratka, J., *J. Chromatogr.* **1991,** *543*, 1-7.

10. Kallury, K. M. R.; Macdonald, P. M.; Thompson, M., *Langmuir* **1994,** *10*, 492-499.

11. Fowler, C. E.; Burkett, S. L.; Mann, S., *Chem. Commun.* **1997**, 1769-1770.

12. Juvaste, H.; Iiskola, E. I.; Pakkanen, T. T., *J. Mol. Catal. A* **1999,** *150*, 1-9.

13. Juvaste, H.; Pakkanen, T. T.; Iiskola, E. I., *Organometallics* **2000,** *19*, 1729-1733.

14. Timonen, S.; Pakkanen, T. T.; Iiskola, E. I., *J. Organomet. Chem.* **1999,** *582*, 273-278.

15. Kanan, S. A.; Tze, W. T. Y.; Tripp, C. P., *Langmuir* **2002,** *18*, 6623-6627.

16. Wulff, G.; Heide, B.; Helfmeier, G., *React. Polym.* **1987,** *6*, 299-310.

17. Wulff, G.; Heide, B.; Helfmeier, G., *J. Am. Chem. Soc.* **1986,** *108*, 1089-1091.

18. Hwang, K. O.; Sasaki, T., *J. Mater. Chem.* **1998,** *8*, 2153-2156.

19. Hwang, K. O.; Yakura, Y.; Ohuchi, F. S.; Sasaki, T., *Mat. Sci. Eng. C* **1995,** *3*, 137-141.

20. Katz, A.; Davis, M. E., *Nature* **2000,** *403*, 286-289.

21. Zaitsev, V. N.; Skopenko, V. V.; Kholin, Y. V.; Donskaya, N. D.; Mernyi, S. A., *Zh. Obshch. Khim.* **1995,** *65*, 529-537.

22. Pangborn, A. B.; Giardello, M. A.; Grubbs, R. H.; Rosen, R. K.; Timmers, F. J., *Organometallics* **1996,** *15*, 1518-1520.

23. Cha, J. S.; Chun, J. H.; Kim, J. M.; Kwon, O. O.; Kwon, S. Y.; Lee, J. C., *Bull. Kor. Chem. Soc.* **1999,** *20*, 400-402.

24. The imine has limited solubility in common NMR solvents. As a result of this, NMR spectra showed very broad peaks, preventing the determination of multiplicity.

25. Zhao, D. Y.; Feng, J. L.; Huo, Q. S.; Melosh, N.; Fredrickson, G. H.; Chmelka, B. F.; Stucky, G. D., *Science* **1998,** *279*, 548-552.

26. Zhao, D. Y.; Huo, Q. S.; Feng, J. L.; Chmelka, B. F.; Stucky, G. D., *J. Am. Chem. Soc.* **1998,** *120*, 6024-6036.

27. Engelhardt, G.; Michel, D., *High Resolution Solid-State NMR of Silicates and Zeolites*. ed.; John Wiley and Sons: New York, 1988.

28. Sindorf, D. W.; Maciel, G. E., *J. Am. Chem. Soc.* **1983,** *105*, 3767-3776.

29. Sudholter, E. J. R.; Huis, R.; Hays, G. R.; Alma, N. C. M., *J. Colloid. Interf. Sci.* **1985,** *103*, 554-560.

30. Baranska, H.; Labudzinka, A.; Terpinski, J., *Laser Raman Spectroscopy*. ed.; John Wiley and Sons: New York, 1987.

CHAPTER 3

SYNTHESIS, CHARACTERIZATION, AND TESTING OF IMMOBILIZED TI-CGC INSPIRED COMPLEXES[†]

3.1 Introduction

To build a truly single-site CGC on an amino-silica surface via a multi-step grafting technique, a well-defined aminosilica (ideally with uniform, isolated sites) is required as a starting material. We have recently reported a patterning protocol (discussed in Chapter 2) that allows for the preparation of a well-defined amine-functionalized silica, with amine sites which behave as if they are isolated and uniform[1]. Using this patterned aminosilica as a scaffold, we have subsequently developed a protocol to synthesize a supported titanium constrained-geometry-inspired catalyst on the surface[2]. Here we report the detailed description of the supported patterned CGC[3] and demonstrate its applicability in the catalytic polymerization of ethylene using both methylaluminoxane (MAO) and borane/trialkyl aluminum co-catalysts. In particular, we probe the role of the site isolation on the polymerization performance of the titanium precatalysts and focus on the impact of leaching of the supported metal complexes on the possibility of preparing well-defined, truly single-site model polymerization catalysts using this methodology.

3.2 Experimental Section

General Considerations. The following chemicals were commercially available and used as received: 3,3,3-Triphenylpropionic acid (Acros), 1.0 M $LiAlH_4$ in tetrahydrofuran

[†] This work has been published in part in J. Am. Chem. Soc. 2004, 126, 3052-3 and J. Catal. 2004, 227, 186-201.

(THF) (Aldrich), pyridinium dichromate (Acros), 2,6 di-tert-butylpyridine (Acros), dichlorodimethylsilane (Acros), TEOS (Aldrich), 3-aminopropyltrimethoxysilane (Aldrich), hexamethyldisilazane (Aldrich), tetrakis(diethylamino)titanium (Aldrich), trimethyl silyl chloride (Aldrich), trimethylaluminum (Aldrich), triisobutylaluminum (Aldrich), methylaluminoxane (Aldrich, 10 wt% in toluene), and n-butyllithium in hexanes (Aldrich). Tetramethyl-cyclopentadiene (Aldrich) was distilled prior to use. Anhydrous toluene (Acros) was distilled over sodium metal prior to use. Tris(pentafluorophenyl)borane (Aldrich) was purified via sublimation before use. Anhydrous methanol (Acros) was further dried over 4-Å molecular sieves prior to use. Anhydrous ether, anhydrous THF, anhydrous dichloromethane, and anhydrous hexanes were obtained from a packed bed solvent purification system utilizing columns of copper oxide catalyst and alumina (ether, hexanes) or dual alumina columns (tetrahydrofuran, dichloromethane)[4]. All air- and moisture-sensitive compounds were manipulated using standard vacuum line, Schlenk, or cannula techniques under dry, deoxygenated argon or in a drybox under a deoxygenated nitrogen atmosphere. Ethylene was passed over a metallic catalyst (Matheson 641-01 cartridge) to remove oxygen and water, before being fed to the reactor.

Synthesis of SBA-15. SBA-15 with approximately 50 Å diameter pores was synthesized via literature methods[5, 6]. Calcination of the material was done in air using the following temperature program: (1) increasing the temperature (1.2 °C/min) to 200 °C, (2) heating at 200 °C for 1 h, (3) increasing at 1.2 °C/min to 550 °C, and (4) holding at 550 °C for 6

h. Prior to use, the SBA-15 was dried under vacuum at 150 °C for 3 h and stored in a drybox.

Catalyst Synthesis Densely-loaded and patterned aminosilica materials were prepared using a SBA-15 host as described previously[1].

Reaction of Chlorodimethyl(2,3,4,5-tetramethyl-2,4-cyclopentadien-1-yl)silane with Amine Functionalized Silica Materials (6). Chlorodimethyl-(2,3,4,5-tetramethyl-2,4-cyclopentadien-1-yl)silane (excess) was added to a mixture of amine-functionalized silica with hexanes in a drybox. A proton sponge, 2,6-Di-tert-butylpyridine (excess), was added. The mixture was then allowed to stir for 24 h. The solid was collected by filtration, which was followed by washing with hexanes and THF in the drybox. The solid was then contacted with another aliquot of chlorodimethyl-(2,3,4,5-tetramethyl-2,4-cyclopentadien-1-yl)silane and the procedure was repeated.

Metallation of Amino-Cp Silica Material (7). The solid was packed into a flask in the glovebox with toluene (15 mL). $Ti(NEt_2)_4$ (excess) was diluted with toluene (5 mL), and both mixtures were cooled. In the drybox, the solution of $Ti(NEt_2)_4$ in toluene was added to the flask dropwise while stirring. After the reaction mixture had warmed to room temperature, it was refluxed for half an hour. The solution was filtered off, and the resulting light yellow solid was washed with toluene and pentane. The resulting orange-brown solid was filtered, washed with toluene, dried under vacuum at room temperature overnight, and then stored in a drybox

Ligand Exchange (8). In a drybox, **7** was added to a flask with anhydrous hexanes and excess chlorotrimethyl silane. The reaction was allowed to stir overnight at room temperature. The solid was filtered and washed with hexanes in the drybox. The orange-

brown solid was recovered, dried under vacuum overnight at room temperature, then stored in a drybox.

Synthesis of Homogeneous complex 9. $Me_4CpSiMe_2Cl$ (1.07 g, 5 mmol) was dissolved in 50 ml of hexane and cooled to -78°C. To this mixture n-propylamine (0.6 g, 10.2 mmol) was added via syringe and the reaction mixture was stirred overnight at and allowed to warm to room temperature. The n-propylamine/HCl salt was removed by filtration under argon and the solvent was removed under vacuum yielding the crude product as a yellow oil. Next, 2 mmol of the this crude product $C_5Me_4HSiMe_2NH(CH_2)_2CH_3$ was added via syringe to 2 mmol of $Ti(NEt_2)_4$ dissolved in 20 ml of toluene at -70°C. The mixture was heated under reflux overnight and the product was obtained as a clear brown oil after the by-products were removed at 130°C under high vacuum. The product was then added to a flask with excess chlorotrimethylsilane and hexanes. The reaction was allowed to stir overnight and then the solvent and excess silane were removed under vacuum. NMR (C_6D_6): δ = 0.21 (6H, $Si(CH_3)_2$), 1.05 (3H, $CH_2C\mathit{H}_3$), 1.58 (2H, $CH_2C\mathit{H}_2CH_3$), 1.75 (6H, $CpC\mathit{H}_3$), 1.90 (6H, $CpC\mathit{H}_3$), 2.6 (2H, $NC\mathit{H}_2CH_2$). Anal Calc. for $C_{14}H_{21}NCl_2SiTi$, C 48.0%, H 6.0%, N 4.0%, Cl 20.3%, Ti 13.7%. Found C 48.4%, H 5.7%, N 4.6%, Cl 21.5%, Ti 12.9%.

Characterization. FT-Raman spectra were obtained on a Bruker FRA-106. At least 256 scans were collected for each spectrum, with a resolution of 2-4 cm^{-1}. Cross-polarization magic angle spinning (CP-MAS) NMR spectra were collected on a Bruker DSX 300-MHz instrument. Samples were spun in 7-mm zirconia rotors at 5 kHz. The ^{13}C CP-MAS parameters were 10000 scans, a 90 pulse length of 4 s, and a delay of 4 s between scans.

The ^{29}Si CP-MAS parameters were 2000 scans, a 90 pulse length of 5 s, and a delay of 10 s between scans. Nitrogen physisorption measurements were conducted on a Micromeritics ASAP 2010 at 77K. Samples were pretreated by heating under vacuum at 150 ºC for 8 hours. Diffuse reflectance ultraviolet-visible (UV-VIS) spectroscopy was performed on solid materials in a drybox with an Ocean Optics USB2000 Fiber Optic Spectrometer using a PTFE diffuse reflectance standard. Solution UV-VIS spectroscopy was performed using a Hewlett Packard Model 8453 spectrometer with anhydrous hexanes as a solvent. Thermogravimetic analysis (TGA) was performed on a Netzsch STA409. Samples were heated under air from 30 to 1000° C at a rate of 5 °C/min. The organic loading was measured by determining the weight loss from 200 to 650 °C. Elemental analysis was performed by Desert Analytics. Gel Permeation Chromatography was performed at the University of Massachusetts, Amherst with Polymer Laboratories PL-220 high temperature GPC equipped with a Wyatt MiniDawn (620 nm diode laser) high temperature light scattering detector and refractive index detector at 135 °C using 1,2,4-trichlorobenzene as solvent and calibrated using polystyrene standards. Polyethylene was extracted from silica at 130 °C using trichlorobenzene as the solvent prior to the GPC analysis.

Ethylene Polymerizations

MAO Co-catalyst: The immobilized precatalyst was added to the reactor with toluene and methyl alumoxane (800 Al:1 Ti) in a drybox. The solution was stirred for 20 minutes to allow for sufficient activation of the catalyst. The reactor was then sealed and removed from the glovebox, placed in a 25 °C waterbath, and subsequently connected to

an ethylene source at 60 psi. The ethylene was delivered for a prescribed amount of time and the polymerization was terminated by releasing the ethylene pressure and adding acidic ethanol. The precipitated polymers were washed with ethanol, then dried at 70 ºC.

Borane co-catalyst: In a typical polymerization, the immobilized precatalyst was added to the reactor with toluene, tris(pentafluorophenyl) borane (1.5 B:1 Ti), and either trimethyl aluminum or triisobutyl aluminum (400:1 Al:Ti ratio) in a drybox. The mixture was allowed to stir for 30 minutes to allow for sufficient activation of the catalyst. The reactor was then sealed and removed from the glovebox, placed in a 25 °C waterbath, and ethylene at 60 psi was introduced as described above. The polymerization was allowed to continue for a prescribed amount of time, then terminated as noted above. The precipitated polymers were washed with ethanol, then dried at 70 °C.

Leaching Experiments: The immobilized precatalyst, toluene, and methyl alumoxane (800 Al:1 Ti) were added to a flask in a drybox. The mixture was allowed to stir for 20 minutes. The mixture was then filtered in the drybox, and the filtrate was added to the reactor with toluene and an additional portion of MAO (200:1 Al:Ti). The reactor was then removed from the glovebox, placed in a 25 °C waterbath, and contacted ethylene at 60 psi as described above. The polymerization was allowed to continue for a prescribed amount of time and then terminated by adding acidic ethanol. The precipitated polymers were washed with ethanol, then dried at 70 °C.

3.3 Results and Discussion

3.3.1 Materials Synthesis and Characterization

Using the unique patterned aminosilica material discussed in Chapter 2 (Scheme 3.1) as a scaffold, potentially site-isolated organometallic catalysts can be prepared[2].

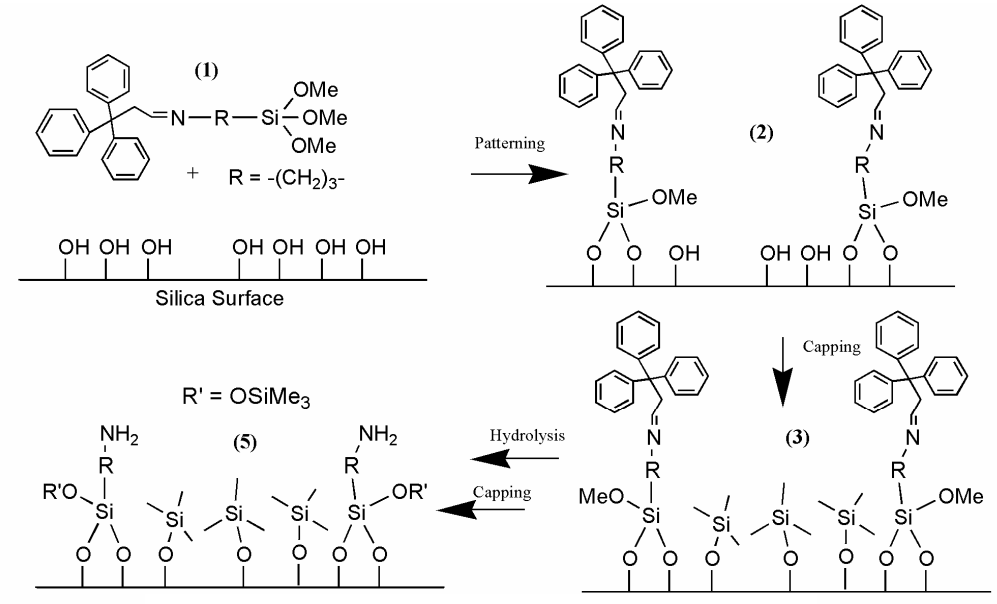

Scheme 3.1 Aminosilica Patterning Protocol

Scheme 3.2 shows a synthetic protocol that has been developed to prepare immobilized Ti-CGC inspired species. The first step in the synthesis of the supported complex is the reaction of the supported amine with chlorodimethyl(2,3,4,5-tetramethyl-2,4-cyclopentadien-1-yl)silane (Cp-silane). After contacting with two aliquots of the silane, there is quantitative reaction of the silane with the supported amines, as determined by TGA and elemental analysis. When the same procedure is followed using a densely functionalized amino-silica, only two-thirds of the amines react with the silane

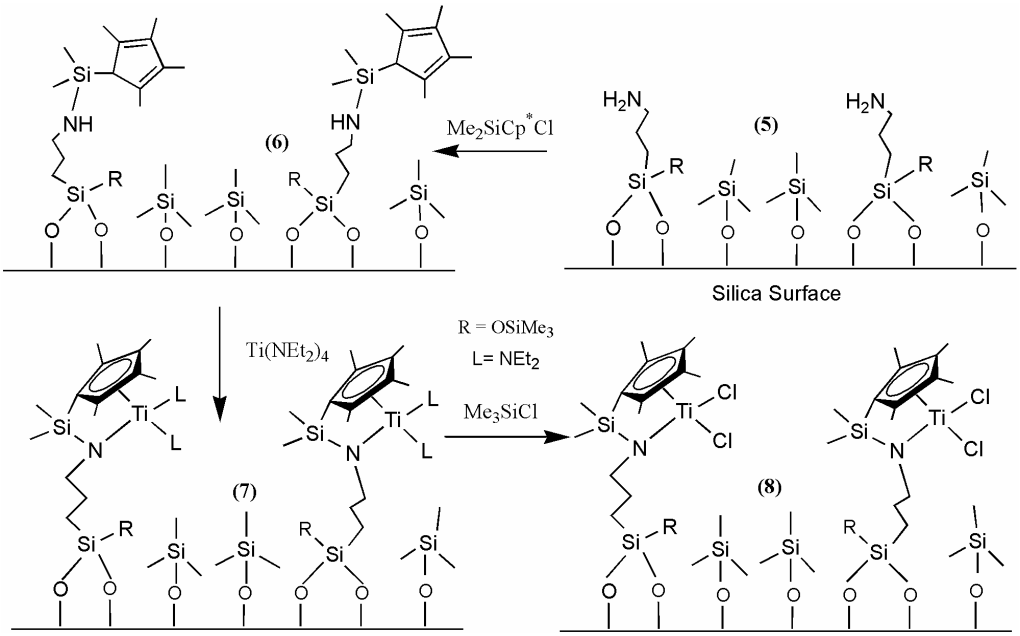

Scheme 3.2 Ti-CGC Synthetic Protocol

functionality. This is comparable to results reported in the literature where following treatment with n-butyl lithium, roughly 70% of the amine groups on a densely-functionalized surface react with the chlorodimethyl(2,3,4,5-tetramethyl-2,4-cyclopentadien-1-yl)silane[7-11]. Thus, the ill-defined nature of the densely-loaded silica surface results in multiple types of amine sites. In contrast, on the patterned material, the amine sites behave in a more uniform manner. As previously reported, there is no reaction of the chlorodimethyl(2,3,4,5-tetramethyl-2,4-cyclopentadien-1-yl)silane with capped, amine-free SBA-15, as verified via TGA and UV-Vis[1]. In contrast, contacting bare SBA-15 with excess Cp-silane resulted in a pink colored solid, with a loading of 1.07 mmoles silane/g solid. These results provide evidence that for reactions on amine-

containing solids, the silane reacts with the amine functionalities on the surface, and does not open siloxane bridges.

A common synthetic route for the preparation of homogeneous metallocenes or CGCs utilizes an alkyl lithium reagent in the next step to deprotonate the Cp ring followed by metallation with the metal tetrachloride salt. However, as mentioned previously, with silica-supported systems where a single type of site is desired, alkyl lithium reagents must be avoided. Hence, an alternate metallation strategy is required. In this work, after functionalization by the tetramethylcyclopentadienyl silane (Cp'), the support is metallated via an amine elimination method[12, 13]. Additional metallation strategies, such as reaction of the ligand with $CpMCl_3$ (Royo method), are also possible[14-17]. Following metallation, the diethylamine ligands on the titanium are exchanged with chlorides, by contacting the complex with trimethylsilyl chloride. Elemental analysis showed essentially quantitative metallation of the amines by the titanium (slightly above 100%, but within experimental error). This compares to ~50% amine metallation on densely functionalized materials[7-9, 18]. The ligand exchange on the patterned material (**7**) results in nearly quantitative conversion to the chloride form. Elemental analysis shows a chloride loading of 0.72 mmoles/g for the patterned material (**8**), resulting in a chlorine to titanium ratio of 1.89 (ideal ratio = 2.0). A chloride loading of 0.95 mmoles/g was determined for the densely functionalized material (**12**), which yields a Cl:Ti ratio of 1.81 (ideal ratio = 2.0). These Cl:Ti ratios suggest the protocol developed (Scheme 3.2) allows for the titanium metal center to be supported with exchangeable ligands intact. Overall, these elemental analysis results, summarized in Table 3.1, provide evidence that the use of the novel support with isolated amines leads to a material with more uniform

sites than when traditional synthetic techniques are used. However, the potential for side reactions, especially of the titanium source with traces of residual silanols during metallation, can not be ruled out.

Table 3.1 Material Synthesis Summary

	Patterned Silica	Control 11	Control 12	Control 13 ("dense")	Control 14 ("random")
Material Description	Patterned Silica	Preformed Complex on SBA	Step-wise method using n-BuLi	Step-wise method without alkyllithiums	Step-wise method without alkyllithiums
Amine Loading (mmol/g)	0.35[a,b]	NA	1.25[a]	1.25[a]	0.46[a]
Cyclopentadienyl Loading (mmol/g)	0.35[a,b]	NA	0.84[a,b]	0.81[a,b]	0.32[a]
Ti Loading (mmol/g)	0.38[b]	0.17[b]	0.65[b]	0.53[b]	0.38[b]

a: Loading determined by TGA; b: Loading determined by Elemental Analysis

It could be theorized that the incomplete Cp-silane grafting and metallation found on the densely functionalized material is the result of steric constraints on the densely-loaded aminosilica, rather than the formation of multiple types of sites with inherently different reactivities. In attempt to probe this, a low-loading randomly functionalized aminosilica was synthesized by contacting 3-aminopropyltrimethoxysilane with SBA-15, such that 0.46 mmoles amine/g solid was supported, giving roughly the same amine loading as the patterned solid. Upon contacting the low-loading randomly functionalized aminosilica with chlorodimethyl(2,3,4,5-tetramethyl-2,4-cyclopentadien-1-yl)silane, 0.32 mmoles of silane/g solid was grafted onto the silica surface, which corresponds to 70% of the amine reacting. After metallation with tetrakis(diethylamino)titanium, elemental

analysis showed a titanium loading of 0.38 mmoles/g solid (material **14**). This corresponds to an amine metallation of 83%, which is higher than material **13** but still less than the quantitative metallation seen in **8**. However, this level of metallation is equivalent to 119% cyclopentadienyl metallation. This result suggests the formation of multiple types of metal sites on the surface, as the titanium could react with surface silanols, amines on the surface, or immobilized cyclopentadienyl functionalities. These observations may be attributed to two potential causes. First, the randomly and densely functionalized solids could indeed have amine sites with different reactivities as outlined in our previous report[1]. Or, an alternate cause for this behavior could be the steric constraints imparted by amine sites that exist on the surface in patches even at low loadings[19]. After the first few amine sites in a region react with the Cp-silane moiety, there simply may not be enough room for additional Cp-silane molecules to react with adjacent unreacted amines. Additional studies probing these two hypotheses are underway.

Nitrogen physisorption was used to characterize the silica framework throughout the synthesis. The results are summarized in Table 3.2. The surface area and average pore diameter decrease upon functionalization of the amine with the cyclopentadienyl functionality, and then decrease again upon metallation with the titanium source. As the mesoporous pore structure is still present, significant pore blockage has not occurred during functionalization. However, the decrease in average pore diameter (from 52 to 39 Å) suggests Ti-CGC inspired sites were constructed in the pores or along the pore openings.

Table 3.2. Nitrogen Physisorption Results

Sample	BET surface area (m^2/g of SiO_2)	Average pore diameter[a] (Å)
SBA-15	650	52
5	589	49
6	433	44
7	376	39

a: Determined from desorption isotherm

The materials were also characterized by ^{13}C and ^{29}Si CP-MAS NMR. Figure 3.1 shows the ^{29}Si CP-MAS NMR spectra of the patterned materials **5**, **6**, and **8**. In each spectra, the resonances for the Q^2, Q^3, Q^4 silicon resonances can be seen at –92, -100, and –107 ppm respectively [20]. The alkyl linkages to the surface can be characterized by the Si-C bond resonances. These resonances, seen at –45, -56, and –67 ppm, corresponding to the reaction of 1, 2, and 3 silylmethoxy groups with the surface silanols [21]. The peak at

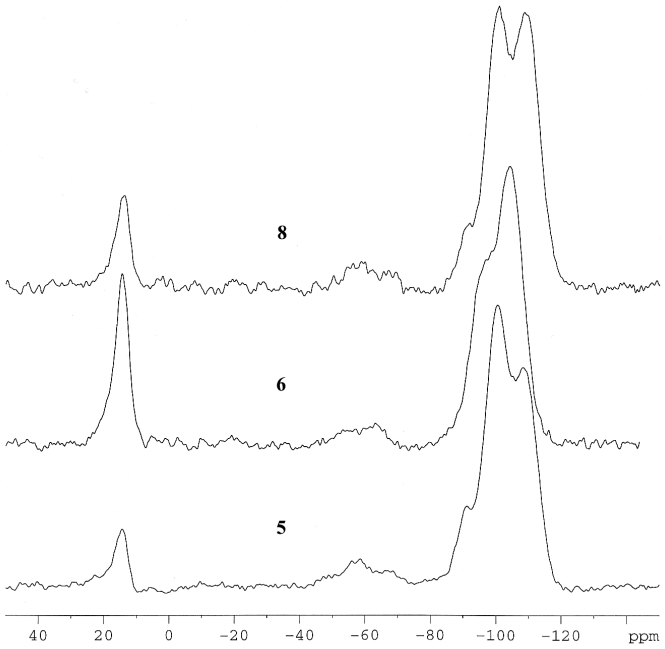

Figure 3.1 ^{29}Si CP-MAS NMR spectra of patterned aminosilica (**5**), patterned cyclopentadienyl functionalized SBA-15 (**6**) and metallated Ti CGC-inspired material (**8**).

14 ppm is associated with the Si-C bond found in the capping agent and on the cyclopentadienyl functionality. Although peak heights should not be used to make conclusions since CP-MAS NMR is not a quantitative technique, the presence of the signals discussed above suggest the formation of a covalently-immobilized surface species.

The ^{13}C NMR spectrum in Figure 3.2 shows the result of the reaction of the cyclopentadienyl functionality with the patterned aminosilica (**6**). Also illustrated is the spectrum of the metallated solid after ligand exchange (**8**). Specific band assignments are given in Table 3.3. These NMR spectra show the expected carbon-containing surface functionalities are present, although even with the use of cross-polarization techniques, the signal to noise ratio is poor. The important resonances present include the carbons in the tetramethylcyclopentadienyl functionality, which can be found at 10-14 ppm, 20-25 ppm, and 128 ppm. The signal at 67 ppm is a spinning side band. Upon metallation and

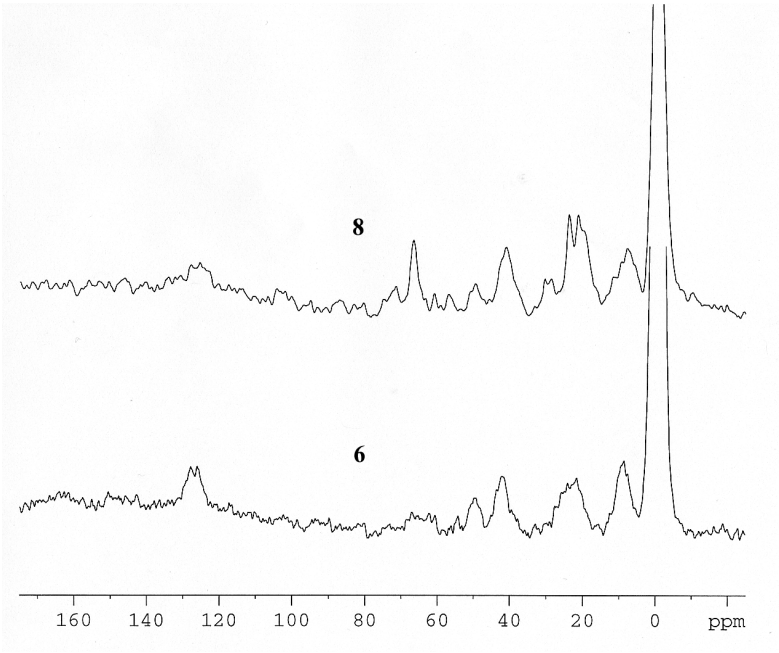

Figure 3.2 ^{13}C CP-MAS NMR spectra of patterned cyclopentadienyl functionalized SBA-15 (**6**) and metallated Ti CGC-inspired material (**8**)

ligand exchange, little change is expected in the ^{13}C NMR spectra. Therefore, complementary techniques must be used to further probe the structure of the metallated materials.

Table 3.3 ^{13}C CP-MAS NMR Assignments

Assignment	Resonance (ppm)
Capping Agent: -Si-($\mathbf{C}H_3$)$_x$	0
Propyl linker: -Si-$\mathbf{C}H_2$-CH_2 Cp' ring substituents: ($\mathbf{C}H_3$)$_4C_5$	10-14
Propyl linker: -CH_2-$\mathbf{C}H_2$-CH_2 Cp' ring substituents: ($\mathbf{C}H_3$)$_4C_5$	20-25
Propyl linker: -N-**C**H2-CH2	43
Methoxy: -O$\mathbf{C}H_3$	50
Cp' ring: (CH_3)$_4\mathbf{C}_5$	128

.

Hence, FT-Raman spectroscopy has been also used to characterize the materials. The spectrum of the patterned amino-silica (**5**) is shown in Figure 3.3. The large signals at ~2900 cm^{-1} are associated with aliphatic C-H stretches from the patterned amine and capping agent. The small peak at ~3050 cm^{-1} corresponds with aromatic C-H stretches due to a small fraction of the trityl imine remaining on the surface. Upon reaction with the cyclopentadienyl silane (material **6**), the signals corresponding to aliphatic carbon-hydrogen vibration (~2900 cm^{-1}) increase as expected. The small amount of aromatic vibrations at 3050 cm^{-1} are still apparent as well. Upon metallation (material **8**), a significant change in the spectra was not expected nor seen, as the organic groups on the surface should not change. The disappearance of some peaks (i.e. the unreacted trityl imine C-H stretches at 3050 cm^{-1}) might be attributable to the reactivity of the residual

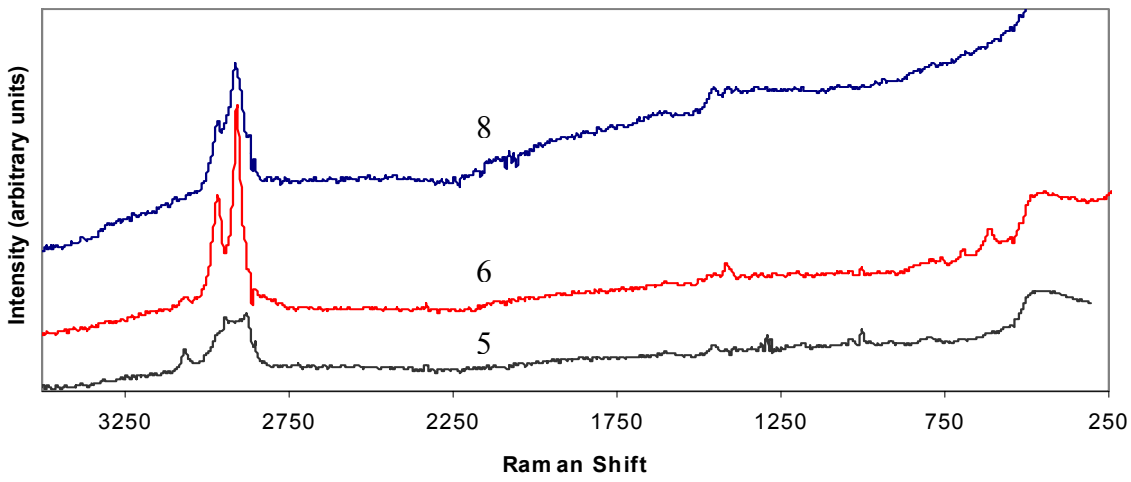

Figure 3.3 FT-Raman spectra of patterned aminosilica (**5**), patterned cyclopentadienyl functionalized SBA-15 (**6**), and metallated Ti-CGC inspired material (**8**)

trityl groups with the tetrakis(diethylamino)titanium. Alternately, the loss of these signals may be an artifact of the poorer signal to noise ratio and elevated baseline associated with sample fluorescence of the metallated material. It is noteworthy that the spectrum of the metallated species cannot always be obtained due to fluorescence resulting from the dark orange-brown color of the supported Ti-CGC complex. The combined data from the above techniques is consistent with the presence of the intended surface organic functionalities on the surface. However, as in previous works, little information has been gained concerning the bonding of the transition metal atoms [9-11, 22-24].

Characterization of the supported complexes is difficult due to the fact that traditional techniques such as NMR, FTIR, and FT-Raman rarely give useful information concerning the bonding of many transition metal centers when the metal species are present at such low concentrations. Hence, in this work, the materials were also characterized by UV-VIS spectroscopy in an attempt to elucidate the speciation of the

metal center (spectra shown in Figure 3.4). The UV-VIS spectrum for the bare SBA-15 silica has a peak absorbance at 220 nm and a smaller signal at 260 nm. The patterned aminosilica has a broader peak at 220 nm and a shoulder that starts at approximately 240 nm. After reaction of the amines with cyclopentadienyl silane, the spectrum changes further. The peak absorbance seen in material **6** at 310 nm is assigned to a π to π* transition of the cyclopentadienyl functionality [25]. Upon metallation to produce material (**8**), the characteristic UV-VIS signals change to a peak at 245 nm, likely a transition of the titanium metal center, and a ligand to metal charge transfer (LMCT) signal (from the complexed cyclopentadienyl ligand to the titanium) appearing as a shoulder at 330 nm [25].

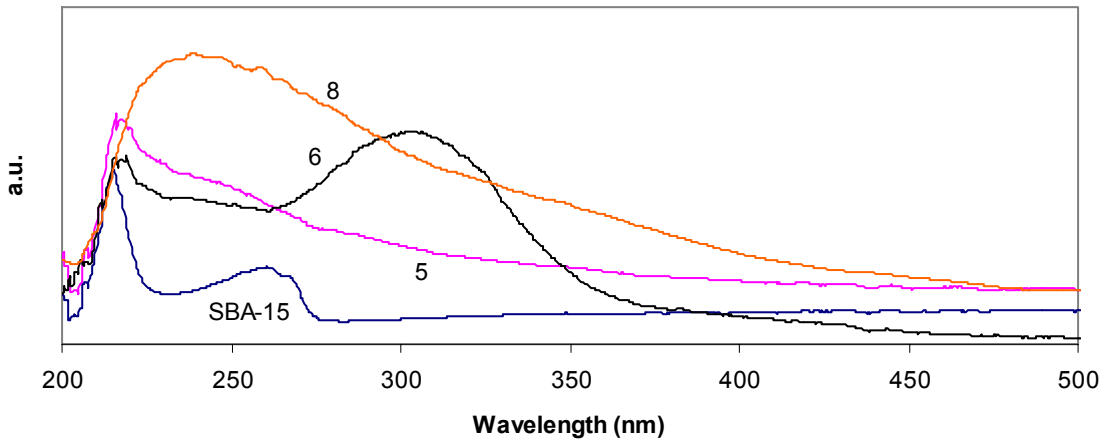

Figure 3.4 Diffuse reflectance UV-VIS spectra of bare SBA-15, patterned aminosilica (**5**), patterned cyclopentadienyl-functionalized SBA-15 (**6**), and metallated Ti CGC-inspired material (**8**)

To attempt to make more definitive assignments, spectra were obtained for several control materials. Two homogeneous CGC complexes (Scheme 3.3) were prepared and their UV-VIS spectra were obtained. The spectra of the patterned material

8 and homogeneous complexes **9** and **10** are shown in Figure 3.5. The homogeneous CGC complex (**9**) has a peak at 260 nm and a shoulder can be seen at about 335 nm.

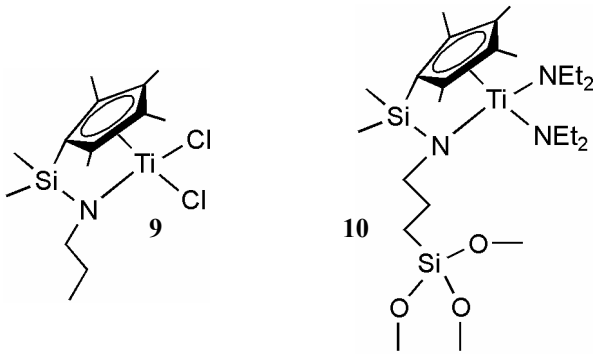

Scheme 3.3 Homogeneous CGC Analogs

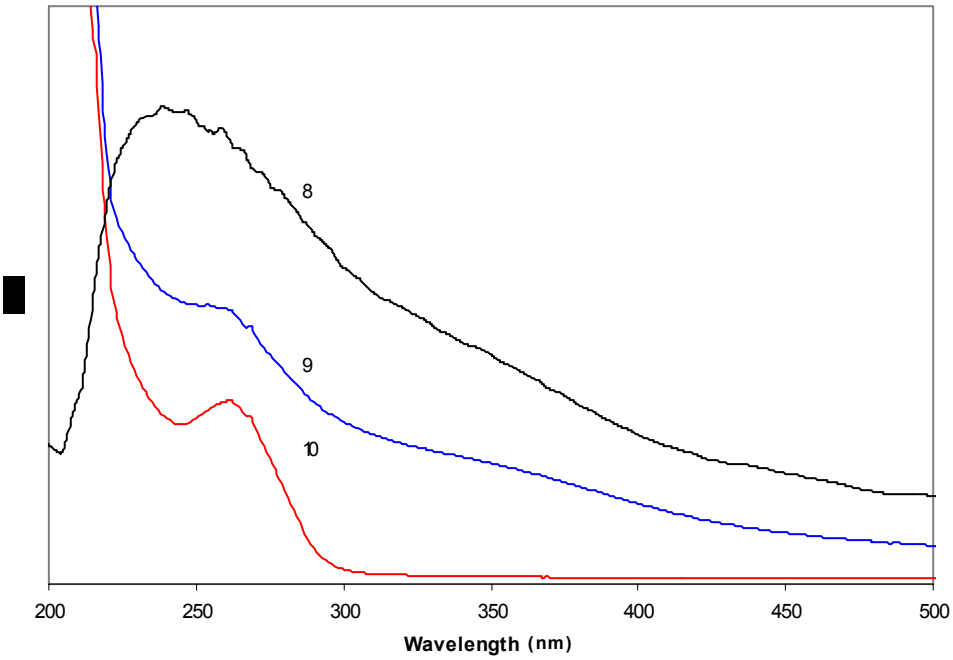

Figure 3.5 UV-VIS spectra of metallated Ti-CGC inspired material (**8**), homogeneous CGC complex (**9**), and homogeneous CGC complex (**10**)

These transitions are similar to the ones seen in material **8**. The homogeneous CGC complex (**10**) has a different spectrum than the other two materials. It has a single broad signal centered at 265 nm. In solution, the shoulder at 330 nm was not observed. The transitions at 260 nm for the complexes in the homogeneous solution can be assigned to a transition involving the metal center. The large peak near 200 nm seen in both homogeneous samples is the result of the λ_{end} of the solvent, hexanes. In the supported Ti-CGC (**8**), there is a broad signal with a maximum intensity at 245 nm. It is unclear as to the exact structure to which this transition can be assigned. The breadth of the peak could suggest it may be the amalgamation of the 220 nm signal seen in the silica support (Figure 3.4) and the transition from titanium (expected to appear around 260 nm). The homogeneous complex **9** and the patterned material **8** both contain the shoulder at 330nm, a region where the LMCT from the Cp ring to the Ti to appear. It is noteworthy that this band appears in both samples that contain Ti-Cl ligands (**8**, **9**) but it is absent in the material with Ti-amine ligands (**10**).

Although the similarity between the spectra for the homogeneous control material and the supported complexes is promising, definitive assignments can not be made until the spectra of several potential structures that could result from side-reactions during the synthesis are examined. In addition, the CGC-inspired materials made via traditional techniques need to be probed.

Figure 3.6 shows a comparison of the UV-VIS spectra of the patterned material **8** to those of several titanium CGC-inspired control materials. Solid control material **11** was made by supporting the preformed homogeneous complex on silica following Eisen's protocol [22]. Control material **12** was made following Pakkanen's method that

utilizes a step-wise grafting approach including n-butyl lithium in the treatments [9-11]. Finally, the control materials **13** (high loading) and **14** (low loading) were made using the same protocol as shown in Scheme 3.2, with the exception that a densely functionalized aminosilica support (**13**, high loading) instead of the patterned aminosilica was used. In all of the metallated materials, there is a broad signal centered around 240 nm. In control material **11**, a material that contains supported Ti-amine species, the transition seen in the homogeneous complex **9** at 330 nm is notably absent. In contrast, in materials **8** and **13**, materials that are chloride exchanged, this band is quite strong. Based on UV-VIS analysis, the patterned material **8** and all the control materials **11, 13** and **14** appear qualitatively similar to the homogeneous analogue **10**. Only the n-butyl lithium treated material, **12**, stands out as distinctly different, with virtually no intensity beyond 300 nm.

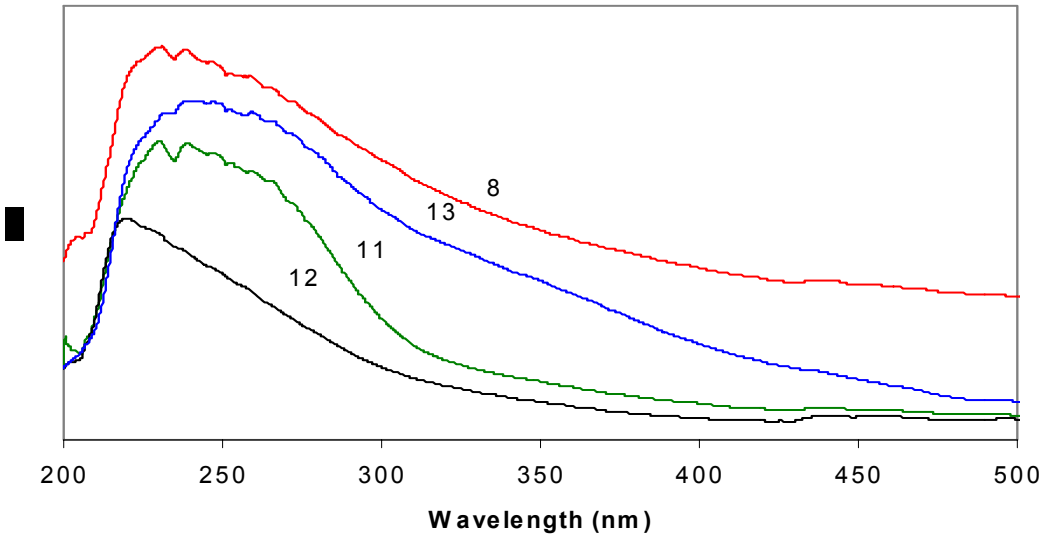

Figure 3.6 Diffuse reflectance UV-VIS spectra of metallated Ti-CGC inspired material (**8**), control material (**11**), control material (**12**), and control material (**13**)

The supported CGC-inspired complex **8** was also compared to additional titanium-containing materials. One sample was synthesized by contacting tetrakis(diethylamino)titanium with SBA-15, to give a material that should contain Ti-O-Si linkages [26], species that might be expected if the titanium source reacted with any residual silanols. The UV-Vis spectrum was taken of this sample before (contains Ti-N and Ti-O linkages) and after (contains only Ti-O linkages) calcinations in air. An additional control material was synthesized by contacting homogeneous complex **9** with bare SBA-15 and capped SBA-15.

The tetrakis(diethylamino)titanium-contacted silica control material has a peak absorption at 240 nm, similar to the transition seen in **8** (Figure 3.7). As in the supported CGC case, this broad peak is likely the result of the signal from the silica support and a transition associated with titanium. Additionally, there is a strong signal at 410 nm, possibly the result of the formation of octahedral Ti-O structures [27, 28]. There is also a shoulder present around 310 nm. After calcination in air at 100 °C, the signals at 240 nm broadens but is still present as is the peak at 410 nm (shown in Figure 3.7). However, the shoulder at 310 nm is less apparent. When the calcination was carried out at 300 °C, the UV-Vis spectrum (not shown) is identical to material that was calcined at 100 °C. Overall, the patterned CGC-inspired material appears distinctly different from this control material, especially in the region near 400 nm.

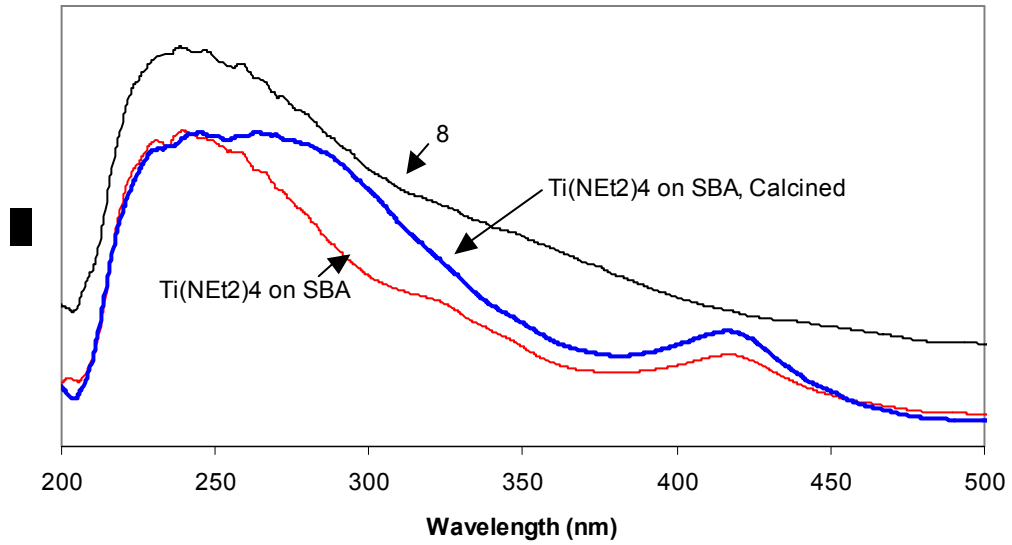

Figure 3.7 Diffuse reflectance UV-VIS spectra of metallated Ti-CGC inspired material (**8**), $Ti(NEt_2)_4$ treated SBA-15, and calcined $Ti(NEt_2)_4$

The homogeneous complex **9** was contacted with both bare and capped SBA-15 to try and produce a material with Ti-CGC species but with direct complex-silanol interactions. The spectrum of the resulting solid can be seen in Figure 3.8, along with material **8** and complex **9** immobilized on silanol-capped silica. Both materials containing complex 9 and silica have a broad peak spanning from 220 to 260 nm. In addition, a shoulder is present at around 330 nm, as seen in the spectrum of the homogeneous complex **9** in solution. Overall, it is evident that the spectra for both materials are strikingly similar to the CGC-inspired material **8**, providing evidence that the intended CGC structure may have been formed in the patterned material.

While the UV-Vis spectrum of the patterned material is consistent with the formation of a constrained geometry catalyst structure being synthesized on the surface,

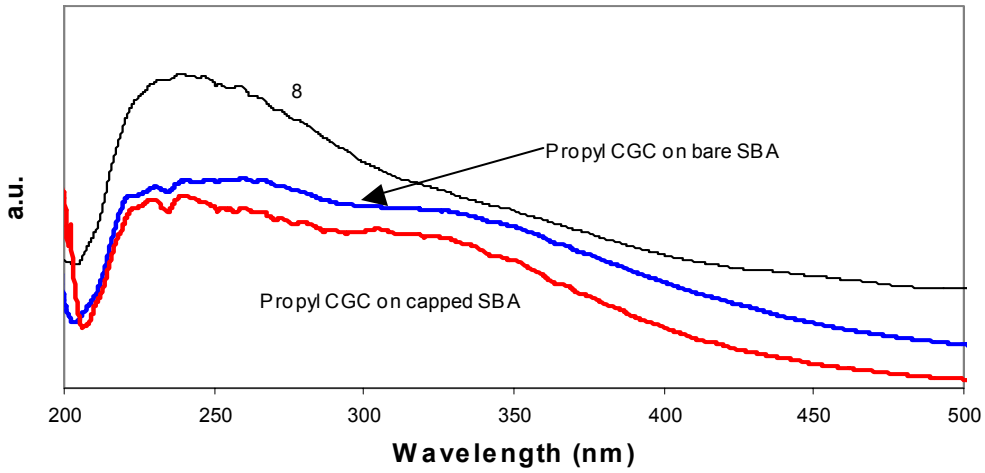

Figure 3.8 Diffuse reflectance UV-VIS spectra of metallated Ti-CGC inspired material (**8**), homogeneous control (**9**) on bare SBA, and homogeneous control (**9**) on capped SBA.

conclusive assignments of the ligand structure around the titanium based solely on the spectroscopic evidence presented above can not be made. The transitions associated with the CGC structure are also roughly comparable with many other Ti coordinations with wholly inorganic ligands, for example titanium dioxide and the material made by contacting tetrakis(diethylamino)titanium with silica followed by calcination. However, these materials show no significant catalytic activity for the polymerization of ethylene. Titanium dioxide only produced trace amounts of polymer and no polymer was formed using the tetrakis(diethylamino)titanium solid. This is in stark contrast to the CGC-inspired materials as noted below, suggesting the transitions seen are the result of CGC formation.

Through the characterization techniques discussed above, the confirmation of CGC sites cannot be explicitly proven, although the similarity between the UV-VIS spectra of **8** and the homogeneous CGC in solution **9** is consistent with the hypothesis

that immobilized CGC sites were formed. When this data is combined with the inactivity of supported titanium species with wholly inorganic ligands, it shows the active Ti species supported via the new protocol developed are very likely ligated by organic ligands. Additional characterization directly probing the metal center is underway.

3.3.2 Ethylene Polymerization

The catalytic activity of the materials was evaluated in the polymerization of ethylene. The patterned materials were again compared to the control materials described above: homogeneous analogs **9** and **10** synthesized following literature methods [22]; a solid control material **11** made by supporting the preformed homogeneous complex on silica following Eisen's protocol [22]; control material **12** made following Pakkanen's method that utilizes a step-wise grafting approach including n-butyl lithium in the treatments [9-11]; and control material **13** was made using the same protocol as shown in Scheme 3.2, with the exception that a densely functionalized aminosilica support instead of the patterned aminosilica was used. Control **14** is identical to **13** except a randomly functionalized aminosilica with a lower amine loading was used as the scaffold for the CGC. Scheme 3.4 depicts cartoons of the various supported control materials used in this study[29]. The results of ethylene polymerizations utilizing MAO as a co-catalyst are compiled in Table 3.4. The patterned catalyst was found to have an activity of 16-20 kg polymer/mol Ti-hr. In comparison to the materials made from densely-loaded aminosilica (**12, 13, 14**), the patterned material has an activity that is 4-5 times higher. However, the activity of control **11** was found to be higher than the patterned material.

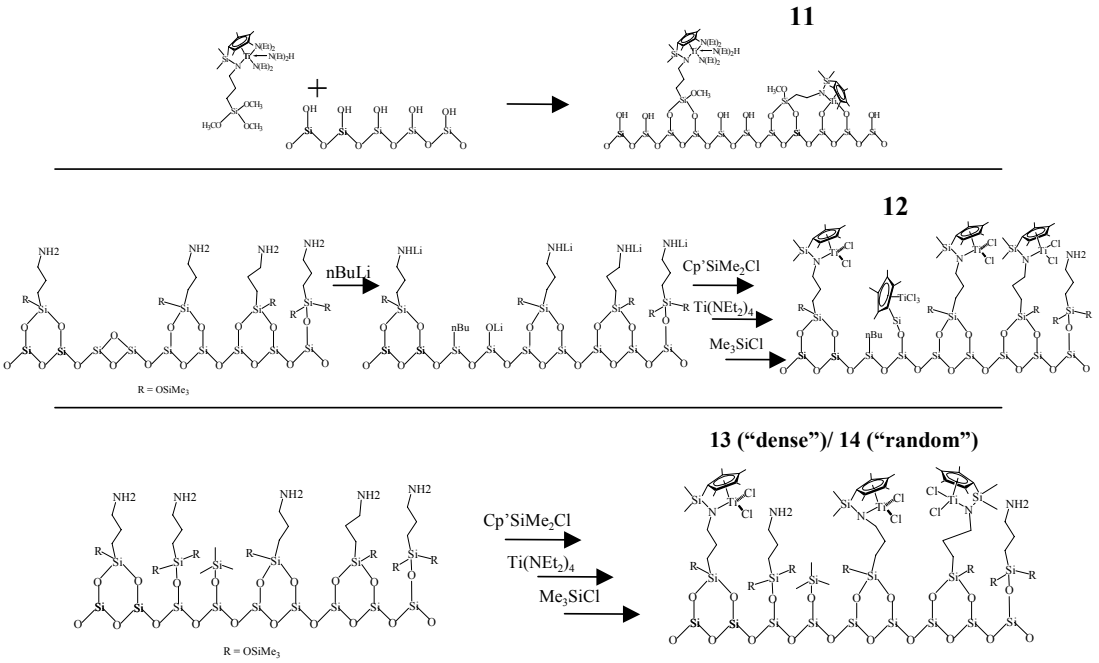

Scheme 3.4 Idealized Cartoons of Ti-CGC Control Materials

As this material is believed to produce a distribution of sites [22], including some metal-surface interactions, this result was interesting.

In considering this data, it is important to note that MAO is capable of leaching organometallic species from the silica support [30-34]. To test whether this phenomenon was affecting the precatalysts used in this work, leaching studies were undertaken. The pre-catalyst was contacted with MAO (800:1 Al:Ti) and toluene in a drybox. The resulting solution was allowed to stir for 20 minutes, then the catalyst was removed by filtration. The filtrate was then added to the reactor with an additional portion of MAO. This solution was subsequently exposed to ethylene (60 psig) using the typical polymerization protocol. If the MAO caused leaching of the organometallic complex from the surface, the filtrate should be active in ethylene polymerization. The results of these studies are depicted in Figure 3.9.

Table 3.4 Ethylene Polymerization Results using MAO as a Co-catalyst

Entry	Catalyst	Ti loading[a] (mmol/gcat)	Activation Time (min)	Total Productivity[b] (kg PE/mol Ti-hr)	MW (x10^5)	PDI
1	8 – patterned	0.38	60	15.8	5.7	2.4
2	8 – patterned	0.38	20	19.7	8.9	2.3
3	9 – control	2.83	20	11.4	---	---
4	9 – control	2.83	20	13.5	---	---
5	10 – control	1.6	20	6	---	---
6	10 – control	1.6	20	5.8	---	---
7	11 – control	0.17	20	26.5	7.8	2.3
8	12 – control	0.65	60	4.1	---	---
9	12 – control	0.65	20	4.2	---	---
10	13 – control	0.53	60	4.5	---	---
11	13 – control	0.53	20	5.7	4.1	4.6
12	13 – control	0.53	20	5.9	2.5	5.1
13	14 – control	0.38	20	5.4	---	---

a) Titanium loadings determined by elemental analysis; b) polymerization conditions: T = 25 ºC; co-catalyst: MAO; Al/Ti = 800; solvent: toulene; ethylene pressure: 60 psi; reaction time: 10 min.

It is important to note that it is difficult to accurately determine the amount of *active* titanium which leached from the solid. As the leached complexes can be much more active than the supported species, a small fraction of the metal sites may leach (and an even smaller fraction may actually be active) yet they may provide almost all of the activity observed using the solid catalyst. To determine the amount of leaching from the solid, a nominal activity was calculated based on the total amount of titanium in the solid contacted with the MAO and toluene. By calculating an activity based on the total

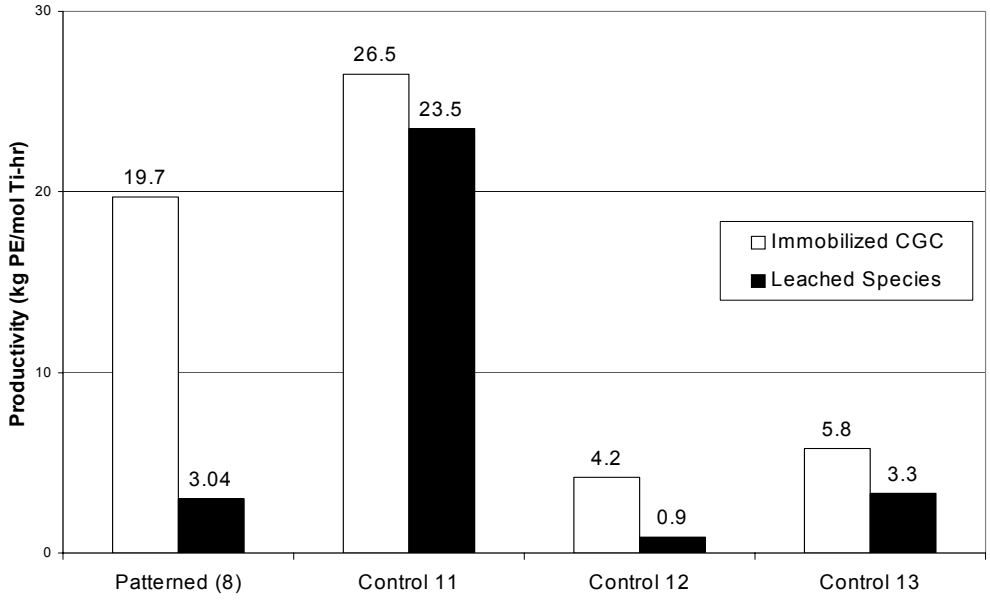

Figure 3.9 Comparison of the polyethylene productivity of the supported catalysts with the leached filtrate using methylaluminoxane as a co-catalyst.

titanium in a given sample, the percentage of supported activity for a given solid resulting from leaching can be estimated. The results of these experiments should be viewed as a lower bound on the activity of the leached species. The activated species are extremely sensitive, and although all manipulations are performed in a dry box, it is possible there is deactivation through handling.

The patterned catalyst shows 20-30% of its activity is the result of leached species. The control catalyst made via a step-wise approach also shows approximately 20-30% of its activity resulting from leached species. The other control materials showed a greater percentage of their activity could be attributed to leaching. Approximately 50% of the activity of the densely functionalized control (**13**) may be attributed to leached species. Almost 90% of the activity of the catalyst made via pre-formed complex addition (**11**) is attributed to leaching. Thus, this material is more active than the

patterned material because highly active, leached Ti species are produced. These results show the significant impact leaching can have on this type of polymerization system. The fact that at least 20% of the activity of the patterned catalyst can be attributed to leached metal complex makes it difficult to make conclusions as to the effect of the patterned scaffold on a supported CGC. Thus, molecular level insight into the supported Ti-CGC-inspired catalysts will likely not be achieved when using MAO as the co-catalyst.

It would be preferable to have a system in which the leaching was negligible or non-existent. In recent years, it has been shown that an effective class of co-catalysts for metallocenes/constrained geometry catalysts are borane/alkylaluminum systems [35, 36]. In borane-activated polymerizations, the supported precatalyst is contacted with a molecular borane (i.e. tris[pentafluorylphenyl]borane) and a trialkylaluminum (trimethylaluminum or triisobutylaluminum). An advantage of these types of systems is that the combination of molecular species is more well-defined than the oligomeric MAO activator [37]. Leaching experiments were carried out in a similar manner to those described above. The solid pre-catalysts were contacted with toluene and trimethylaluminum or triisobutylaluminum in the dry box. After allowing the solution to stir for 30 minutes, the solid was removed by filtration. The filtrate was then added to the reactor with an aliquot of MAO. This mixture was then exposed to ethylene (60 psig) using the typical polymerization protocol. There was no polymer formed from the filtrate, suggesting that the alkyaluminums do not leach active catalytic sites from the silica. Studies were also undertaken to determine whether the borane/alkylaluminum systems leached inactive titanium species. After contacting the patterned catalyst with trimethylaluminum and

toluene as in the leaching studies, the filtrate and solid was analyzed for titanium. By elemental analysis, none of the supported titanium leached via exposure to an alkylaluminum (less 5 parts per million). Additionally, the patterned catalyst was contacted with trimethylaluminum and tris[pentafluorylphenyl]borane, the solid was removed by filtration. The titanium content of the filtrate was determined by elemental analysis, which showed no detectable titanium present. This suggests using the borane/trialkylaluminum co-catalyst systems will allow for the productivity of the immobilized species to be more accurately evaluated.

Figure 3.10 depicts the results of the polymerizations utilizing TMA and TIBA in conjunction with tris[pentafluorylphenyl]borane as an activator. The same data are tabulated in Table 3.5 along with physical properties of the polymers produced. Given that this co-catalyst system does not cause detectable leaching of active species, catalytic results with this system may be attributable to immobilized catalysts.

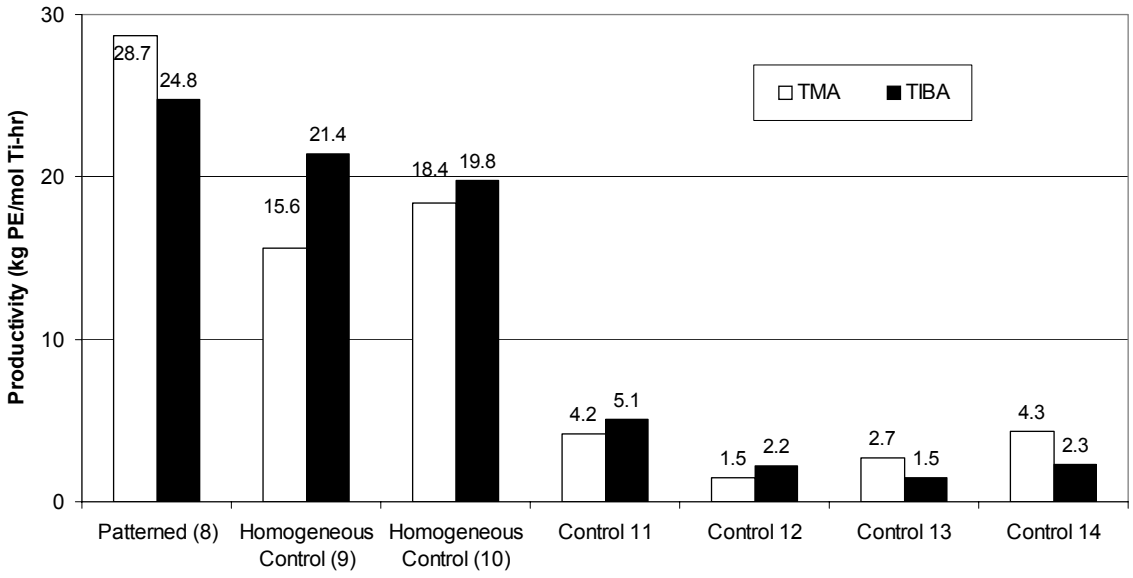

Figure 3.10 Polyethylene productivity of the precatalysts using tris(pentafluorophenyl)-borane and trimethylaluminum or triethylaluminum as a co-catalyst.

Table 3.5 Ethylene Polymerization Results using Borane/Alkyl Aluminum Co-catalysts

Entry	Catalyst	Ti loading[a] (mmol/gcat)	Alkyl Aluminum	Productivity[d] (kg PE/mol Ti-hr)	Tm (°C)	Mw (polymer)	PDI
1	8 - patterned	0.38	TMA[b]	28.7	134.1	660,000	3.1
2	8 - patterned	0.38	TIBA[c]	24.8	133.8	1,000,000	1.9
3	9 - control	2.83	TMA	15.6			
4	9 - control	2.83	TIBA	21.4			
5	10 - control	1.6	TMA	18.4	133.9		
6	10- control	1.6	TIBA	19.8	132.8	470,000	2.8
7	11 – control	0.17	TMA	4.2	131.5	ND	ND
8	11 – control	0.17	TIBA	5.1	132.6	620,000	2.5
9	12 - control	0.65	TMA	1.5	131.9		
10	12 - control	0.65	TIBA	2.2	133.2		
11	13- control	0.53	TMA	2.7	133.5	500,000	broad
12	13- control	0.53	TIBA	1.5	133.1	1,000,000	2
13	14 – control	0.38	TMA	4.3			
14	14 - control	0.38	TIBA	2.3			

a) Titanium loadings determined by elemental analysis; b) TMA = trimethylaluminum; c) TIBA = triisobutylaluminum; d) polymerization conditions: T = 25 ºC; co-catalyst: tris(pentafluorophenyl)borane; Al/Ti = 400; solvent: toulene; ethylene pressure: 60 psi; reaction time: 10 min;

Using the borane/trialkylaluminum systems, the patterned system was observed to be significantly more active than the control materials, including the two homogeneous controls **9** and **10**. This mirrors the results seen in the MAO study. The results also give insight into the unexpectedly high activity of **11** using MAO as co-catalyst – most of this activity is attributable to leached species. As the alkylaluminums do not leach the metal complex from the surface, the activity of **11** is greatly decreased compared to the MAO polymerizations. In fact, the activity of the patterned material appears to be slightly enhanced when using a borane co-catalyst. Indeed, there is ample precedence in the literature for activities to be significantly influenced by the nature of the co-catalyst [38, 39].

The combination of characterization and polymerization studies show that using a patterned aminosilica as a scaffold for the preparation of a CGC-inspired complex allows for a material which is significantly more active than catalysts assembled on densely

functionalized materials. The patterned silica allows for sites which may be uniform and isolated to be synthesized, although the exact mechanism for the increased reactivity is not yet certain. One possible explanation is the patterning protocol produces a metal center that cannot interact with free amines on the surface, as the data suggests essentially all of the amines are functionalized, in contrast to the densely and randomly functionalized materials (**12-14**). To elucidate the impact of the amines, the catalytic productivity of the materials with free amines in solution was determined. The catalysts were activated as discussed above, using both MAO and borane/alkylaluminum systems. After activation of the catalyst, propyl amine (200:1 N:Ti) was added to the mixture, which was then exposed to ethylene as previously described. The results are summarized in Table 3.6. In comparison to the catalytic results shown in Tables 3.4 and 3.5, adding free amine to the polymerization caused a significant decrease in the productivity of the catalysts. As the free amines can ligate to the metal center, it is possible that the open site on the titanium necessary for monomer coordination is filled by the propyl amine. While

Table 3.6 Polymerizations in the Presence of Free Amine

Entry	Catalyst	Ti loading[a] (mmol/gcat)	Cocatalyst	Amine Equivalents	Productivity[e] (kg PE/mol Ti-hr)
1	8 - patterned	0.38	Borane[b]/TMA[c]	200	6.3
2	8 - patterned	0.38	Borane[b]/TMA[d]	200	6.9
3	8 – patterned	0.38	MAO	200	5.1
4	9 – control	2.83	Borane[b]/TMA[c]	200	0.5
5	9 - control	2.83	Borane[b]/TMA[d]	200	Trace
6	9 - control	2.83	MAO	200	Trace
7	13 - control	0.53	Borane[b]/TMA[c]	200	1.0
8	13 - control	0.53	Borane[b]/TMA[d]	200	Trace
9	13 - control	0.53	MAO	200	0.7
7	14 - control	0.38	Borane[b]/TMA[c]	200	1.6
8	14 - control	0.38	Borane[b]/TMA[d]	200	2.4
9	14 - control	0.38	MAO	200	1.1

a) Titanium loadings determined by elemental analysis; b) Borane = tris(pentafluorophenyl)borane; c) TMA = trimethylaluminum; d) TIBA = triisobutylaluminum; e) polymerization conditions: T = 25 ºC; solvent: toulene; ethylene pressure: 60 psi; reaction time: 10 min

the presence of the co-catalyst in the polymerization can continue to create the necessary active species, the amine is shown to reduce the efficiency of this process. These results may suggest an explanation for the decreased activity of the densely functionalized materials compared to the patterned catalysts. It is possible the supported metal centers interact with amines in close proximity on the surface, forming a less active catalytic site. Indeed, in another work, we have recently shown that complexes that are formed through interaction of Zr with Cp and amine groups that are not directly linked are substantially less active than catalysts that have the true CGC structure[17]. However, it is highly unlikely that this can completely explain the decreased rates over the non-patterned catalysts. It is noteworthy that 200 equivalents of added amine reduced the activity of **8** by 80%. However, this reduced activity was still 50-150% higher than the densely-loaded material in the absence of added amine. As the dense material has roughly 0.5 equivalents of extra surface amines (compared 200x excess in the homogeneous case described above) and the amines are not as mobile as the homogeneous amines, it is clear that the additional amine can not account for all or even most of the observed activity difference.

It is noteworthy that the patterned material **8** is found to be unique in two aspects – its metallation efficiency (~1 Ti:N) and its catalytic productivity. This supports the hypothesis that preparation of accessible, potentially more uniform surface species is the likely cause of the observed elevated productivity (in lieu of the preparation of different, more active species on the patterned aminosilica[40]). The isolation could improve polymerization activity by allowing for more efficient and complete activation of the metal center. It could also allow for faster diffusion of the monomer to the reactive

center. At this point, it is difficult to determine whether the spatial patterning, removal of surface silanols through capping, or some combination of the two make the patterned precatalyst a more active species than the control materials. Work is currently underway to help shed light on this issue.

It should be noted that there are limitations associated with the polymerization reactor used in the work reported here. The activity was determined by collecting the polymer produced in the reactor and averaging this productivity over the time of monomer exposure. Through this method, it is impossible to determine the initial activity, deactivation rates, or steady-state productivity of the catalysts. It is desirable to be able to monitor the activity of the catalyst throughout the duration of the polymerization. This will allow for better conclusions to be drawn regarding the performance of the patterned catalyst versus the control materials. Experiments along these lines are an area for future studies.

3.4 Summary

An immobilized Ti constrained-geometry-inspired catalyst was prepared using a well-defined, site-isolated aminosilica. In using this patterned aminosilica, the synthesis of well-defined, single-sited immobilized Ti-CGC species was desired. The functionalization of the patterned silica proceeded at practically quantitative conversion, unlike when traditionally-prepared aminosilica materials were used as scaffolds. The synthesis of the supported complexes was evaluated at each stage by multiple techniques. The compilation of data is consistent with the formation of the desired species on the silica surface, although definitive proof of sites with the CGC structure could not be

obtained. While UV-Vis spectroscopy provided evidence that the immobilized metallated species could have the CGC structure, conclusive assignment of the titanium bonding could not be made due to similarities of the spectra of the CGC-inspired materials and the control materials. Indeed, it appears that UV-Vis spectroscopy, while helpful, may not be the best probe for elucidating the titanium bonding in these systems.

The ethylene polymerization productivity of the patterned catalyst was compared to control materials made by literature protocols. Using MAO as a co-catalyst, the patterned material was significantly more productive than most of the control materials. However, these results are skewed by the leaching phenomenon caused by interaction of the MAO with the supported materials. As such, this yields an ambiguous system, making analysis of the immobilized species difficult. To truly compare the supported materials, a borane/alkylaluminum co-catalyst system was used, which did not cause detectable leaching in the catalysts studied. Using tris(pentafluorophenyl)borane, along with either trimethylaluminum or triisobutylaluminum, it was found the patterned materials have a productivity of 5-10 times that of any solid supported control material evaluated here.

These polymerization results, when combined with the synthesis and characterization data, suggest the patterned aminosilica scaffold yields a polymerization catalyst which behaves as if its sites are more accessible and uniform than those resulting from literature protocols. This relatively well-defined system is a good candidate for future structural studies.

3.5 References

1. McKittrick, M. W.; Jones, C. W., *Chem. Mater.* **2003,** *15*, 1132-1139.

2. McKittrick, M. W.; Jones, C. W., *J. Am. Chem. Soc.* **2004,** *126*, 3052.

3. The complexes are referred to as CGCs here, although there is no evidence that the surface complexes prepared in previous works on immobilized CGCs actually have the CGC structure. Although some evidence is presented that CGCs are in fact formed in this work, a better term would be "CGC-Inspired" complexes as described in the title of this chapter.

4. Pangborn, A. B.; Giardello, M. A.; Grubbs, R. H.; Rosen, R. K.; Timmers, F. J., *Organometallics* **1996,** *15*, 1518-1520.

5. Zhao, D. Y.; Feng, J. L.; Huo, Q. S.; Melosh, N.; Fredrickson, G. H.; Chmelka, B. F.; Stucky, G. D., *Science* **1998,** *279*, 548-552.

6. Zhao, D. Y.; Huo, Q. S.; Feng, J. L.; Chmelka, B. F.; Stucky, G. D., *J. Am. Chem. Soc.* **1998,** *120*, 6024-6036.

7. Juvaste, H.; Iiskola, E. I.; Pakkanen, T. T., *J. Organomet. Chem.* **1999,** *587*, 38-45.

8. Juvaste, H.; Iiskola, E. I.; Pakkanen, T. T., *J. Mol. Catal. A* **1999,** *150*, 1-9.

9. Juvaste, H.; Pakkanen, T. T.; Iiskola, E. I., *Organometallics* **2000,** *19*, 4834-4839.

10. Juvaste, H.; Pakkanen, T. T.; Iiskola, E. I., *Organometallics* **2000,** *19*, 1729-1733.

11. Juvaste, H.; Pakkanen, T. T.; Iiskola, E. I., *J. Organomet. Chem.* **2000,** *606*, 169-175.

12. Diamond, G. M.; Jordan, R. F.; Petersen, J. L., *J. Am. Chem. Soc.* **1996,** *118*, 8024-8033.

13. Carpenetti, D. W.; Kloppenburg, L.; Kupec, J. T.; Petersen, J. L., *Organometallics* **1996,** *15*, 1572-1581.

14. Kasi, R. M.; Coughlin, E. B., *Organometallics* **2003,** *22*, 1534-1539.

15. Ciruelos, S.; Cuenca, T.; Gomez, R.; Gomez Sal, P.; Manzanero, A.; Royo, P., *Organometallics* **1996,** *15*, 5577-5585.

16. Royo, B.; Royo, P.; Cadenas, L. M., *J. Organomet. Chem.* **1998,** *551*, 293-297.

17. Yu, K.; McKittrick, M. W.; Jones, C. W., *Organometallics* **2004,** *23*, 4089-4096.

18. Iiskola, E. I.; Timonen, S.; Pakkanen, T. T.; Harkki, O.; Lehmus, P.; Seppala, J. V., *Macromolecules* **1997,** *30*, 2853-2859.

19. Yoshitake, H.; Yokoi, T.; Tatsumi, T., *Chem. Mater.* **2002,** *14*, 4603-4610.

20. Engelhardt, G.; Michel, D., *High Resolution Solid-State NMR of Silicates and Zeolites*. ed.; John Wiley and Sons: New York, 1988.

21. Sindorf, D. W.; Maciel, G. E., *J. Am. Chem. Soc.* **1983,** *105*, 3767-3776.

22. Galan-Fereres, M.; Koch, T.; Hey-Hawkins, E.; Eisen, M. S., *J. Organomet. Chem.* **1999,** *580*, 145-155.

23. Timonen, S.; Pakkanen, T. T.; Iiskola, E. I., *J. Organomet. Chem.* **1999,** *582*, 273-278.

24. Timonen, S.; Pakkanen, T. T.; Iiskola, E. I., *J. Mol. Catal. A* **1999,** *148*, 235-244.

25. Calleja, G.; van Grieken, R.; Garcia, R.; Melero, J. A.; Iglesias, J., *J. Mol. Catal. A* **2002,** *182*, 215-225.

26. Anwander, R.; Gorlitzer, H. W.; Gerstberger, G.; Palm, C.; Runte, O.; Spiegler, M., *J. Chem. Soc. Dalton* **1999**, 3611-3615.

27. Capel-Sanchez, M. C.; Campos-Martin, J. M.; Fierro, J. L. G., *J. Catal.* **2003,** *217*, 195-202.

28. Reddy, E. P.; Davydov, L.; Smirniotis, P. G., *J. Phys. Chem. B* **2002,** *106*, 3394-3401.

29. The cartoons depict hypothesized surface structures for 11-14. There is no direct evidence that these specific titanium sites are formed - they are derived from chemical intuition.

30. Tian, J.; Wang, S. T.; Feng, Y. D.; Li, J. M.; Collins, S., *J. Mol. Catal. A* **1999,** *144*, 137-150.

31. dos Santos, J. H. Z.; Ban, H. T.; Teranishi, T.; Uozumi, T.; Sano, T.; Soga, K., *J. Mol. Catal. A* **2000,** *158*, 541-557.

32. Lee, B. Y.; Oh, J. S., *Macromolecules* **2000,** *33*, 3194-3195.

33. Uusitalo, A. M.; Pakkanen, T. T.; Iskola, E. I., *J. Mol. Catal. A* **2002,** *177*, 179-194.

34. Cheng, X. L., O.W.; Deck, P.A., *J. Mol. Catal. A* **2004,** *212*, 121-126.

35. Yang, X. M.; Stern, C. L.; Marks, T. J., *J. Am. Chem. Soc.* **1994,** *116*, 10015-10031.

36. Ewen, J. A. E., M.J. 0,427,697, 1991.

37. Chen, E. Y. X.; Marks, T. J., *Chem. Rev.* **2000,** *100*, 1391-1434.

38. Chen, Y. X.; Stern, C. L.; Yang, S. T.; Marks, T. J., *J. Am. Chem. Soc.* **1996,** *118*, 12451-12452.

39. Mohammed, M.; Nele, M.; Al-Humydi, A.; Xin, S. X.; Stapleton, R. A.; Collins, S., *J. Am. Chem. Soc.* **2003,** *125*, 7930-7941.

40. Utilizing the patterned aminosilica support in conjunction with a different metallation strategy, the evidence supports the formation of different, more active transition metal species on the silica surface

CHAPTER 4

COMPARISON OF METALLATION METHODS FOR SYNTHESIS OF IMMOBILIZED CGC COMPLEXES[†]

4.1 Introduction

In recent years, constrained geometry catalysts (CGC) have emerged as an important class of organometallic complexes[1]. Used mainly as olefin polymerization catalysts, these homogeneous species offer unique advantages due to the environment around the metal center. The open nature of the reactive center allows for the production of very high molecular polymers, as well as long-chain and short-chain branched polymers.

A common synthetic route for the preparation of homogeneous metallocenes or CGCs utilizes an alkyllithium reagent to deprotonate the cyclopentadienyl ring. This is proceeded by metallation with the metal tetrachloride salt. However, as previously discussed, with silica-supported systems this methodology can result in side reactions with the surface. For example, metal chlorides can react directly with the surface instead of the Cp ring, leading to the formation of multiple types of sites. The alkyllithium reagent can also react with the silica surface by opening siloxane bridges, again resulting in the possible formation of a multi-sited material[2]. Therefore alkyllithium reagents must be avoided where a single type of site is desired.

In the synthesis of homogeneous CGCs, there are two additional major methods of metallation which have been shown to be more amenable for immobilization protocols. The amine elimination route was developed by Jordan and coworkers for making Group IV metallocenes, then applied to the synthesis of CGCs[3, 4]. In this case, for CGCs,

[†] This work has been submitted to J. Molecular Catalysis: A (2005).

tetrakis(diethylamino)titanium is reacted with a cyclopentadienyl functionalized amine. Two of the amine ligands are replaced in the titanium coordination environment, being substituted for ligation to the cyclopentadienyl ligand and the tethered amine. Another major method was developed by Royo and coworkers[5]. This method entails the reaction of a piano stool type complex with an amine to form the CGC. This metallation schemes requires both the metal and silyl chloride to react with a single amine.

Both amine elimination and the Royo method have been used in the synthesis of supported catalysts where the CGC structure was targeted. For example, Pakkanen and co-workers reacted a cyclopentadienyl ligand on an amine-functionalized silica surface then metallated the surface with a variety of Group IV tetrakis(dialkylamino) complexes[6-10]. Coughlin and co-workers have synthesized supported CGC-type complexes using the Royo method on amine functionalized polystyrene[11].

We have recently reported a patterning protocol that allows for the preparation of a well-defined amine-functionalized silica (Scheme 4.1), with amine sites which behave as if they are isolated and uniform[12]. Using this patterned aminosilica as a scaffold, protocols to synthesize supported constrained-geometry-inspired catalysts on the surface were subsequently developed. We previously reported the synthesis of a supported titanium CGC-inspired complex made via an amine elimination route, which is shown in Scheme 4.2[13, 14]. Additionally, the synthesis of a silica supported zirconium CGC-inspired complex via the Royo method, as shown in Scheme 4.3, was also reported[15].

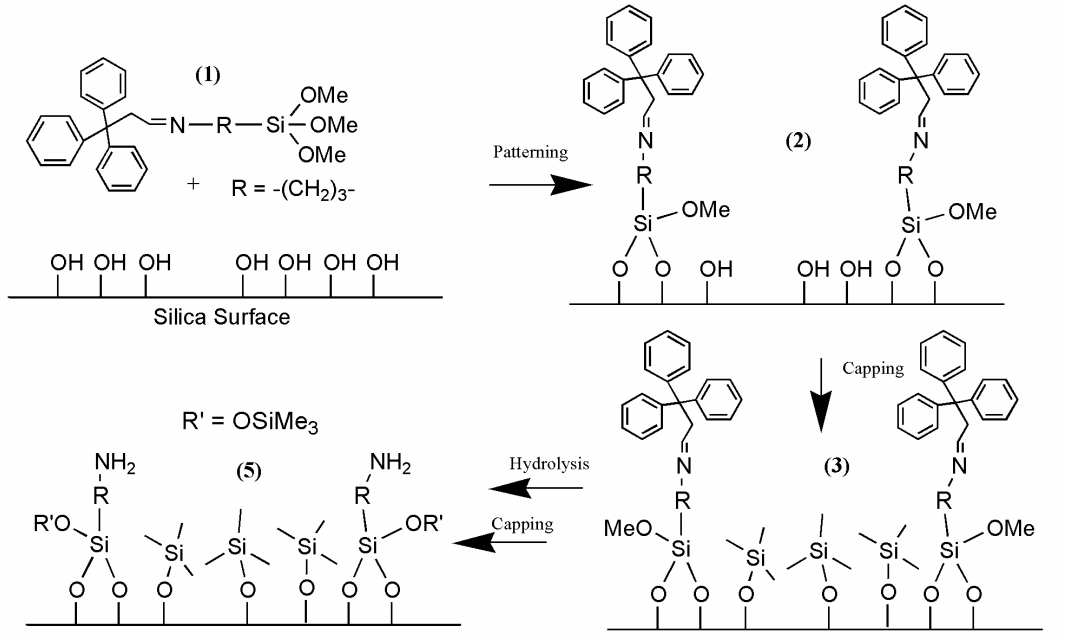

Scheme 4.1 . Patterned Aminosilica Synthesis

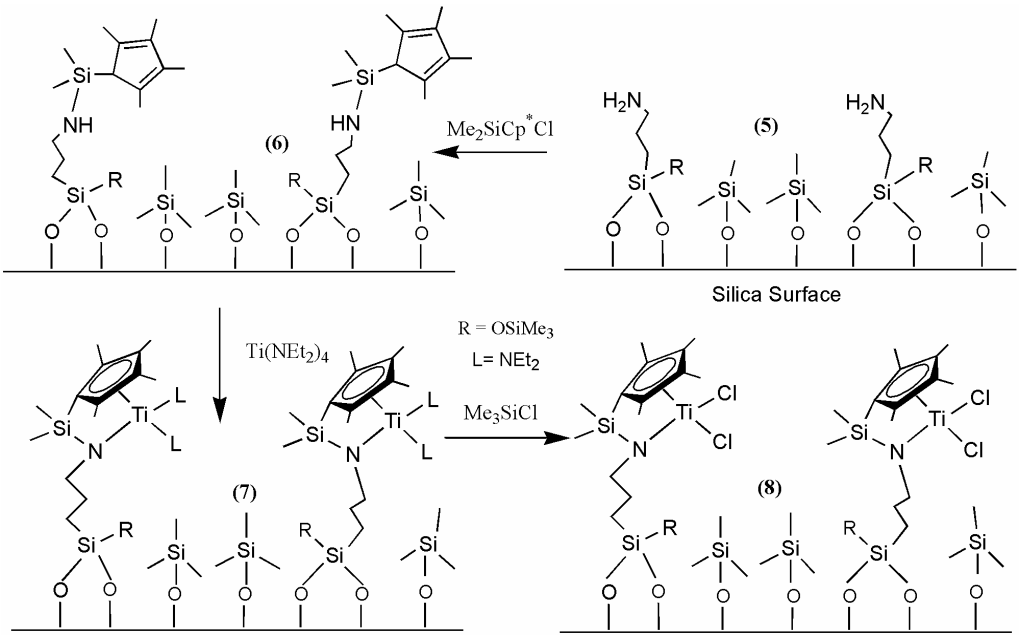

Scheme 4.2 Ti-CGC Synthetic Protocol via Amine Elimination Route

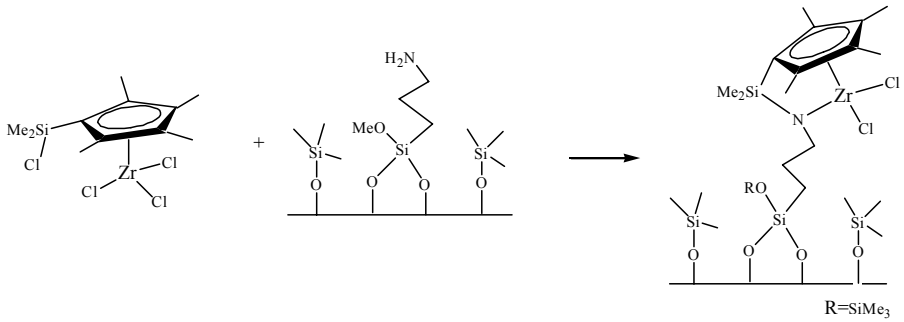

Scheme 4.3 Zr-CGC Synthetic Protocol via Royo method

As shown in the literature, these metallation methods have been used to synthesize supported CGC type complexes which are active for the polymerization of ethylene and other olefins[6-11, 13-15]. However, it is of interest to determine the impact of the metallation method on the catalyst performance and resulting polymer properties, as there are no reports that directly compare catalysts with similar intended structures prepared by both the Jordan and Royo methods. There are several

difficulties in truly comparing the efficiency of the metallation route in making an active polymerization catalyst. Using the popular, and easy to prepare, synthesized densely functionalized aminosilicas can cause complications. For example, as reported previously, there is evidence of the formation of "bridging complexes", as shown in Scheme 4.4[15]. As the amines are in close proximity to one another, there is the possibility of the piano stool complex reacting with more than one immobilized amine, which leads to the formation of a multi-sited material, with each site having different catalytic productivities. The sites formed as shown in Scheme 4.3 are significantly more active in ethylene polymerization than the sites shown in Scheme 4.4[15]. By using the

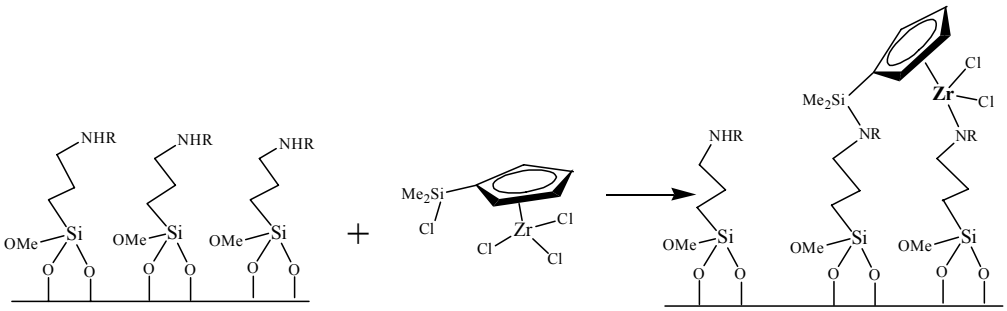

Scheme 4.4 Bridged Piano-stool Complexes

patterned aminosilica scaffold as a support, this bridging phenomenon appears to be significantly reduced, or possibly eliminated. In both metallation schemes, the use of densely functionalized aminosilica as a scaffold can lead to a multi-sited material. Metal centers can interact with other catalyst sites or unfunctionalized amines. As the aminosilica produced by the patterning protocol allows for the synthesis of well-defined, isolated amine sites on the silica surface, this provides a unique scaffold to probes the effect of metallation protocol on catalyst synthesis, performance, and resulting polymer properties.

4.2 Experimental

General Considerations. The following chemicals were commercially available and used as received: 3,3,3-Triphenylpropionic acid (Acros), 1.0 M $LiAlH_4$ in tetrahydrofuran (THF) (Aldrich), pyridinium dichromate (Acros), 2,6 di-tert-butylpyridine (Acros), dichlorodimethylsilane (Acros), TEOS (Aldrich), 3-aminopropyltrimethoxysilane (Aldrich), hexamethyldisilazane (Aldrich), tetrakis(diethylamino)titanium (Aldrich),

trimethyl silyl chloride (Aldrich), trimethylaluminum (Aldrich), triisobutylaluminum (Aldrich), methylaluminoxane (Aldrich, 10 wt% in toluene), and n-butyllithium in hexanes (Aldrich). Tetramethyl-cyclopentadiene (Aldrich) was distilled prior to use. Anhydrous toluene (Acros) was distilled over sodium metal prior to use. Tris(pentafluorophenyl)borane (Aldrich) was purified via sublimation. Anhydrous methanol (Acros) was further dried over 4-Å molecular sieves prior to use. Anhydrous ether, anhydrous THF, anhydrous dichloromethane, and anhydrous hexanes were obtained from a packed bed solvent purification system utilizing columns of copper oxide catalyst and alumina (ether, hexanes) or dual alumina columns (tetrahydrofuran, dichloromethane)[16]. All air- and moisture-sensitive compounds were manipulated using standard vacuum line, Schlenk, or cannula techniques under dry, deoxygenated argon or in a drybox under a deoxygenated nitrogen atmosphere. Ethylene was passed over a metallic catalyst (Matheson 641-01 cartridge) to remove oxygen and water, before being fed to the reactor.

Catalyst Synthesis: Materials **1-8** were synthesized by literature procedures[12-14]. Complex **9** was synthesized via literature procedure[11].

Immobilization via Royo Method. The immobilization protocol was adapted from literature procedure[15]. Complex 9 (50mg, 0.14mmol) and the proton scavenger, 2,6-di-tert-butyl-pyridine (200mg, 1.05mmol) were added into a toluene (40 ml) suspension of patterned amine-functionalized SBA-15 (300mg). The reaction mixture was stirred at room temperature for 24 h, at which point it was filtered in a dry box and washed

extensively with dichloromethane, hexane, and toluene. The resulting silica supported catalyst was dried under high vacuum for several hours. A similar procedure was used for immobilizing the complex on densely functionalized aminosilica.

Synthesis of SBA-15. SBA-15 with approximately 100 Å diameter pores was synthesized via literature methods[17, 18]. Calcination of the material was done in air using the following temperature program: (1) increasing the temperature (1.2 °C/min) to 200 °C, (2) heating at 200 °C for 1 h, (3) increasing at 1.2 °C/min to 550 °C, and (4) holding at 550 °C for 6 h. Prior to use, the SBA-15 was dried under vacuum at 200 °C for 3 h and stored in a drybox.

Characterization. Diffuse reflectance ultraviolet-visible (UV-VIS) spectroscopy was performed on solid materials in a drybox with an Ocean Optics USB2000 Fiber Optic Spectrometer using a PTFE diffuse reflectance standard. Thermogravimetic analysis (TGA) and differential scanning calorimetry was performed on a Netzsch STA409. TGA samples were heated under air from 30 to 1000° C at a rate of 5 °C/min. The organic loading was measured by determining the weight loss from 200 to 650 °C. DSC samples to determine polymer melting points were heated under nitrogen with a heating cycle from 30 to 160 ºC at 2º/min, cooling to 100 ºC at 2º/min, then repeating the cycle. The melting point was taken from the second heating cycle. Elemental Analysis was performed by Desert Analytics.

Ethylene Polymerizations

MAO Co-catalyst: The immobilized precatalyst was added to a pressure glass reactor with toluene and methyl alumoxane (800 Al:1 Ti) in a drybox. The solution was stirred for 20 minutes to allow for sufficient activation of the catalyst. The reactor was then sealed and removed from the glovebox, placed in a 25 °C waterbath, and subsequently connected to an ethylene source at 60 psi. The ethylene was delivered for a prescribed amount of time and the polymerization was terminated by releasing the ethylene pressure and adding acidic ethanol. The precipitated polymers were washed with ethanol, then dried at 70 ºC.

Borane co-catalyst: In a typical polymerization, the immobilized precatalyst was added to the pressure glass reactor with toluene, tris(pentafluorophenyl) borane (1.5 B:1 Ti), and either trimethyl aluminum or triisobutyl aluminum (400:1 Al:Ti ratio) in a drybox. The mixture was allowed to stir for 30 minutes to allow for sufficient activation of the catalyst. The reactor was then sealed and removed from the glovebox, placed in a 25 °C waterbath, and ethylene at 60 psi was introduced as described above. The polymerization was allowed to continue for a prescribed amount of time, then terminated as noted above. The precipitated polymers were washed with ethanol, then dried at 70 °C.

Leaching Experiments: The immobilized precatalyst, toluene, and methyl alumoxane (800:1 Al:Ti) or alkylaluminum (400:1 Al:Ti) were added to a flask in a drybox. The mixture was allowed to stir for 20 minutes. The mixture was then filtered in the drybox,

and the filtrate was added to the pressure glass reactor with toluene and an additional portion of MAO (200:1 Al:Ti). The reactor was then removed from the glovebox, placed in a 25 °C waterbath, and contacted ethylene at 60 psi as described above. The polymerization was allowed to continue for a prescribed amount of time and then terminated by adding acidic ethanol. The precipitated polymers were washed with ethanol, then dried at 70 °C.

4.3 Results and Discussion

4.3.1 Catalyst Synthesis and Characterization

Two aminosilica scaffolds were used in this work. Patterned aminosilica was synthesized via the protocol shown in Scheme 4.1. Traditionally grafted densely-functionalized aminosilica was made via literature methods[12]. The patterning protocol afforded 0.57 mmols NH_2/g SiO_2. Grafting 3-aminopropyltrimethoxysilane onto the silica surface in a material with a loading of 1.35 mmols NH_2/g SiO_2.

In the amine-elimination route, as shown in Scheme 4.2, the aminosilica is functionalized first with a tetramethylcyclopentadienyl-silane (Cp'Si). On the patterned amine, this reaction is nearly quantitative, as was seen previously[12]. Next, 0.54 mmol of Cp'/g SiO_2 were reacted with the surface bound amines, corresponding to 94.7% functionalization of the patterned amines. Metallation via an amine elimination route with tetrakis(diethylamino)titanium resulted in 0.56 mmols Ti /g, a nearly quantitative metallation of the Cp' (within experimental error). The ligand exchange, accomplish by reacting the metallated solid with trimethylsilylchloride, afforded 1.05 mmol Cl/g SiO_2.

This suggests nearly all of the immobilized Ti species retain their exchangeable ligands (94%). Elemental analysis results are tabulated in Table 4.1.

The densely functionalized aminosilica was used in the same synthetic protocol shown in Scheme 4.2. This material had a loading of 1.35 mmols amine/g SiO_2. Upon reaction with multiple aliquots of Cp'Si, 62% of the amines were found to react which is a loading of 0.84 mmols Cp'Si/g SiO_2. This proportion of amine functionalization is similar to previous results[12]. Metallation via amine elimination yielded 0.68 mmol Ti/g SiO_2, this is approximately a 75% metallation of immobilized Cp'Si and ~50% metallation of immobilized amine sites. After exchanging the diethylamino ligands with chlorides, elemental analysis showed 1.22 mmol Cl/g SiO_2. 89% of the titanium sites have retained their exchangeable ligands in the immobilization process.

Using the same aminosilica supports, the Royo method for synthesizing supported CGC-type complexes was used. From the patterned silica, the supporting protocol shown in Scheme 4.5 afforded 0.12 mmol Ti/g and 0.34 mmol Cl/g. With densely functionalized silica, 0.34 mmols Ti were immobilized and 0.82 mmols Cl/g were retained on the complex. Elemental analysis of these materials are also shown in Table 4.1.

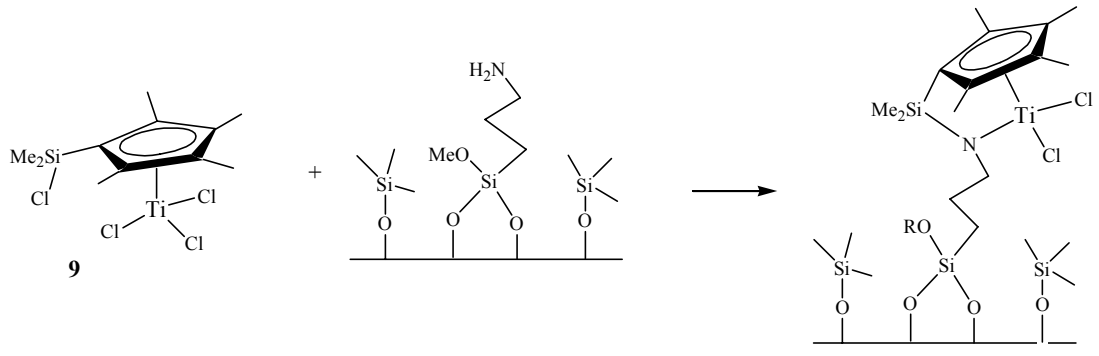

Scheme 4.5 Immobilization of titanium piano-stool complex via the Royo method

Table 4.1 Material Characterization

	Amine Elimination		Royo Method	
Material Description	Patterned Silica	Densely-Functionalized	Patterned Silica	Densely-Functionalized
Amine Loading (mmol/g)	0.57[a,b]	1.35[a,b]	0.57[a,b]	1.35[a,b]
Cyclopentadienyl Loading (mmol/g)	0.54[a,b]	0.84[a,b]	NA	NA
Reaction Yield[c]	94.7%	62.2%	----	----
Ti Loading (mmol/g)	0.56[b]	0.68[b]	0.12[b]	0.34[b]
Reaction Yield[c]	98.2%	50.4%	21.1%	25.2%

a: Loading determined by TGA; b: Loading determined by Elemental Analysis; c: Reaction Yield based on functionalization of immobilized amines

The amine elimination route provides nearly quantitative metallation of the patterned amine, evidenced by the ~1:1 N:Ti ratio. The densely functionalized aminosilica shows an amine to titanium ratio of 2:1. This ratio is similar to previous results[14]. It appears the amine elimination route provides a more efficient means of metallation when compared to Royo method. With a patterned aminosilica support, metallation with **9** gave a N:Ti ratio of roughly 5:1. Densely functionalized materials provided similar results. There are several possibilities for this result. As the pore diameter of the SBA-15 is approximately 100 Å, it is more likely a number of the amine sites will be located in the pore channel. As the piano stool complex has more steric bulk than the individual reactants in the amine elimination metallation, it may block access to

some amines in the pore structure. Additionally, the formation of bridged complexes would result in a larger amine-titanium ratio.

Characterization of supported complexes is difficult due to the fact that traditional spectroscopic techniques, such as NMR, FT-IR, and FT-Raman, rarely give useful information concerning the bonding of many transition metal centers when the metal species are present at such low concentrations. As previously shown, characterization by UV-VIS spectroscopy can be used in an attempt to elucidate the speciation of the metal center[14, 15]. The comparison of the materials in this work can be seen in Figure 4.1.

In the patterned amine elimination materials, there is a broad signal with a maximum intensity at 250 nm. In our previous work, this transition could not be correlated to an exact structure, however it was suggested the peak could be an amalgamation of the 220 nm signal from the SBA-15 scaffold and the transition from

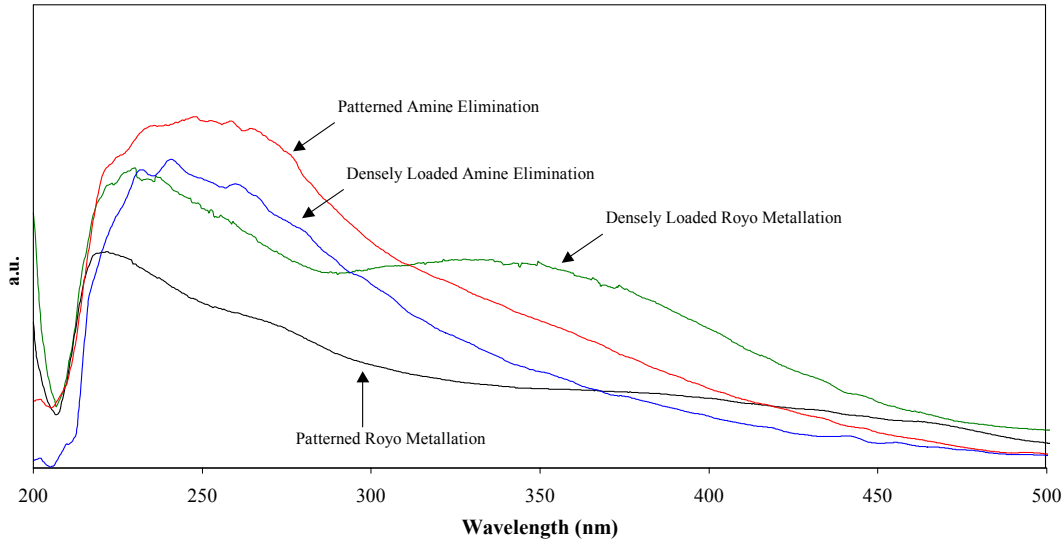

Figure 4.1 Diffuse-reflectance UV-Vis spectra of patterned amine elimination material, densely loaded amine elimination material, patterned Royo material, and densely loaded amine elimination material.

titanium (expected to appear around 260 nm)[14]. The shoulder centered around 330nm is attributed to the ligand to metal charge transfer (LMCT) from the cyclopentadienyl ring to the Ti[19]. The densely-loaded amine elimination material showed a broad signal with a maximum intensity at 240 nm, the LMCT expected around 350 nm is not as prominent as in the patterned material. As noted earlier[14], the UV-Vis spectra for materials made via amine elimination look similar on both densely functionalized and patterned silica. Thus this technique does not provide direct evidence for formation of different types of Ti species on the two supports.

In the patterned Royo material, there is a signal at 220 nm, likely from the silica scaffold. The transition at 260 nm can be attributed to the immobilized titanium complex. A second peak assigned to the LMCT can be seen starting at approximately 325 nm. In the densely functionalized Royo material, there is a broad transition centered around 225 nm, again assigned to a combination of the silica transition and titanium transition. The LMCT is much pronounced than in the other materials, while also beginning at a lower wavelength (280 nm). This large LMCT shoulder is likely the result of incomplete complex formation or formation of the bridging species, similar to those shown in Scheme 4.4. This was tested by synthesizing a densely functionalized secondary aminosilica and using it as a scaffold for complex immobilization (shown in Scheme 4.4 as R = Me). With this secondary amine functionalized silica, it is not possible to form a CGC and there is a high probability of incomplete complex formation or bridged titanium species. As seen in Figure 4.2, the UV-Vis of this material is nearly identical to that of the densely functionalized Royo material. This suggests the high

density of the amine sites on traditionally grafted materials creates a different main Ti site.

Characterization via UV-Vis failed to provide conclusive evidence of the formation of different sites from the different metallation methods. While, the UV-Vis spectra of the materials made via amine elimination show some variations from the Royo materials, the basic transitions expected in an immobilized CGC are present in both materials, albeit with differing intensities which are likely the result of the titanium loadings on the respective samples. The major structural variation seen via this technique in the large LMCT in the densely loaded Royo materials, attributed to the bridging complexes.

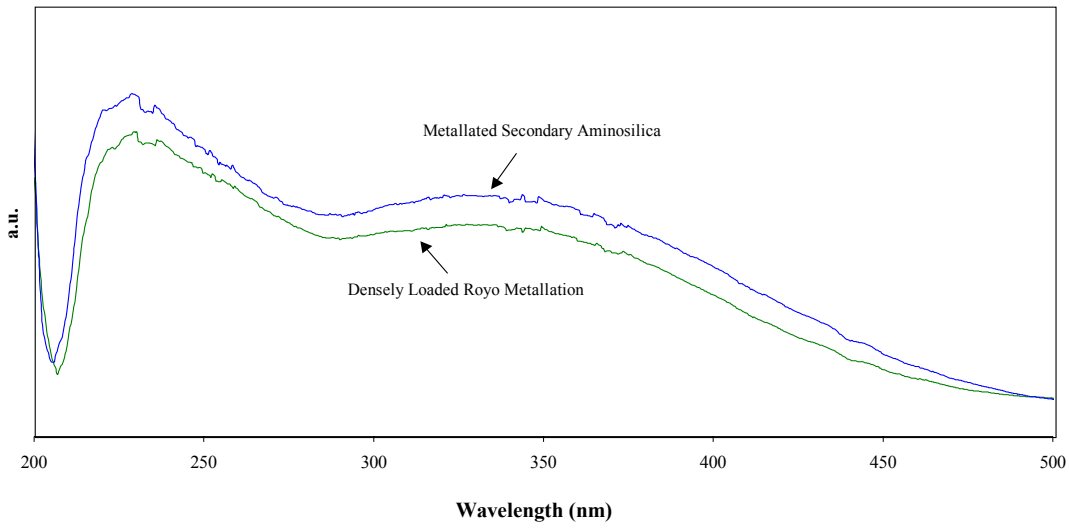

Figure 4.2 Diffuse-reflectance UV-Vis spectra of densely loaded Royo materials using primary and secondary aminosilica scaffolds

4.3.2 Polymerization Results

The ethylene polymerization behavior of the patterned and densely functionalized catalysts made via the two metallation routes was studied. The polymerizations were performed with methylaluminoxane (MAO) and borane/alkylaluminum co-catalysts. The results of the polymerizations using MAO are shown in Table 4.2. As shown, the patterned catalysts made via the Royo method are significantly more active than those made via the amine elimination method. This result is also seen in comparing the densely functionalized materials. The results suggest the Royo method does in fact make a more productive catalysts, however there are difficulties working with MAO as a co-catalyst.

As seen previously in work with these supported CGC-type complexes, the MAO co-catalyst can leach metal complex from the support. This makes it more difficult to

Table 4.2 Ethylene polymerization results using MAO as a co-catalyst

Metallation Method	Support	Productivity (kg PE/mol Ti-hr)
Amine Elimination	Patterned	22.1
Amine Elimination	Patterned	19.0
Amine Elimination	Densely-Loaded	8.0
Amine Elimination	Densely-Loaded	8.6
Royo	Patterned	58.1
Royo	Patterned	61.2
Royo	Densely-Loaded	15.5
Royo	Densely-Loaded	14.3

determine the active species, whether it is the leached species, immobilized species, or some combination of the two. To quantify this leaching phenomenon, the supported pre-catalyst and MAO co-catalyst were stirred in the drybox with toluene. After a prescribed period of time, the mixture was filtered and the filtrate was collected. The filtrate was added to the reactor along with additional co-catalyst and exposed to ethylene as described previously. The results are shown in Figure 4.3. The filtrate from the patterned catalyst made via the Royo method showed an activity of 38.9 kg polymer/mol Ti h, nearly 70% of the activity of the supported catalysts. The catalysts made via amine elimination also show significant leaching, over 50% of the activity is due to leached metal complex. The leached activities determined are a lower bound of the effect of leaching on the overall catalyst activity. Due to handling issues during the leaching

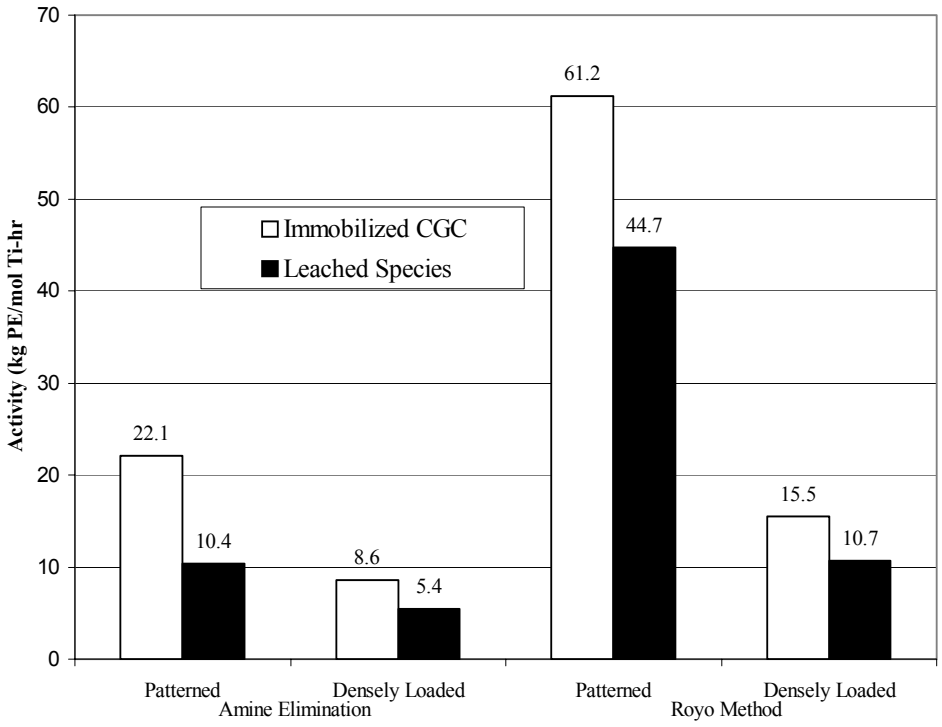

Figure 4.3 Comparison of the polyethylene productivity of the supported catalysts with the leached filtrate using methalumoxane as a co-catalyst.

experiments, there is the possibility for deactivation of active species.

To probe the activity of the actual immobilized species, it has been shown a borane/alkylaluminum co-catalyst does not leach metal complex from the surface[14]. The leaching tests described above were repeated using the catalysts in this work, but contacting the catalysts with alkylaluminums (either trimethylaluminum or triisobutylaluminum). The filtrate collected showed no polymerization activity upon exposure to ethylene. This suggests the activity seen in the studies performed with borane systems provide the productivity of the immobilized active species.

The results of the ethylene polymerization with the supported pre-catalysts and a borane/alkylaluminum co-catalyst can be seen in Table 4.3. Again the patterned catalysts made via the Royo method are significantly more active than those made via the amine

Table 4.3. Ethylene Polymerizations using Borane/alkylaluminum co-catalysts

Metallation Method	Support	Cocatalyst	Productivity (kg PE/mol Ti-hr)
Amine Elimination	Patterned	Borane/TMA	12.1
Amine Elimination	Patterned	Borane/TIBA	10.4
Amine Elimination	Densely-Loaded	Borane/TMA	1.4
Amine Elimination	Densely-Loaded	Borane/TIBA	1.3
Royo	Patterned	Borane/TMA	20.1
Royo	Patterned	Borane/TIBA	15.3
Royo	Densely-Loaded	Borane/TMA	Trace
Royo	Densely-Loaded	Borane/TIBA	2.8

elimination route. However, the magnitude of all the productivities decreased compared to the MAO results, confirming the results of the leaching studies. The patterned Royo material is still 1.5-2 times more active than the patterned amine elimination material.

These results suggest the methodology of the Royo method may allow for the synthesis of fewer, yet on average more accessible sites on the aminosilica scaffold. The SBA-15 material used for a support in this work had a pore diameter of approximately 100 Å. In the amine-elimination method, the aminosilica is first functionalized with a cyclopentadienyl then metallated. With a porous silica support, a number of these metal sites will be immobilized on the interior of the pore wall. When ethylene is added, polymerization at sites near the pore entrance can lead to pore blockage, preventing monomer from reaching other sites. In comparison, the Royo method uses a single-step immobilization protocol. Despite using identical aminosilica scaffolds, the materials made via the Royo method have significantly lower titanium loading than the materials made via amine elimination. If a piano-stool complex molecule reacts with an immobilized amine site near the entrance of a pore, it would be difficult for additional piano-stool complex to pass by to react with amines further down the pore. This effect would be larger in the Royo method than reacting the individual components as takes place in the amine elimination route. The formation of the CGC decreases the effective pore diameter, preventing a greater number of amines from reacting. As such, there are fewer immobilized CGCs within the pore which will be blocked once polymerization begins.

In the work previous reported by this group on using the Royo method for immobilization of CGC complexes, a zirconium piano-stool complex was used[15]. The

activities of the Ti-Royo materials reported here are several orders of magnitude lower than the Zr-Royo materials reported previously. However, it is difficult to compare the two studies due to the use of different aminosilica scaffold materials, polymerization vessel, and polymerization conditions.

4.4 Summary

The results presented here provide evidence that using a Royo metallation scheme to synthesize an immobilized constrained geometry catalyst may lead to a more active catalyst than those prepared by an amine elimination route. The catalysts synthesized by the Royo method were more productive per mole of supported titanium. However, the disadvantages of this method include a larger leaching effect when MAO is used as a co-catalyst. Additionally, the Royo method has significantly lower metallation efficiency than the amine elimination route, which showed nearly quantitative functionalization. As a result of this nearly quantitative functionalization, the amine elimination materials had a much greater loading of titanium, which allows them to produce more polyethylene per gram of supported *catalyst* than the Royo materials.

4.5 References

1. McKnight, A. L.; Waymouth, R. M., *Chem. Rev.* **1998,** *98*, 2587-2598.

2. Uusitalo, A. M.; Pakkanen, T. T.; Iskola, E. I., *J. Mol. Catal. A* **2002,** *177*, 179-194.

3. Diamond, G. M.; Rodewald, S. R.; Jordan, R. F., *Organometallics* **1995,** *14*, 5-7.

4. Diamond, G. M.; Jordan, R. F.; Petersen, J. L., *J. Am. Chem. Soc.* **1996,** *118*, 8024-8033.

5. Royo, B.; Royo, P.; Cadenas, L. M., *J. Organomet. Chem.* **1998,** *551*, 293-297.

6. Juvaste, H.; Pakkanen, T. T.; Iiskola, E. I., *Organometallics* **2000,** *19*, 4834-4839.

7. Juvaste, H.; Iiskola, E. I.; Pakkanen, T. T., *J. Organomet. Chem.* **1999,** *587*, 38-45.

8. Timonen, S.; Pakkanen, T. T.; Iiskola, E. I., *J. Organomet. Chem.* **1999,** *582*, 273-278.

9. Timonen, S.; Pakkanen, T. T.; Iiskola, E. I., *J. Mol. Catal. A* **1999,** *148*, 235-244.

10. Iiskola, E. I.; Timonen, S.; Pakkanen, T. T.; Harkki, O.; Lehmus, P.; Seppala, J. V., *Macromolecules* **1997,** *30*, 2853-2859.

11. Kasi, R. M.; Coughlin, E. B., *Organometallics* **2003,** *22*, 1534-1539.

12. McKittrick, M. W.; Jones, C. W., *Chem. Mater.* **2003,** *15*, 1132-1139.

13. McKittrick, M. W.; Jones, C. W., *J. Am. Chem. Soc.* **2004,** *126*, 3052.

14. McKittrick, M. W.; Jones, C. W., *J. Catal.* **2004,** *227*, 186-201.

15. Yu, K.; McKittrick, M. W.; Jones, C. W., *Organometallics* **2004,** *23*, 4089-4096.

16. Pangborn, A. B.; Giardello, M. A.; Grubbs, R. H.; Rosen, R. K.; Timmers, F. J., *Organometallics* **1996,** *15*, 1518-1520.

17. Zhao, D. Y.; Feng, J. L.; Huo, Q. S.; Melosh, N.; Fredrickson, G. H.; Chmelka, B. F.; Stucky, G. D., *Science* **1998,** *279*, 548-552.

18. Zhao, D. Y.; Huo, Q. S.; Feng, J. L.; Chmelka, B. F.; Stucky, G. D., *J. Am. Chem. Soc.* **1998,** *120*, 6024-6036.

19. Calleja, G.; van Grieken, R.; Garcia, R.; Melero, J. A.; Iglesias, J., *J. Mol. Catal. A* **2002,** *182*, 215-225.

CHAPTER 5

ETHYLENE-NORBORNENE COPOLYMERIZATIONS WITH SUPPORTED TI-CGC COMPLEXES

5.1 Norbornene Polymerizations

The homopolymerization of norbornene can proceed via several routes to produce three different types of polymer as shown in Scheme 5.1. The three routes are via ring-opening metathesis polymerization, a radical/cationic polymerization, and a vinyl-type polymerization. The most studied of these methods is ring-opening metathesis polymerization (ROMP). An interesting aspect of polynorbornenes made via ROMP is the presence of double bonds in the polymer backbone, which can allow for cross-linking of the polymer. Industrially, a $RuCl_3$/HCl catalyst in butanol is used for ROMP processes[1]. Other processes use tungsten, molybdenum, rhenium, or ruthenium complexes (i.e. metal halides or metal chlorides) in conjuction with co-catalysts. More

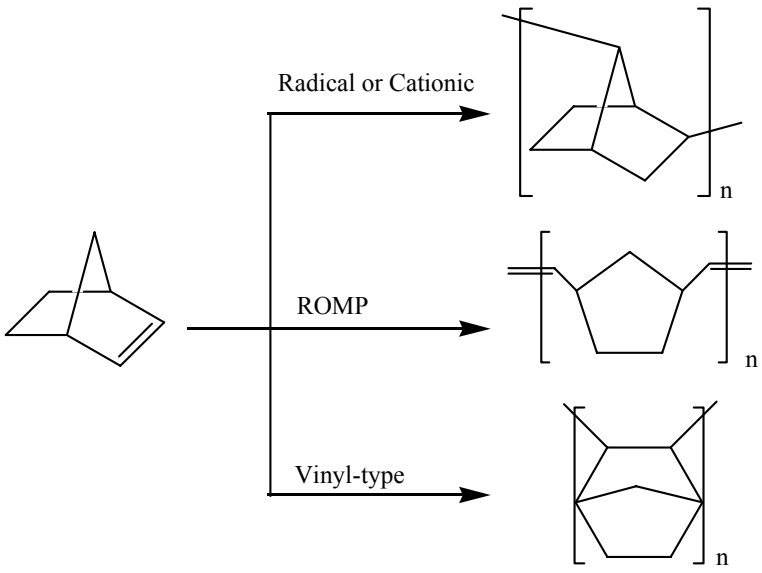

Scheme 5.1 Polymerization routes for norbornene

well-defined small molecule homogeneous catalysts are used in academic research, typically metal-carbene complexes. Among the transition metals used in these ROMP catalysts are tungsten, molybdenum, and ruthenium.

The radical polymerization of norbornene was first reported in 1968[2]. Typical protocols use traditional radical initiators, such as azoisobutyronitrile (AIBN). These polymerizations result in low-mass oligomers. As such, there is not a great deal of research done in this area.

Addition or vinyl polymerization of norbornene maintains the bicyclic structure of the monomer unit. Polynorbornene made via this method has mechanical properties, thermal stability, and clarity that makes it ideal for a number of applications. Specifically, there is particular interest in using these polymers for microelectronic applications, such as low k dielectric materials, photoresist materials, and liquid crystal displays[1, 3, 4].

5.2 Ethylene-Norbornene Copolymerizations

While there is considerable interest in the vinyl homopolymerization of norbornene, there are also an increasing number reports of cyclo-olefin copolymers (COCs). For example, ethylene-norbornene copolymers (Scheme 5.2) have properties,

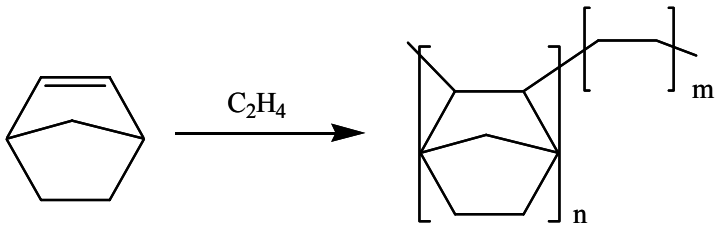

Scheme 5.2. Norbornene/Ethylene Copolymerization

such as high glass transition temperatures, high thermal stability, and high clarity, which make them viable for applications in microelectronics, pharmaceutical packaging, and optical media[5]. In addition, the copolymerization of a functionalized norbornene monomer with ethylene (and other olefins) can yield materials with tailored properties, such as solubility or increased Tg. There have been many reports in the literature of using homogeneous catalysts for these polymerizations, most often late transition metal (Pd and Ni) catalysts. For example, Brookhart and coworkers reported the use of cationic α-diimine nickel catalysts for polymerization of various olefins, such as shown in Figure 5.1[6-8]. This system was commercialized by Dupont as the Ni-Versipol™ Catalyst System[9]. Without sufficient steric bulk at R/R', oligomers are produced from these catalysts. However, increasing steric bulk at R/R' decreases the catalytic activity. Brian Goodall of Promerus (formerly of B.F. Goodrich) has also reported the synthesis of several homogeneous catalysts for the polymerization of functionalized norbornenes with olefins[10, 11]. In addition, Goodall combines ring-opening metathesis polymerization with addition polymerizations[10].

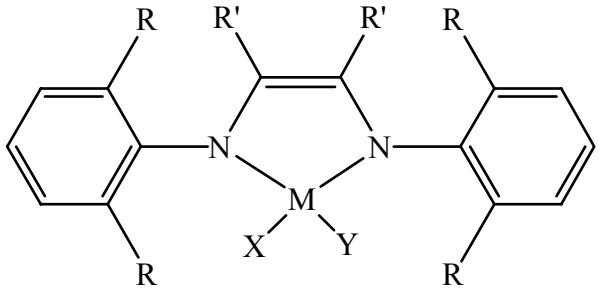

M = Ni, Pd

Figure 5.1 Late-transition metal catalyst for olefin polymerization

The mechanism for late metal (i.e. Ni, Pd) olefin polymerizations can be seen in Scheme 5.3[6]. This is similar to the mechanism for olefin polymerization by metallocenes and CGCs. The metal complex is activated by a co-catalyst, usually methalumoxane or a borane/alkylaluminum system. The co-catalyst abstracts one of the ligands, creating a cationic metal center, which is the active species for polymerization, and simultaneously producing a weakly coordinated anion. The initial coordination of monomer, shown as ethylene, is more facile than in metallocene polymerizations. This facile ligation has allowed this species to be identified by NMR spectroscopy, enabling detailed mechanistic studies. After coordination of ethylene, a four-member transition state is formed in the turnover limiting step. The rearrangement of the abstracted hydrogen yields another cationic metal center with an open coordination site, allowing for the incorporation of another monomer unit[8].

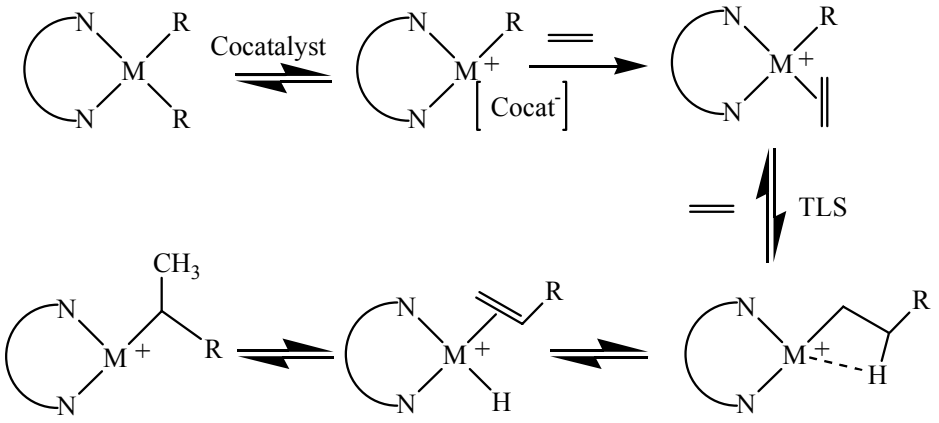

Scheme 5.3 Olefin polymerization mechanism for late metal catalysis

Unfortunately, most transition metal based olefin polymerization systems are not very tolerant of functionalities present in polar monomers, especially if the functionality is close to the C=C bond. In particular, early transition metals are highly oxophilic, resulting in inhibition of polymerization by oxygen-containing functionalities in the monomer. Even with late transition metals, inhibition of polymerization due to coordination of functionalities in the monomer or in the polymer chain can and does occur[12]. Despite this, several factors suggest Group IV catalysts would provide a more viable route to novel ethylene-norbornene copolymers. Typically, late transition-metal catalysts produce polyolefins with lower molecular weights than Ti or Zr metallocenes and CGCs[8]. If high molecular weights are required, the Ni and Pd systems are more difficult to use. Additionally, the Group IV metallocenes show a unique behavior in the copolymerization of ethylene with non-functionalized norbornenes. It has been reported in the literature, after incorporating an ethylene monomer unit, the incorporation of a norbornene unit is highly favored, leading to an overall increase in polymerization rate[13-16]. This observation has been supported by computational studies as well[17]. Ziegler and coworkers calculated that a less sterically hindered reactive center of CGCs allows for a stronger bond between the metal center and ethylene, raising the transition state energy[18]. Therefore increasing the congestion around the active site, such as adding a norbornene comonomer, makes the insertion of the monomers more favorable, allowing for a rate enhancement.

As discussed above, early transition metals are more oxophilic than late transition metals. However, there have been a number of reports in the literature of the polymerization of polar monomers using Group IV catalysts. Using metallocene type

complexes for the polymerization of monomers with polar functionalities can be difficult due to unwanted interactions between the metal center and monomer. A polar functionality, such as an alcohol or amine, has been shown to lead to deactivation of the metal center[8, 19]. However, several approaches have been developed to allow polymerization of polar monomers with homogeneous Group IV metallocenes and CGCs.

A common strategy is to employ a protecting group to prevent catalytic deactivation. For example, Waymouth and co-workers polymerized alpha-olefins containing silyl-protected amines and alcohols[20]. Several amino-olefins (for example, 5-*N*,*N*-Diisopropylamino-1-pentene) were also polymerized using dialkyl or diphenyl substitutients on the nitrogen[21]. A similar protection scheme also allowed for copolymerization of the amino-olefins with 1-hexene or 4-methyl-1-pentene[22]. Hydroxy functionalized styrene can also be polymerized after silyl protection of the polar group[23].

Another route to polymerization of phenolic monomers is modification of the monomer to sterically hinder reactions between the phenol and the metal center. Näsman and co-workers have reported the copolymerization of 6-tert-Butyl-2-(1,1-dimethylhept-6-enyl)-4-methylphenol with propylene and ethylene[24, 25]. The tert-butyl group limits deactivation of the catalytic site compared to an unhindered phenolic monomer.

Most transition metal complexes require co-catalysts (such as methylalumoxane or borane/alkylaluminums) to become active catalysts for olefin polymerization. These co-catalysts are Lewis-acidic, likely creating acid-base interactions with polar functionalities on the monomer (i.e. alcohols, esters, amines). Most polar monomers will interact with the co-catalyst (due to the large excess of Al present) during polymerization, if not protected prior to contact. These possible pairings makes it difficult to determine if

the monomer is polymerized in a protected or unprotected form, as monomers not protected prior to contact with co-catalysts will likely react with the aluminum species in situ[19].

Trialkylaluminums are often pre-contacted with the monomer, so that they maybe used as a protecting group when polymerizing alcohol-functionalized monomers. There have been a number of reports of prereacting an alcohol and/or amine functionalized olefin (i.e. ethylene, propylene, norbornene, etc.) with trimethylaluminum or methylalumoxane, followed by copolymerization of the protected monomer with ethylene using a metallocene catalyst[26-31]. This approach has also been successful when triisobutylaluminum was used as the protecting group for alcohol and carboxylic acid functionalized olefins[32-34]. In that work, Fink was also able to polymerize a protected polar monomer with a supported zirconocene catalyst[32]. The supported catalyst was synthesized by contacting the silica support with MAO, then adding in the homogeneous metallocene. This is the only known example of polymerization of polar norbornene monomer with a supported metallocene-type catalyst.

Another route to polar functionalized polyolefins is via post-polymerization transformations. Jiang and Wang reported the copolymerization of ethylene and 5-ethylidene-2-norbornene catalyzed by a zirconocene. The copolymer contains ethylidene groups, which upon reaction with a hydrogen borane can be converted into hydroxyl groups[35].

The polymerization of acrylates, as well as the copolymerization of acrylates and ethylene, has also been studied[36-39]. These polymerizations can proceed without any protection schemes for the acrylate functionality. However, it is likely the

polymerization of acrylates proceeds via a different mechanism than ethylene and propylene polymerization. It has been suggested this mechanism is a radical pathway, however, not a classical free radical mechanism[40].

As noted in Chapters 3 and 4, a synthetic protocol has been developed to support a constrained geometry-inspired complex on a silica scaffold such that the sites are more well-defined and isolated than materials synthesized via traditional methods. In typical olefin (i.e. ethylene and propylene) polymerizations, the use of supported metallocenes and CGCs allows for synthesis of polymers with higher densities and higher degrees of crystallinity. If this control extends to these ethylene-norbornene copolymers, material properties could be tailored for a specific application, for example increasing the crystallinity to increase the thermal decomposition temperature.

In this chapter, the activity of the patterned catalysts in the copolymerization of ethylene with various norbornene monomers is evaluated. This is the first report of using a tethered catalyst in this polymerization. The patterned catalyst had significant productivity in the copolymerization of ethylene-norbornene, showing very similiar polymerization productivity of the copolymer compared to an ethylene homopolymerization. Furthermore, the "patterned" catalysts even display increased activity compared to the analogous homogeneous system. Heterogeneous tethered catalysts prepared via typical methods on densely loaded supports showed no activity for the copolymerization, in contrast to results seen using only ethylene. Functionalized norbornenes, including monomers containing strongly-coordinating, polar groups such as quinoline-functionalized norbornene, were also readily polymerized using the patterned pre-catalysts.

5.3 Experimental Section

Catalysts were synthesized as described previously[41, 42].

5-Nonyl-bicyclo[2.2.1]hept-2-ene and 5-[(6-Bicyclo[2.2.1]hept-5-en-2-yl-hexylamino)-methyl]-quinolin-8-ol were provided by Amy Meyers (Weck Group, School of Chemistry and Biochemistry, Georgia Institute of Technology) and synthesized as reported in literature[43, 44].

Norbornene Homopolymerizations: In a nitrogen drybox, precatalyst, co-catalyst, and toluene are added into a small glass pressure tube reactor. The mixture is then stirred to allow for activation of the precatalyst. Norbornene monomer is then added to the reactor, which is then sealed and removed from the drybox. The tube is allowed to stir at 50 °C for a given time. The polymerization is quenched via addition of acidic ethanol. The polymer is collected via filtration with washing by acetone. The resulting product is then dried overnight.

Ethylene/Norbornene Copolymerizations: In a nitrogen drybox, precatalyst, toluene, and co-catalyst to a pressure glass reactor. The mixture is then stirred to allow for activation of the precatalyst. The norbornene monomer is then added to the reactor, which is then sealed and removed from the drybox. Ethylene (60 psi) was added to the reactor for ten minutes at 25 °C. The polymerization is quenched via addition of acidic ethanol. The polymer is collected via filtration and washing with acetone. The resulting product is then dried overnight.

Leaching Experiments: The immobilized precatalyst, toluene, and methyl alumoxane (800 Al:1 Ti) were added to a flask in a drybox. The mixture was allowed to stir for 20 minutes. The mixture was then filtered in the drybox, and the filtrate was added to the pressure glass reactor with toluene and an additional portion of MAO (200:1 Al:Ti). The norbornene monomer is then added to the reactor, which is then sealed and removed from the drybox. The reactor is then placed in a 25 °C waterbath, and contacted ethylene at 60 psi as described above. The polymerization was allowed to continue for a prescribed amount of time and then terminated by adding acidic ethanol. The precipitated polymers were washed with acetone, then dried at 70 °C.

Polymer Characterization: Differential Scanning Calorimetry analysis was conducted by heating samples under nitrogen with a heating cycle from 30 to 200 ºC at 2º/min, cooling to 100 ºC at 2º/min, then repeating the cycle. The thermal transition was taken from the second cycle. ^{13}C NMR was performed on a Bruker AMX 400 at 125 ºC. The polymers (>100 mgs) were dissolved in a 4:1 mixture of 1,2,4 trichlorobenzene and 1,1,2,2 tetrachloroethane (d_2) and placed in a 10 mm NMR tube. At least 1000 scans were run for each sample. Elemental analysis was performed by Desert Analysis.

5.4 Results and Discussion

5.4.1 Catalyst Synthesis

A protocol to support a constrained geometry-inspired complex on an aminosilica scaffold such that the sites are more well-defined and isolated than materials synthesized via traditional methods was previously reported (Scheme 5.1). These "patterned" precatalysts are significantly more active in the polymerization of ethylene than the control materials, including homogeneous analogs. Two control catalysts were used for comparison to the patterned material. The first control, a homogeneous analog of the supported complex (Figure 5.2), was synthesized as previously reported[41, 42]. The second control, a densely-loaded catalyst, was synthesized by the same methodology as the patterned material. However, in this catalyst, a traditionally grafted aminosilica material with a dense surface loading of amines was used as the scaffold for the synthesis of the immobilized complex.

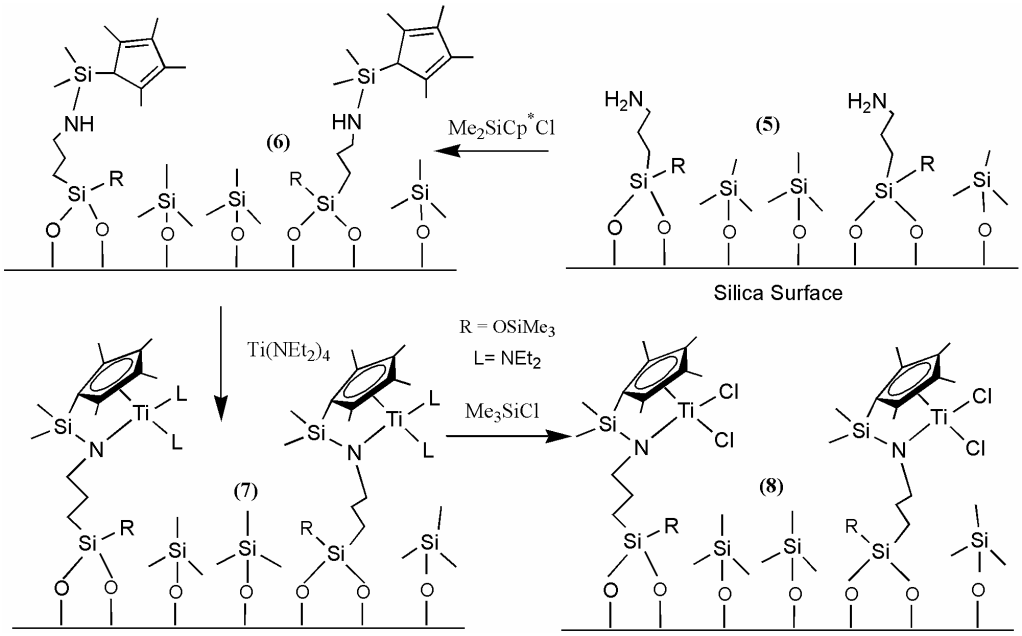

Scheme 5.4 Ti-CGC Synthetic Protocol

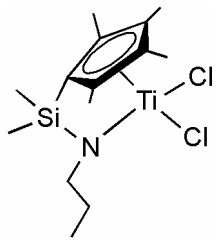

Figure 5.2 Homogeneous CGC Analog

5.4.2 Norbornene Homopolymerizations

The productivity of the catalysts in the homopolymerization of norbornene was tested and the results are shown in Table 5.1. It is noteworthy that the densely functionalized catalyst showed no activity towards the polymerization of norbornene. The homogeneous catalyst showed the ability to produce polymer, albeit at a very low rate. In comparison, the patterned precatalyst was significantly more productive in the norbornene polymerization. Using MAO as a co-catalyst led to a more active system than the borane/alkylalumium co-catalysts. The increased activity of the patterned precatalyst is not unexpected when compared to previous studies of ethylene polymerization. The patterned catalysts were also 5-10 times more active in the polymerization of ethylene compared to the control materials[41, 42]. As UV-Vis spectroscopy provided no evidence to suggest different types are formed on the different aminosilica scaffolds, the higher activity of the patterned catalyst was previously hypothesized to be associated with greater accessibility to the tethered metal centers. These norbornene polymerization results further suggest the patterned catalyst has a more accessible active site than the densely functionalized catalyst. As norbornene has a greater steric presence than ethylene, a more isolated catalytic site would be more

Table 5.1 Norbornene Homopolymerization Results

Catalyst	Ti Loading (mmol/g)	Co-catalyst	Productivity (kg polymer/mol Ti-hr)	DSC Transitions (ºC)
Patterned	0.38	MAO	39.1	185
Patterned	0.38	MAO	36.5	185
Patterned	0.38	Borane/TIBA	21.1	182
Patterned	0.38	Borane/TIBA	23.4	183
Homog.	2.83	MAO	0.9	183
Homog.	2.83	Borane/TIBA	2.4	186
Densely Loaded	0.53	MAO	Trace	----
Densely Loaded	0.53	Borane/TIBA	0	----

a: Loading determined by Elemental Analysis; b: co-catalyst: MAO; Al/Ti = 800; c: co-catalyst: borane/triisobutylaluminum; Al/Ti = 400.

capable of polymerizing the monomer. The homogeneous CGC shows a lower activity than the patterned catalyst as well, which is similar to results previously seen in ethylene polymerizations. The propyl chain on the homogeneous CGC was chosen as it is a closer analog of the supported species than a tert-butyl, or other sterically bulky functionality, as seen in some commercial catalysts[45].

Differential Scanning Calorimetry (DSC) was used to study the thermal transitions in the homopolymers. These results are also listed in Table 5.1. The polynorbornenes produced by the patterned materials showed transitions between 180-185 ºC. The polymers produced with the homogeneous analog had transitions at very

similar temperature to those seen in the polymers made via patterned materials. While it is difficult to assign DSC transitions to a specific polymer structure, these results are consistent with a poly(norbornene). Shiono and coworkers reported various norbornene-ethylene copolymers polymerized via titanium complexes with identical norbornene content having varied glass transition temperatures and melting points[46]. It was determined that the norbornene content, distribution, and stereochemistry in the polymer all have an effect on the thermal properties of the polymer.

5.4.3 Ethylene-norbornene copolymers

The catalysts were also tested in the production of ethylene-norbornene copolymers. The catalytic productivities in the copolymerizations are tabulated in Table 5.2. Also shown in the table are the results for ethylene homopolymerization as previously reported with these catalyts (Chapter 3)[42]. Similar to the results seen in the norbornene homopolymerization, the patterned catalyst again shows the most activity, the homogenous catalysts shows a low productivity of copolymer, and the densely functionalized catalyst is practically inactive in this polymerization, although using MAO as a co-catalyst gives trace productivity. With the patterned catalyst, the copolymerization productivity is higher than the norbornene hompolymerization activity. Using a borane/alkylaluminum co-catalyst, the patterned precatalyst shows a similar copolymer productivity and ethylene productivity. Yet with MAO as co-catalyst, the system is significantly more active than in the ethylene homopolymerization, similar to literature results discussed above[13-17].

Table 5.2 Ethylene Norbornene Copolymerization Results

Entry	Catalyst	Ti loading[a] (mmol/gcat)	Co-catalyst	Ethylene Productivity[f] (kg PE/mol Ti-hr)	Copolymer Productivity (kg polymer/mol Ti-hr)[g]
1	Patterned	0.38	Borane[b]/TMA[c]	28.7	27.9
2	Patterned	0.38	Borane[b]/TIBA[d]	24.8	25.2
3	Patterned	0.38	MAO[e]	19.7	54.2
4	Homog.	2.83	Borane[b]/TMA[c]	15.6	3.6
5	Homog.	2.83	Borane[b]/TIBA[d]	21.4	3.4
6	Homog.	2.83	MAO[e]	13.5	5
7	Traditional.	0.53	Borane[b]/TMA[c]	2.7	No activity
8	Traditional.	0.53	Borane[b]/TIBA[d]	1.5	No activity
9	Traditional.	0.53	MAO[e]	5.9	0.8

In previous work with these catalysts, it has been shown that metal complex leached by contact with MAO accounts for a large portion of the activity seen in ethylene polymerization[42]. Leaching studies were undertaken to determine if this phenomenon would explain the high activity of the patterned systems. The leaching tests were conducted as described in the experimental section and the results are shown in Figure 5.3. The ethylene-norbornene copolymerization activity of the leached species accounts for about 7% of the total activity seen from the MAO system. Interestingly, while the overall magnitude of the leached species activity is similar when compared to ethylene homopolymerization, the percent contribution is much lower. As the leached homogeneous catalyst is several times more active in ethylene polymerization than in the copolymerization, this suggests the bulk of the activity seen in the patterned system may be from metal sites attached to the surface. As previously reported, the patterned system

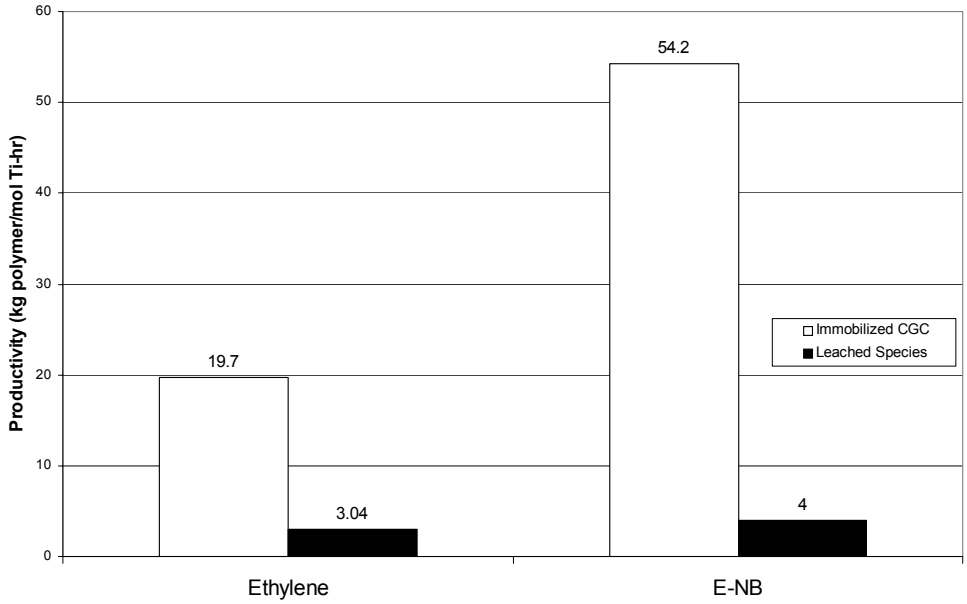

Figure 5.3. Leaching studies in copolymerization

showed no detectable titanium leaching when a borane/alkylaluminum co-catalyst system was used[42]. The results of these experiments should be viewed as a lower bound on the activity of the leached species. The activated species are extremely sensitive, and although all manipulations are performed in a dry box, it is possible there is deactivation through handling. Thus, the actual catalytic productivity of leached species could be higher.

Some of the copolymers synthesized were characterized by ^{13}C NMR. The characteristic carbons for an ethylene/norbornene copolymers can be seen in Figure 5.4, with the corresponding resonances shown in Table 5.3[14]. The spectrum of the patterned copolymer is also shown in Figure 5.4. The characteristic signals for norbornene incorporation into the polymer can be seen. Equation 1 shows the calculation of percent incorporation of norbornene into the copolymer using ^{13}C NMR peak integrations[46].

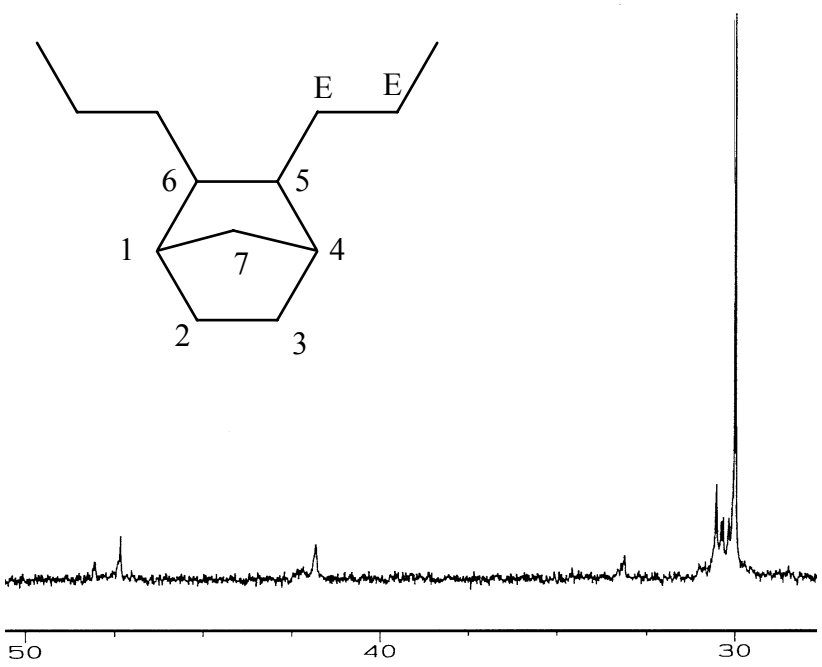

Figure 5.4 ^{13}C Spectrum of copolymer produced via Patterned Catalysts and MAO co-catalyst

Table 5.3 Ethylene-Norbornene Copolymer ^{13}C NMR assignments

^{13}C chemical shifts (ppm)	assignment
27-32.7	C5, C6, CE
33.0-36.7	C7
37-44	C1, C4
44.5-56	C2, C3

$$\text{mol \% NB} = \frac{1/3(I_{C2/3} + I_{C1/4} + 2_{IC7})}{I_{CE} + I_{C5/6}} \times 100 \qquad (1)$$

This calculation gives a percent norbornene incorporation of 20%. It is important to note, in a ^{13}C NMR spectrum the area of each peak is not simply proportional to the number of carbons giving rise to the signal because the Nuclear Overhauser Effect from proton decoupling is not equal for all of the carbons[47]. Thus this percent incorporation should be viewed as an estimate, not an absolute measure of the percent incorporation.

The spectra of the control materials showed no apparent incorporation of norbornene into the copolymer. The only signals seen in these materials were from polyethylene (around 30 ppm). None of the characteristic signals arising from the norbornene carbons (C1-C7) were distinguishable from baseline noise.

The copolymers were also characterized by DSC. The results are tabulated below (Table 5.4). The copolymers showed transitions between 172-175ºC, similar to some ethylene-norbornene copolymers reported in the literature[46, 48]. This confirms the results of the ^{13}C NMR spectra that norbornene is in fact incorporated into the polymer. In contrast, the polymers produced by the homogeneous control catalyst showed a melting point of approximately 140 ºC, as did polymer from the traditionally prepared densely functionalized material. While ethylene-norbornene copolymers have been reported with DSC transitions in the same range, this result is also similar to melting points of typical polyethylenes[41, 42, 49, 50]. Combining the DSC results with results seen in ^{13}C NMR, there is no detectable norbornene incorporation in the polymers produced by the control materials and it is likely that the materials are homopolymers of ethylene. It should be

Table 5.4 DSC Analysis of Copolymers

Catalyst	Co-catalyst	Productivity (kg polymer/mol Ti-hr)	DSC Transitions (°C)
Patterned	Borane/TMA[a]	27.9	175
Patterned	Borane/TIBA[b]	25.2	174
Patterned	MAO[c]	54.2	172
Homog.	Borane/TMA[a]	3.6	141
Homog.	Borane/TIBA[b]	3.4	139
Homog.	MAO[c]	5	120, 144
Traditional.	MAO[c]	0.8	141

a: co-catalyst: borane/trimethylaluminum; Al/Ti = 400; b: co-catalyst: borane/triisobutylaluminum; Al/Ti = 400 c: co-catalyst: MAO; Al/Ti = 800.

noted that while other homogeneous CGCs have shown the ability to copolymerize ethylene-norbornene, these catalysts have also been shown to significantly more active in ethylene homopolymerizations[51, 52].

One desired application of using a supported catalyst for the copolymerization of ethylene-norbornene is the possible removal of the metal, leaving a high-purity polymer. This is unusual in supported metallocene/CGC polymerizations as the high activity of the catalyst results in only a small weight fraction of residual metal in the polymer. However, for microelectronics applications, it would be desirable to have a metal-free polymer. Using the copolymers produced by the patterned precatalysts and MAO, an extraction was performed in an attempt to remove the titanium species from the polymer. Elemental analysis detected no titanium in the resulting polymer (0.001% limit of

detection). This result does not allow the conclusion to be reached that the polymer is completely metal free, however, as the maximum amount of Ti in the polymer would be approximately 0.09%. Nonetheless, there appears to be a significant reduction in metal residue in the copolymer.

Thus, the patterned materials exhibit the capability to incorporate norbornene in a copolymerization with ethylene. However, the addition of bulky polar or nonpolar functional groups to the monomer can drastically change the reactivity of the monomers. To this end, we investigated the copolymerization of ethylene with functionalized norbornenes. The first functionality tested was a long alkyl chain attached to the ring, 5-Nonyl-bicyclo[2.2.1]hept-2-ene (Figure 5.5A). This non-polar, bulky monomer was used in a copolymerization and the observed productivities are illustrated in Figure 5.6. Again the densely loaded catalyst showed very little activity in this polymerization, not unexpected due to its lack of activity in the copolymerization of norbornene and ethylene. The homogeneous catalyst showed some activity for this copolymerization, although the productivity was slightly depressed from the norbornene-ethylene copolymerization. The

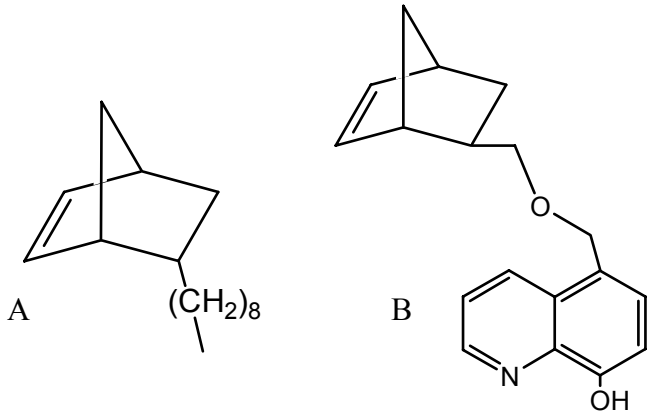

Figure 5.5 A) 5-Nonyl-bicyclo[2.2.1]hept-2-ene; B) 5-[(6-Bicyclo[2.2.1]hept-5-en-2-yl-hexylamino)-methyl]-quinolin-8-ol

patterned catalyst again showed the highest productivity in the polymerization. The polymerization productivity was lower than in the unfunctionalized norbornene studies, however as the nonyl-functionalized monomer is much larger than the unfunctionalized monomer, it can be expected to have a slower incorporation due to steric constraints.

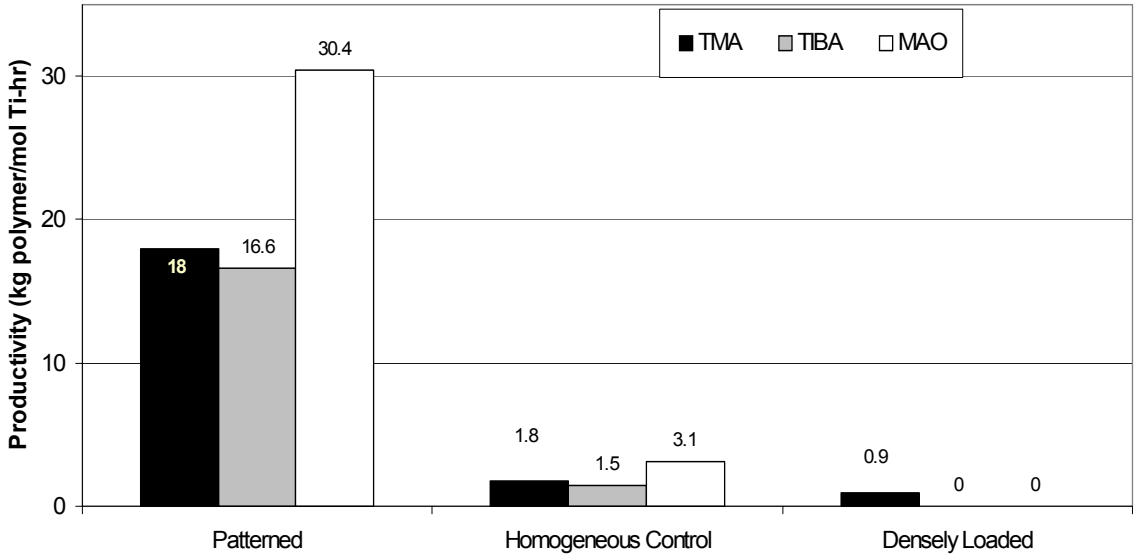

Figure 5.6 Ethylene-5-Nonyl-bicyclo[2.2.1]hept-2-ene copolymerization results

The second functionalized monomer, 5-[(6-Bicyclo[2.2.1]hept-5-en-2-yl-hexylamino)-methyl]-quinolin-8-ol, is illustrated schematically in Figure 5.5B. This is a polar monomer which has been polymerized via ROMP to synthesize polymeric electron transport layers in light-emitting diodes[43, 44]. The results of the copolymerizations with this monomer are shown in Figure 5.7. The control materials are again nearly inactive in the copolymerization. However, the patterned catalyst maintains some polymerization activity in this system. This is unique from two perspectives. First, this norbornene

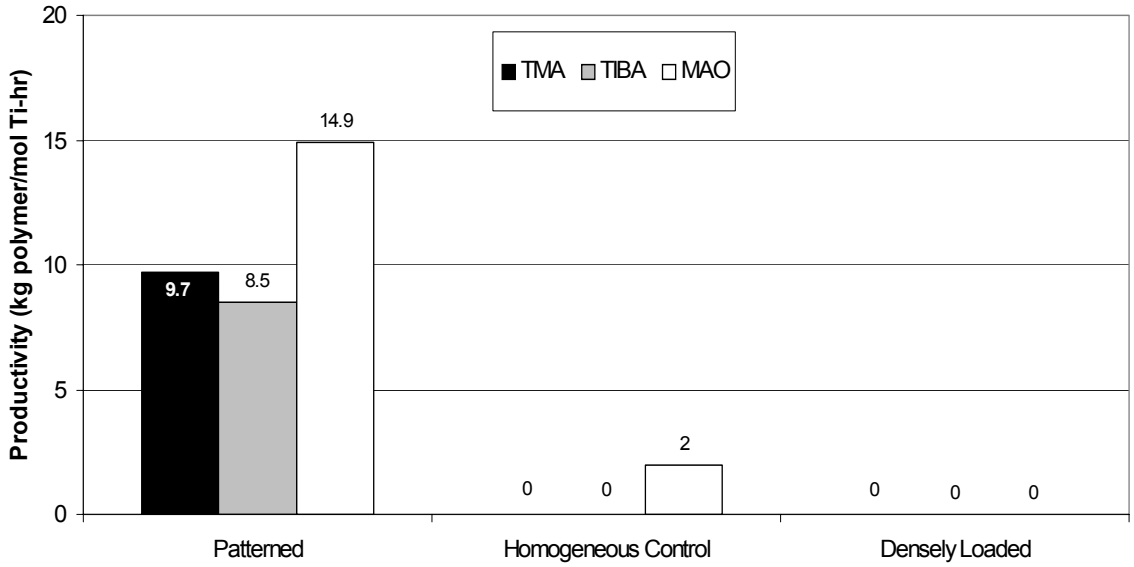

Figure 5.7 Ethylene-quinoline norbornene copolymerization results

monomer contains a quinoline moiety that can easily coordinate with the metal center. However, Meyers and Weck have shown that this ligand coordinates to Al centers. Thus, interactions with the cocatalyst, which is present in a large excess, may decrease the likelihood that the quinoline group coordinates with the Ti center[43, 44]. The second unique aspect is that this is the first example of an immobilized CGC-inspired used in the copolymerization of a functionalized norbornene with ethylene.

The lack of activity by the control catalysts and the depressed rate of the patterned catalyst compared to other polymerizations could be a consequence of several factors. The bicyclic rings on the monomer create a very large steric profile, thus having isolated catalytic sites may allow for better incorporation. The depressed activity of the other copolymerizations could be the result of monomer-catalyst interactions. It is possible the titanium metal center interacts with the polar functionalities, creating titanium sites which

are unavailable for polymerization. This can be seen in the lack of activity of the homogeneous CGC with the borane/alkylaluminum cocatalysts. As the homogeneous CGC is much more mobile in the polymerization solution, it has a greater chance of reacting with the polar end of the monomer, creating an inactive system.

As the quinoline functionality has been used for aluminum coordination, it is likely the aluminum based co-catalysts are also reacting with the functionality. This may protect the metal center from unwanted interactions, however the aluminum coordination is an equilibrium process, so there will be available functionalities with which the titanium can react. In experiments where the catalyst is not activated before exposure to the quinoline functionalized monomer, there is no polymerization activity seen. As discussed previously, it has been previously shown that protecting a polar monomer with a trialkylaluminum can allow for polymerization[26-34]. This process is likely to occur when the monomer is added to the catalyst/co-catalyst solution.

5.5 Summary

The patterned catalysts developed here shown activity towards the copolymerization of ethylene and various functional norbornenes. The catalysts also showed a higher activity in the copolymerization than in the homopolymerizations of ethylene and norbornene, confirming results seen in homogeneous and computational studies[13-17]. In comparison, control materials made via literature techniques showed little or no activity in copolymerizations and characterization of the resulting polymer shows no apparent incorporation of the comonomer. These results further provide evidence of the enhanced activity achieved through the use of the patterning protocol discussed

above. The polymerization of functionalized norbornenes, both polar and non-polar, was also able to be accomplished. The polymerization of the polar monomer was likely facilitated by interactions between the aluminum co-catalysts and the polar functionality. This "in-situ protection" may have allowed for the comonomer to be polymerized. Additionally, reduction of residual titanium content in the polymer was achieved, allowing for potentially high-purity copolymers to be produced.

5.5 References

1. Janiak, C.; Lassahn, P. G., *Macromol. Rapid Comm.* **2001,** *22*, 479-492.

2. Kennedy, J. P.; Makowski, H. S., *J. Polym. Sci. Pol. Sym.* **1968**, 247.

3. Janiak, C.; Lassahn, P. G., *J. Mol. Catal. A* **2001,** *166*, 193-209.

4. Kaminsky, W.; Engehausen, R.; Kopf, J., *Angew. Chem. Int. Edit.* **1995,** *34*, 2273-2275.

5. Monkkonen, K.; Lautanen, J.; Kettunen, V.; Leppanen, V. P.; Pakkanen, T. T.; Jaaskelainen, T., *J. Mater. Chem.* **2000,** *10*, 2634-2636.

6. Johnson, L. K.; Killian, C. M.; Brookhart, M., *J. Am. Chem. Soc.* **1995,** *117*, 6414-6415.

7. Johnson, L. K.; Mecking, S.; Brookhart, M., *J. Am. Chem. Soc.* **1996,** *118*, 267-268.

8. Ittel, S. D.; Johnson, L. K.; Brookhart, M., *Chem. Rev.* **2000,** *100*, 1169-1203.

9. Brookhart, M. S.; Johnson, L. K.; Killian, C. M.; Arthur, S. D.; Feldman, J.; McCord, E. F.; McLain, S. J.; Kreutzer, K. A.; Bennett, A. M. A.; Coughlin, E. B.; Ittel, S. D.; Parthasarathy, A.; Wang, L.; Yang, Z.-Y. 5,866,663, 1997.

10. Goodall, B. L.; Mcintosh, L. H.; Rhodes, L. F., *Macromol. Symp.* **1995,** *89*, 421-432.

11. Goodall, B. L., *Abstr. Pap. Am. Chem. S.* **1998,** *215*, U778-U778.

12. Klabunde, U.; Ittel, S. D., *J. Mol. Catal.* **1987,** *41*, 123-134.

13. Ruchatz, D.; Fink, G., *Macromolecules* **1998,** *31*, 4669-4673.

14. Ruchatz, D.; Fink, G., *Macromolecules* **1998,** *31*, 4674-4680.

15. Ruchatz, D.; Fink, G., *Macromolecules* **1998,** *31*, 4681-4683.

16. Ruchatz, D.; Fink, G., *Macromolecules* **1998,** *31*, 4684-4686.

17. Kim, E. G.; Klein, M. L., *Organometallics* **2004,** *23*, 3319-3326.

18. Woo, T. K.; Fan, L.; Ziegler, T., *Organometallics* **1994,** *13*, 2252-2261.

19. Boffa, L. S.; Novak, B. M., *Chem. Rev.* **2000,** *100*, 1479-1493.

20. Kesti, M. R.; Coates, G. W.; Waymouth, R. M., *J. Am. Chem. Soc.* **1992,** *114*, 9679-9680.

21. Stehling, U. M.; Stein, K. M.; Kesti, M. R.; Waymouth, R. M., *Macromolecules* **1998,** *31*, 2019-2027.

22. Stehling, U. M.; Stein, K. M.; Fischer, D.; Waymouth, R. M., *Macromolecules* **1999,** *32*, 14-20.

23. Kim, Y.; Do, Y., *Macromol. Rapid Comm.* **2000,** *21*, 1148-1155.

24. Wilen, C. E.; Nasman, J. H., *Macromolecules* **1994,** *27*, 4051-4057.

25. Wilen, C. E.; Luttikhedde, H.; Hjertberg, T.; Nasman, J. H., *Macromolecules* **1996,** *29*, 8569-8575.

26. Marques, M. M.; Correia, S. G.; Ascenso, J. R.; Ribeiro, A. F. G.; Gomes, P. T.; Dias, A. R.; Foster, P.; Rausch, M. D.; Chien, J. C. W., *J. Polym. Sci. Pol. Chem.* **1999,** *37*, 2457-2469.

27. Radhakrishnan, K.; Sivaram, S., *Macromol. Rapid. Comm.* **1998,** *19*, 581-584.

28. Hagihara, H.; Tsuchihara, K.; Sugiyama, J.; Takeuchi, K.; Shiono, T., *J. Polym. Sci. Pol. Chem.* **2004,** *42*, 5600-5607.

29. Hagihara, H.; Tsuchihara, K.; Sugiyama, J.; Takeuchi, K.; Shiono, T., *Macromolecules* **2004,** *37*, 5145-5148.

30. Aaltonen, P.; Fink, G.; Lofgren, B.; Seppala, J., *Macromolecules* **1996,** *29*, 5255-5260.

31. Hakala, K.; Helaja, T.; Lofgren, B., *J. Polym. Sci. Pol. Chem.* **2000,** *38*, 1966-1971.

32. Goretzki, R.; Fink, G., *Macromol. Chem. Phys.* **1999,** *200*, 881-886.

33. Wendt, R. A.; Fink, G., *Macromol. Chem. Physic.* **2000,** *201*, 1365-1373.

34. Kaya, A.; Jakisch, L.; Komber, H.; Voigt, D.; Pionteck, J.; Voit, B.; Schulze, U., *Macromol. Rapid Comm.* **2001,** *22*, 972-977.

35. Jiang, G. J.; Wang, T. Y., *J. Chin. Chem. Soc. Taip.* **1998,** *45*, 341-347.

36. Jensen, T. R.; Yoon, S. C.; Dash, A. K.; Luo, L. B.; Marks, T. J., *J. Am. Chem. Soc.* **2003,** *125*, 14482-14494.

37. Arndt, S.; Beckerle, K.; Hultzsch, K. C.; Sinnema, P. J.; Voth, P.; Spaniol, T. P.; Okuda, J., *J. Mol. Catal. A* **2002,** *190*, 215-223.

38. Jin, J. Z.; Chen, Y. X., *Macromol. Chem. Physic.* **2002,** *203*, 2329-2333.

39. Frauenrath, H.; Balk, S.; Keul, H.; Hocker, H., *Macromol. Rapid Comm.* **2001,** *22*, 1147-1151.

40. Tian, G.; Boone, H. W.; Novak, B. M., *Macromolecules* **2001,** *34*, 7656-7663.

41. McKittrick, M. W.; Jones, C. W., *J. Am. Chem. Soc.* **2004,** *126*, 3052.

42. McKittrick, M. W.; Jones, C. W., *J. Catal.* **2004,** *227*, 186-201.

43. Meyers, A.; Weck, M., *Chem. Mater.* **2004,** *16*, 1183-1188.

44. Meyers, A.; Weck, M., *Macromolecules* **2003,** *36*, 1766-1768.

45. Stevens, J. C.; Timmers, F. J.; Wilson, D. R.; Schmidt, G. F.; Nickias, P. N.; Rosen, R. K.; Knight, G. W.; Lai, S. Y. Eur Pat. Appl. 0 416 815 A2, 1991.

46. Hasan, T.; Ikeda, T.; Shiono, T., *Macromolecules* **2004,** *37*, 8503-8509.

47. Skoog, D. A.; Holler, F. J.; Nieman, T. A., *Principles of Instrumental Analysis*. Fifth ed.; Harcourt Brace College Publishers: Philadelphia, 1998.

48. Cho, E. S.; Joung, U. G.; Lee, B. Y.; Lee, H.; Park, Y. W.; Lee, C. H.; Shin, D. M., *Organometallics* **2004,** *23*, 4693-4699.

49. Tritto, I.; Boggioni, L.; Sacchi, M. C.; Locatelli, P.; Ferro, D. R., *Macromol. Symp.* **2004,** *213*, 109-121.

50. Thorshaug, K.; Mendichi, R.; Boggioni, L.; Tritto, I.; Trinkle, S.; Friedrich, C.; Mulhaupt, R., *Macromolecules* **2002,** *35*, 2903-2911.

51. McKnight, A. L.; Waymouth, R. M., *Macromolecules* **1999,** *32*, 2816-2825.

52. McKnight, A. L.; Waymouth, R. M., *Chem. Rev.* **1998,** *98*, 2587-2598.

CHAPTER 6

DEVELOPMENT OF STRUCTURE-REACTIVITY RELATIONSHIPS OF IMMOBILIZED CGC-INSPIRED COMPLEXES

6.1 Structure-Property Relationships

One of the most important advantages of single-site catalysts, such as metallocenes and constrained geometry complexes, is the possibility to rationally alter polymer properties via changes in catalyst structure. Since properties such as complex symmetry, ligand sterics and the electronic structure of the complexes can be tuned by changes in the ligand structure, the chemist or engineer has the possibility to tailor catalyst properties such as reactivity, polymer tacticity and other properties by changes in the catalyst design. However, as many *supported* catalysts prepared via traditional methods result in a distribution of types of sites, it has been very difficult to generate a fundamental understanding of structure/property relationships in *supported* metallocene and CGC systems. Hence, as there has not been a well-characterized, truly single-site supported catalyst, the development of structure-polymer relationships has been very much of an empirical nature to this point. An overriding goal of this thesis has been the development of a well-defined, CGC-Inspired catalyst immobilized on a silica surface. Such a system has been developed, and here the role of various catalyst design parameters on polymerization properties is described.

One of the advantages of homogeneous constrained geometry catalysts is that there are numerous structural components which can be varied. This allows for the catalyst behavior to be tuned. For example, in the CGC shown in Figure 6.1, changing the ligand environment can change the catalyst productivity and polymer properties. Changing the

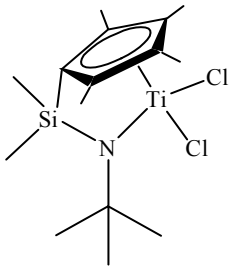

Figure 6.1. Group IV CGC

cyclopentadienyl group from a tetramethylcyclopentadienyl (Cp') ligand (Figure 6.2A) to a cyclopentadienyl (Cp) ligand (Figure 6.2B) to an indenyl ligand (Figure 6.2C) results in a decrease in productivity[1]. Replacing the tert-butyl amido group with a less sterically hindered substituents, such as a phenylamido or propylamido group, also leads to lower productivity[2]. The ligand bite angle also has a role in the catalyst polymerization performance. This angle is most often varied by replacing the dimethylsilyl bridge with a longer version, such as an ethyl bridge, creating a larger bite angle. Due to steric effects, increasing the ligand bite angle decreases the productivity of the catalyst[2].

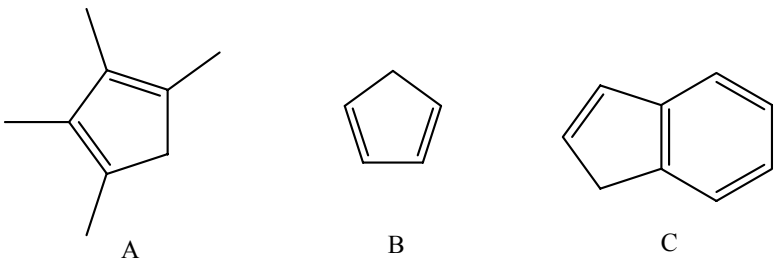

Figure 6.2 A) tetramethylcyclopentadiene; B) cyclopentadiene; C) indene

Changing the metal in the homogeneous CGC also has an effect on catalyst activity and polymer properties. It has been shown in solution polymerizations that zirconium catalysts are slightly more active than analgous titanium and hafnium complexes[3]. However, on a mass basis (grams of polymer per gram of metal), titanium is generally 50% more efficient as a polymerization catalyst than zirconium[3].

In supported CGC-inspired systems made via traditional techniques, Pakkanen and coworkers have synthesized a number of catalysts using various Group IV metals while varying the cyclopentadienyl ligand[4, 5]. In that work, it was reported that the most active metal was zirconium, followed by hafnium, and then titanium (per metal site basis). The zirconium materials synthesized were shown to be more than twice as active as the hafnium materials, and nearly 25-50 times more active than the analogous titanium catalysts. Additionally, two cyclopentadienyl ligands, Cp vs. Cp', were used. The zirconium Cp catalyst was twice as active as the analogous Zr-Cp' system under identical polymerization conditions. This trend held for the other metal systems studied as well. These results, including both the metal and Cp ligand variations, are very different from what has been observed in homogeneous studies [2-5]. For each type of catalyst, the relative activities are shown in Table 6.1. However, as these supported materials can have multiple active-sites, it is difficult to elucidate true structure-reactivity relationships for these systems.

Table 6.1 Relative structure-reactivity relationships of CGC structural variations

Catalyst Structure		Homogeneous Catalyst	Densely Loaded Supported Catalyst
Metal	Ligand		
Ti	Cp'	2	---
Ti	Cp	1	1
Zr	Cp'	2.5	25-50
Zr	Cp	1.3	50-75
Hf	Cp'	0.6	1
Hf	Cp	0.3	15-20

As discussed previously, typical immobilization protocols can produce multi-sited materials. For example, Eisen and co-workers showed that contacting an immobilizable Ti-CGC with a silica surface can result in multiple interactions with the surface creating different types of Ti sites[6]. Pakkanen and coworkers have suggested multiple immobilized ligands can interact with one metal center, again creating a multi-sited CGC-type material when a multi-step grafting synthesis was applied to a densely-loaded aminosilica support[7]. In addition, alkyllithium reagents were used in the synthesis of their materials, which can produce side reactions with the silica surface, again leading to different types of sites.

In this work, we have synthesized several structural variations of the catalyst developed in Chapter 3 using the immobilization protocol shown in Scheme 6.1. In addition to variation in the metal and Cp ligand, a third structural variation unrelated to the active site structure was also studied. By altering the pore size of the support used for immobilization, the role of the pore structure of the silica scaffold on the polymerization was evaluated. The metals studied included titanium, hafnium, and zirconium. These

metals were used in immobilized catalysts with two ligand variations, cyclopentadienyl and tetramethylcyclopentadienyl groups. The effect of support pore size was studied using a tetramethylcyclopentadienyl ligand system with titanium and zirconium catalysts on SBA-15 materials with 50 Å and 100 Å pore diameters.

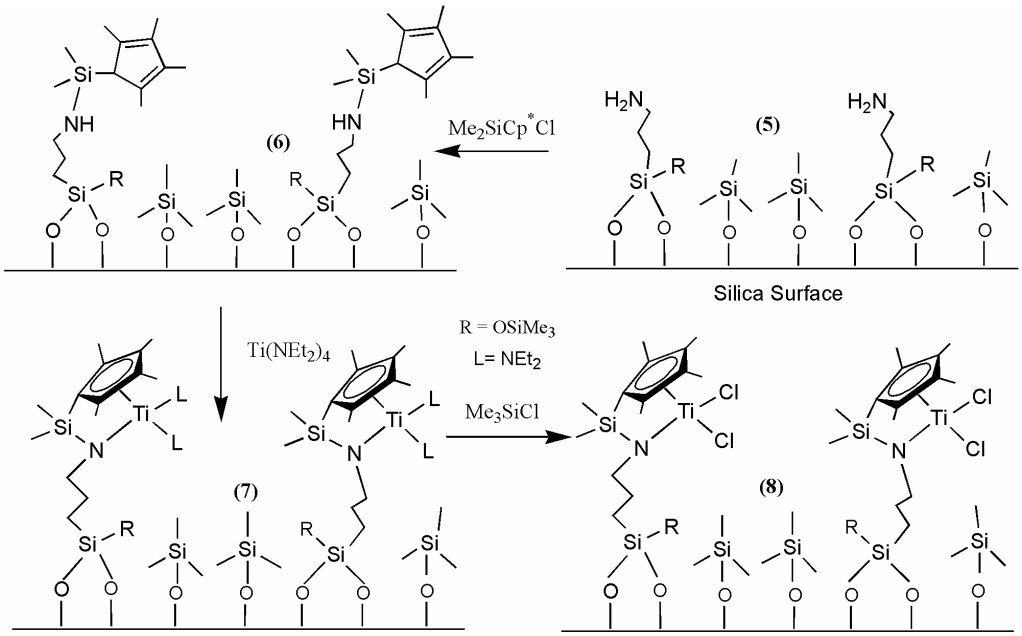

Scheme 6.1 Ti-CGC Synthetic Protocol

6.2 Experimental

Catalyst Synthesis Densely-loaded and patterned aminosilica materials were prepared using a SBA-15 host as described previously[8].

Reaction of chlorodimethyl(cyclopentadienyl)silanes with Amine Functionalized Silica Material. Chlorodimethyl-(2,3,4,5-tetramethyl-2,4-cyclopentadien-1-yl)silane

(excess) was added to a mixture of amine-functionalized silica with hexanes in a drybox. A proton sponge, 2,6-Di-tert-butylpyridine, was added in excess. The mixture was then allowed to stir for 24 h. The solid was collected by filtration, which was followed by washing with hexanes and THF in the drybox. The solid was then contacted with another aliquot of chlorodimethyl-(2,3,4,5-tetramethyl-2,4-cyclopentadien-1-yl)silane and the procedure was repeated.

Metallation of Amino-Cp Silica Materials (M= Ti, Zr, Hf). The solid was packed into a flask in the glovebox with toluene (15 mL). $M(NEt_2)_4$ (1.1 equivalents) was diluted with toluene (5 mL), and both mixtures were cooled. In the drybox, the solution of $M(NEt_2)_4$ in toluene was added to the flask containing the solid dropwise while stirring. After the reaction mixture had warmed to room temperature, it was refluxed for 30 minutes. The solution was filtered off, and the resulting light orange solid was washed with toluene and pentane. The resulting solid was filtered, washed with toluene, dried under vacuum at room temperature overnight on a Schlenk line, and then stored in a drybox

Ligand Exchange. In a drybox, the metallated silica was added to a flask with anhydrous hexanes and excess chlorotrimethyl silane. The reaction was allowed to stir overnight at room temperature. The solid was filtered and washed with hexanes in the drybox. The orange-brown solid was recovered, dried under vacuum overnight at room temperature on a Schlenk line, then stored in a drybox.

Characterization. FT-Raman spectra were obtained on a Bruker FRA-106. At least 256 scans were collected for each spectrum, with a resolution of 2-4 cm^{-1}. Cross-polarization magic angle spinning (CP-MAS) NMR spectra were collected on a Bruker DSX 300-MHz instrument. Samples were spun in 7-mm zirconia rotors at 5 kHz. The ^{13}C CP-MAS parameters were 3000-10000 scans, a 90 pulse length of 4 s, and a delay of 4 s between scans. The ^{29}Si CP-MAS parameters were 1000 scans, a 90 pulse length of 5 s, and a delay of 10 s between scans. Nitrogen physisorption measurements were conducted on a Micromeritics ASAP 2010 at 77K. Samples were pretreated by heating under vacuum at 150 ºC for 8 hours. Average pore diameter was calculated from desorption isotherm. Diffuse reflectance ultraviolet-visible (UV-VIS) spectroscopy was performed on solid materials in a drybox with an Ocean Optics USB2000 Fiber Optic Spectrometer using a PTFE diffuse reflectance standard. Solution UV-VIS spectroscopy was performed using a Hewlett Packard Model 8453 spectrometer with anhydrous hexanes as a solvent. Thermogravimetic analysis (TGA) was performed on a Netzsch STA409. Samples were heated under air from 30 to 1000° C at a rate of 5 °C/min. The organic loading was measured by determining the weight loss from 200 to 650 °C. Elemental analysis was performed by Desert Analytics.

Ethylene Polymerizations

MAO Co-catalyst: The immobilized precatalyst was added to the pressure glass reactor with toluene and methyl alumoxane (800 Al:1 Ti) in a drybox. The solution was stirred for 20 minutes to allow for sufficient activation of the catalyst. The reactor was then sealed and removed from the glovebox, placed in a 25 °C waterbath, and subsequently

connected to an ethylene source at 60 psi. The ethylene was delivered for a prescribed amount of time and the polymerization was terminated by releasing the ethylene pressure and adding acidic ethanol. The precipitated polymers were washed with acetone, then dried at 70 ºC.

Borane co-catalyst: In a typical polymerization, the immobilized precatalyst was added to the pressure glass reactor with toluene, tris(pentafluorophenyl) borane (1.5 B:1 Ti), and either trimethyl aluminum or triisobutyl aluminum (400:1 Al:Ti ratio) in a drybox. The mixture was allowed to stir for 30 minutes to allow for sufficient activation of the catalyst. The reactor was then sealed and removed from the glovebox, placed in a 25 °C waterbath, and ethylene at 60 psi was introduced as described above. The polymerization was allowed to continue for a prescribed amount of time, then terminated as noted above. The precipitated polymers were washed with acetone, then dried at 70 °C.

6.3 Results and Discussion

6.3.1 Catalyst synthesis and characterization

The work previously discussed has focused on a catalyst with a titanium metal center, a coordination environment with a tetramethyl-cyclopentadienyl ligand, and a SBA-15 support with approximately 50 Å pores. In this work, these structural components were varied to begin to develop structure-reactivity relationships for the immobilized catalysts.

The first variation to be studied was changing the metal center of the catalyst. For each metal, a patterned and densely functionalized aminosilica sample was used as a

scaffold. The aminosilica materials were then reacted with chlorodimethyl(2,3,4,5-tetramethyl-2,4-cyclopentadien-1-yl)silane (Cp'-silane). An amine elimination route was again used to metallate the Cp'-silane functionalized solids. The metallation sources used were tetrakis(diethylamino)titanium, tetrakis(diethylamino)zirconium, and tetrakis(diethylamino)hafnium. The elemental analyses of the resulting materials are listed in Table 6.2. Functionalization of the aminosilicas with Cp'-silane proceeded as previously discussed. It should be noted the slight excess of Cp'-silane (compared to amine) detected in the patterned materials used in this work. The magnitude of this excess is very small (less than 3%) and is likely experimental error. As previously shown, Cp'-silane does not react with a capped silica, therefore the only available reactive site for the silane is the immobilized amine[8, 9].

The metallation efficiencies of the three metals on the patterned scaffold are very similar. The titanium loading is 105% of the cyclopentadienyl loading, zirconium is ~100%, and the hafnium is slightly higher at 108%. These are very similar to the results seen previously with titanium, including the observation that all of the metallations on the

Table 6.2 Material Characterization of Various Metallations

	Titanium		Zirconium		Hafnium	
Material Description	Patterned Silica	Densely Functionalized	Patterned Silica	Densely Functionalized	Patterned Silica	Densely Functionalized
Amine Loading (mmol/g)	0.36[a,b]	1.35[a]	0.36[a,b]	1.35[a]	0.36[a,b]	1.35[a]
Cp' Loading (mmol/g)	0.37[b]	0.82[b]	0.37[b]	0.82[b]	0.37[b]	0.82[b]
Metal Loading (mmol/g)	0.39[b]	0.52[b]	0.37[b]	0.41[b]	0.40[b]	0.37[b]

a: Loading determined by TGA; b: Loading determined by Elemental Analysis

patterned material proceeded nearly quantitatively (again, the slight excess is nearly within experimental error). In all cases, the metal loading is very different than with the materials prepared on densely loaded solids, which only show 46-64% metallation efficiencies. These results, when compared to the results of the densely loaded materials, suggest that the metal chosen has little effect on the functionalization of the patterned Cp'-silane material. In comparion, the loading trend on the densely loaded materials appears it may be a function of metal size. Increasing the size of the metal (from Ti to Zr to Hf), leads to a decrease in metal loading.

FT-Raman spectroscopy was also used to characterize the materials. The FT-Raman spectra of the patterned Cp'-silane and Ti-CGC materials were previously reported in Chapter 3 (Figure 3.4). The FT-Raman spectra of the patterned Cp'-silane and hafnium metallated materials are shown below (Figure 6.3). The large signals at ~2900 cm-1 are associated with aliphatic C-H stretches. Sample fluorescence makes

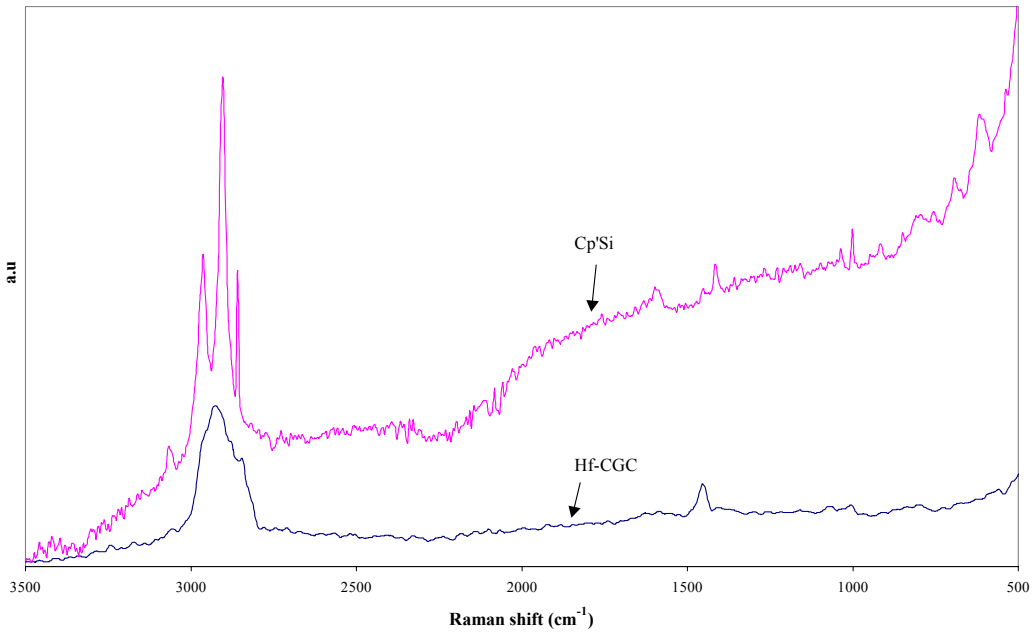

Figure 6.3 FT-Raman Specta of Cp'-silane and Hf-CGC

assignments of additional peaks in the Cp'-silane spectra difficult. The spectrum of the hafnium metallated sample is very similar to the titanium spectrum shown previously. This is to be expected, as the metallation should not alter the Raman shifts of the surface functionalities. The patterned zirconium was not able to be characterized via FT-Raman spectroscopy due to fluorescence of the sample skewing the resulting spectrum.

The various metallated samples were also studied by UV-Vis spectroscopy and the spectra are shown in Figure 6.4. As shown in Chapter 3, while this method does not provide conclusive proof of the formation of a CGC type complex on the surface, it does allow for information to be gathered on the metal center and its cyclopentadienyl ligand. The peak absorbance seen in the Cp'-silane spectra at 310 nm is assigned to a π to π^* transition of the cyclopentadienyl functionality [10]. Upon metallation, the characteristic UV-Vis signal changes to a peak at 245 nm, likely a transition of the metal center, and a ligand to metal charge transfer (LMCT) signal (from the complexed cyclopentadienyl ligand to the metal) appearing as a shoulder at 330 nm [10]. The change in the spectrum is a clear indication of ligation of the Cp groups with the metal centers. The spectra for the

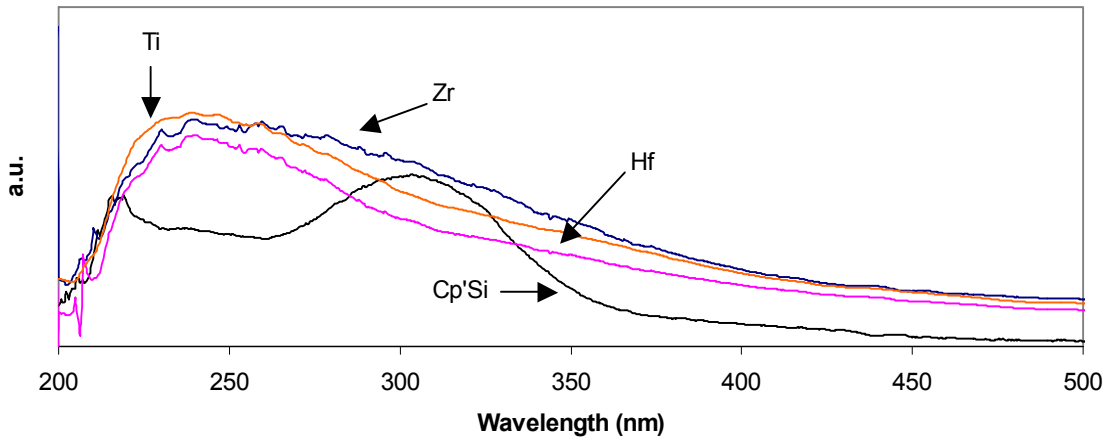

Figure 6.4 UV-Vis Spectra for Metallated Cp' CGC Materials

titanium and hafnium materials are very similar. The signal assigned to the LMCT in the zirconium material is much broader than in the other Group IV metals.

Nitrogen physisorption was used to characterize the surface area and pore size of the materials and the results are tabulated below (Table 6.3). Functionalization of the silica results in a decrease in surface area and pore diameter as expected. However, the pore structure is still maintained, suggesting the synthesis of the immobilized complexes do not result in pore blockage for small probe molecules such as N_2. There are no significant differences in the nitrogen physisorption results for solids with different metal species.

Table 6.3 Nitrogen Physisorption Results

Sample	BET surface area (m^2/g of SiO_2)	Average pore diameter[a] (Å)
SBA-15	675	50
Patterned Aminosilica	575	47
Cp' Functionalized SBA	419	42
Ti-Metallated	384	35
Zr-Metallated	365	34
Hf-Metallated	372	37

a: Determined from desorption isotherm

In addition to variations in the metal center of the immobilized complex, changing the ligand environment of the catalyst can have a significant impact on catalyst activities and polymer properties. As such, we chose to replace the tetramethylcyclopentadienyl ligand used previously with a cyclopentadienyl ligand, chloro-cyclopenta-2,4-dienyl-dimethyl-silane (Cp-silane). The reaction of the supported amine with the Cp-silane was performed in a similar method to the tetramethylcyclopentadienyl group used before.

After contacting with two aliquots of the silane, there is approximately 94% reaction of the patterned amine sites, suggesting the Cp-silane may be slightly less reactive than the Cp'-silane. A homogeneous reaction analog of the Cp-silane/amine reaction was performed using propyl amine instead of a supported amine, which provides additional evidence for lower reactivity of the Cp-silane. This reaction results in a ~65% yield, compared to nearly 80% when the Cp'silane/propyl amine coupling is performed. Metallation of the patterned Cp-silane materials also appears to occur less efficiently than on the Cp'-silane material. The titanium and zirconium reactions showed loadings which correspond to approximately 90% functionalization of the Cp-silane and approximately 83% metallation of the patterned amine sites. The amine elimination with tetrakis(diethylamino)hafnium resulted in 76% metallation of the Cp-silane and 72% metallation of the amines. On the densely functionalized material, roughly 65% of the immobilized amines are functionalized with Cp-silane, very similar to the results seen with the densely functionalized Cp'-silane. Metallation results in a metal loading consistent with 40-60% of the Cp-silane reacting. Elemental analysis of the materials discussed are shown in Table 6.4.

The elemental analysis of the materials suggests that changing the immobilized ligand from a Cp'-silane to a Cp-silane decreases the effectiveness of the metallation reactions. This trend is seen in most of the patterned and densely functionalized materials, with the exception being densely functionalized zirconium materials, which show similar loadings.

Table 6.4 Material Characterization of Cp Functionalized Materials

	Titanium		Zirconium		Hafnium	
Material Description	Patterned Silica	Densely Functionalized	Patterned Silica	Densely Functionalized	Patterned Silica	Densely Functionalized
Amine Loading (mmol/g)	0.36[a,b]	1.35[a]	0.36[a,b]	1.35[a]	0.36[a,b]	1.35[a]
Cp Loading (mmol/g)	0.34[b]	0.89[b]	0.34[b]	0.89[b]	0.34[b]	0.89[b]
Metal Loading (mmol/g)	0.30[b]	0.43[b]	0.31[b]	0.51[b]	0.26[b]	0.36[b]

a: Loading determined by TGA; b: Loading determined by Elemental Analysis

The patterned materials synthesized with a Cp ligand were also characterized by solid state NMR. Figure 6.5 shows the ^{29}Si CP-MAS NMR spectra of the Cp-silane functionalized solid (A) and the zirconium metallated material following ligand exchange (B). In both spectra, the large peak from approximately –95 ppm to –110 ppm corresponds to the Q2, Q3, and Q4 signals of the silica framework[11]. The alkyl linkages to the surface can be characterized by the Si-C bond resonances at -59, and -68 ppm, which correspond to the reaction of 2 and 3 methoxy groups with the silanols on the surface[12]. The ^{29}Si resonance characteristic of the capping agent can be seen at 14 ppm. The broad peak seen in the Cp-silane material (A) at –21 ppm is assigned to the bridging silicon between the immobilized amine and the cyclopentadienyl ring[13]. In comparing the metallated material (B) with the unmetallated material, it is expected that the resonances would not show significant changes. However, the resonance assigned to the bridging silicon disappears in the metallated sample. This is likely the result of coupling associated with the zirconium metal center (vida infra).

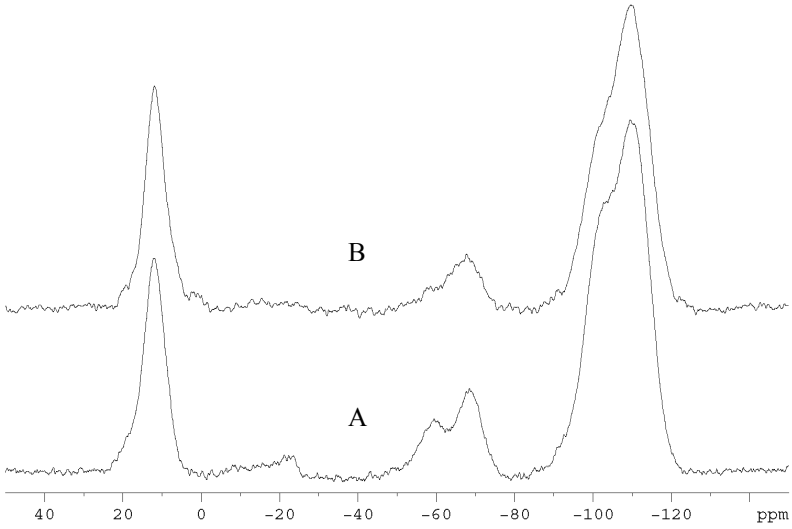

Figure 6.5 ^{29}Si CP-MAS NMR Spectra: A) Patterned Cp-silane functionalized solid; B) Patterned Zr Cp-silane solid

The ^{13}C CP-MAS NMR spectrum in Figure 6.6 shows the result of the reaction of the cyclopentadienyl functionality with the patterned aminosilica (A). Also illustrated is the spectrum of the zirconium metallated solid after ligand exchange (B). Specific band assignments are given in Table 6.5. These NMR spectra show the expected carbon-containing surface functionalities are present, although even with the use of cross-polarization techniques, the signal to noise ratio is poor. The important resonances present include the carbons in the cyclopentadienyl functionality, which can be found at 128 ppm. The signal at 67 ppm is a spinning side band of the peak at 0 ppm. Upon metallation and ligand exchange, little change is expected in the ^{13}C NMR spectra, however, the peak assigned to the cyclopentadienyl carbons is missing similar in the ^{29}Si

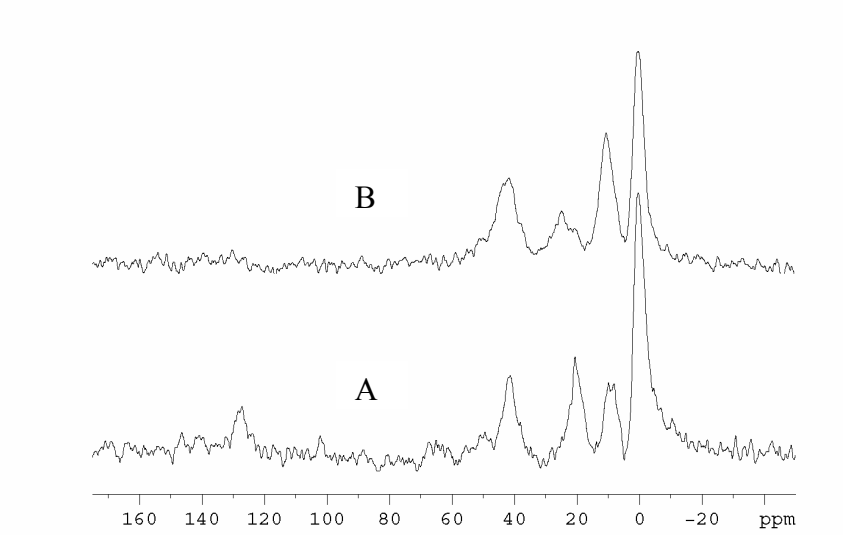

Figure 6.6 ^{13}C CP-MAS NMR Spectra A) Patterned Cp-silane functionalized solid; B) Patterned Zr Cp-silane solid

Table 6.5 ^{13}C CP-MAS NMR Assignments

Assignment	Resonance (ppm)
Capping Agent: -Si-(**C**H_3)$_x$	0
Propyl linker: -Si-**C**H_2-CH_2	10
Propyl linker: -CH_2-**C**H_2-CH_2	20
Propyl linker: -N-**C**H2-CH2	42
Methoxy: -O**C**H_3	50
Cp ring: **C**$_5H_4$	128

spectrum. In a ^{13}C decoupling MAS NMR experiment conducted when this spectrum was taken, these Cp carbons were able to be seen. This suggests the disappearance of these peaks in the cross polarization experiments is likely the result of carbon coupling with zirconium. This coupling allows faster relaxation of the Cp carbons, preventing effective cross-polarization[14].

FT-Raman spectroscopy was also used to characterize the patterned Cp functionalized materials. The results can be seen in Figure 6.7. The characteristic peaks seen in the patterned Cp-silane at ~2900 cm^{-1} are associated with aliphatic C-H stretches. The small peak at ~3050 cm^{-1} corresponds with aromatic C-H stretches due to a small fraction of the trityl imine remaining on the surface. This spectrum has nearly identical features as the tetramethycyclopentadienyl functionalized material (Figure 6.2). This is

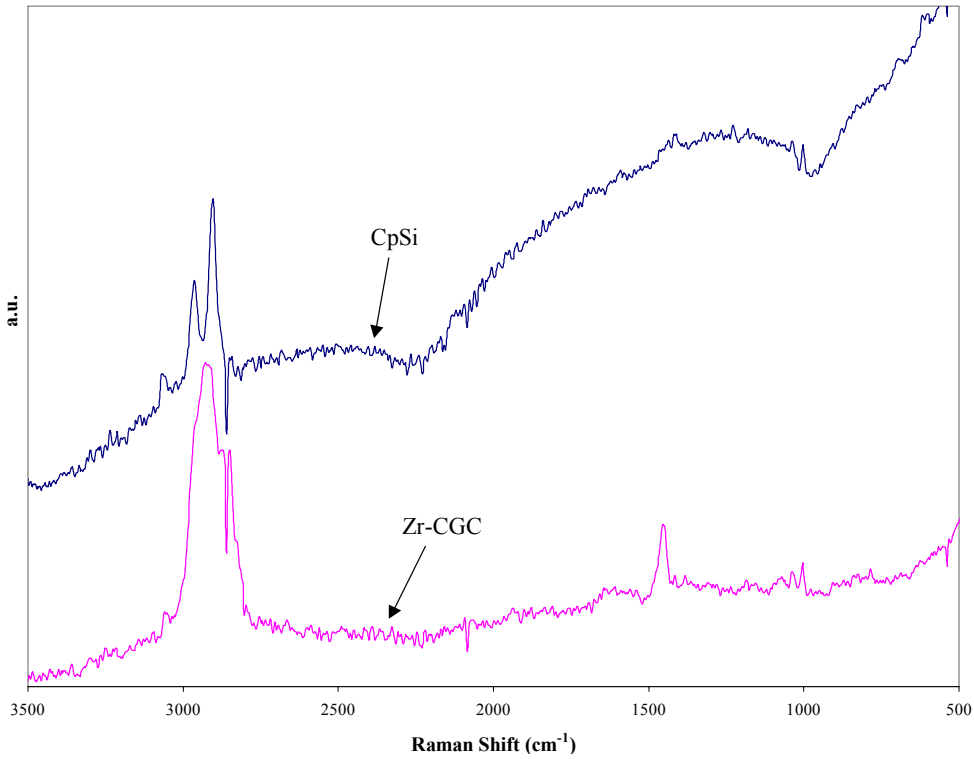

Figure 6.7 FT-Raman Spectra of patterned Cp-silane materials

to be expected as fluorescence hinders peak assignment at lower wavenumbers, which is where C-C stretches would be found. Upon metallation, a significant change in spectra was not expected nor seen in the supported zirconium solid.

The patterned Cp-silane solids were also characterized via UV-Vis spectroscopy. The spectra are shown in Figure 6.8. In the Cp-silane-functionalized solid, the peak absorbance observed at 275 nm is assigned to a π to π* transition of the cyclopentadienyl functionality[10]. This is a different transition than seen in the Cp'-silane materials, as expected. Upon metallation, the characteristic UV-VIS signals change to a peak at 245 nm, likely a transition of the metal center, and a ligand to metal charge transfer (LMCT) signal (from the complexed cyclopentadienyl ligand to the metal) appearing as a shoulder that extends to approximately 350 nm. It should be noted the hafnium and zirconium samples appear to have a larger LMCT signal than the titanium solid. A similar trend was seen in the zirconium-metallated Cp'-silane solid (Figure 6.4). As discussed previously in Chapter 3, UV-Vis was unable to distinguish between the metal sites supported on the patterned aminosilica and densely functionalized aminosilica. Figure

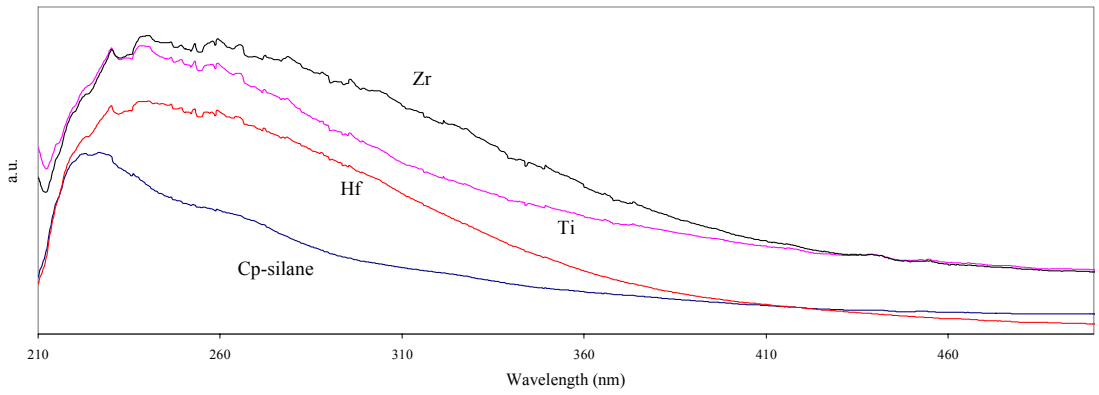

Figure 6.8 UV-Vis comparison of patterned Cp-silane solids

6.8 shows the UV-Vis spectra of patterned and densely functionalized hafnium metallation Cp-silane materials solids. There is no distinguishable difference between the two spectra, confirming the results seen in the Ti-Cp' materials.

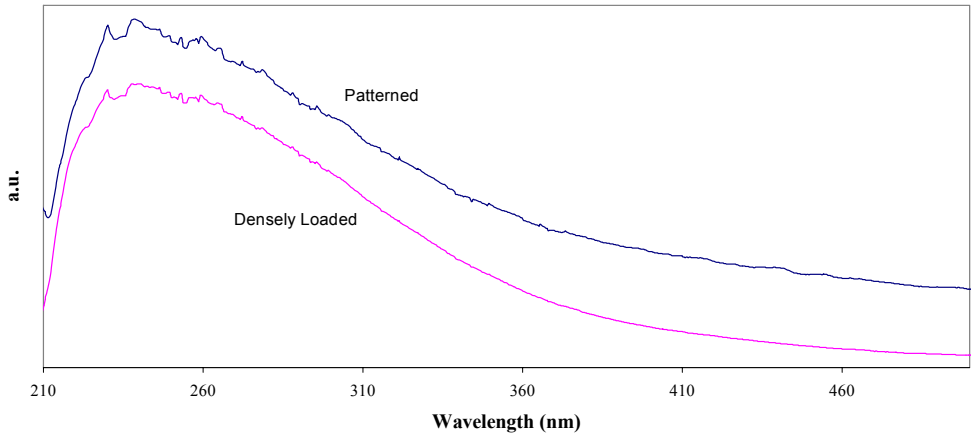

Figure 6.9 UV-Vis comparison of Hf Cp-silane-CGC solids

These materials were also characterized by nitrogen physisorption. The surface areas and average pore diameters determined from these experiments are listed in Table 6.6. The low metallation efficiency of the hafnium source is consistent with the slightly higher surface area of the Hf metallated Cp-silane material than the other metallated samples. The other data are similar to those seen in the Cp'-silane work. Again, the data are consistent with the hypothesis that the mesoporous silica framework is retained throughout the functionalization protocol.

Table 6.6 Nitrogen physisorption comparison of Cp-silane solids

Sample	BET surface area (m^2/g of SiO_2)	Average pore diameter[a] (Å)
SBA-15	675	50
Patterned Aminosilica	575	47
Cp-silane SBA	464	44
Ti-Metallated	368	34
Zr-Metallated	378	39
Hf-Metallated	396	43

a: Determined from desorption isotherm

The final parameter probed in this work is the effect of variation in support pore size. The patterning protocol was developed using SBA-15 with approximately 50 Å pore diameter. In Chapter 4, Ti-CGC complexes were assembled on SBA-15 with larger pores, approximately 100 Å in diameter. Using this support, Ti and Zr complexes with a Cp'-silane ligand were synthesized using a patterned aminosilica scaffold. The material characterization results are tabulated below (Table 6.7). The metallation of the Cp'-silane proceeds at a nearly quantitative level for both Ti and Zr metal complexes.

Table 6.7 Material Analysis for Large Pore CGC-Synthesis

	Titanium		Zirconium	
Material Description	Patterned Silica	Densely-Functionalized	Patterned Silica	Densely-Functionalized
Amine Loading (mmol/g)	0.57[a,b]	1.35[a,b]	0.57[a,b]	1.35[a,b]
Cp'-silane Loading (mmol/g)	0.54[a,b]	0.84[a,b]	0.54[a,b]	0.84[a,b]
Metal Loading (mmol/g)	0.56[b]	0.68[b]	0.53[b]	0.65[b]

a: Loading determined by TGA; b: Loading determined by Elemental Analysis

Nitrogen physisorption was used to characterize the porosity of the materials and the results are shown in Table 6.8. In the adsorption isotherm of the SBA-15 material, there is only the ~100 Å peak present. However, in the desorption isotherm, a small amount of ~35 Å pores can be seen (Figure 6.10). These pores are likely the result of incomplete incorporation of the pore swelling agent used in the SBA-15 synthesis.

Table 6.8 Nitrogen physisorption comparison of Cp-silane solids

Sample	BET surface area (m^2/g of SiO_2)	Average pore diameter[a] (Å)
SBA-15	905	107
Patterned Aminosilica	792	96
Cp' Functionalized SBA	696	85
Ti-Metallated	603	74
Zr-Metallated	621	79

a: Determined from desorption isotherm

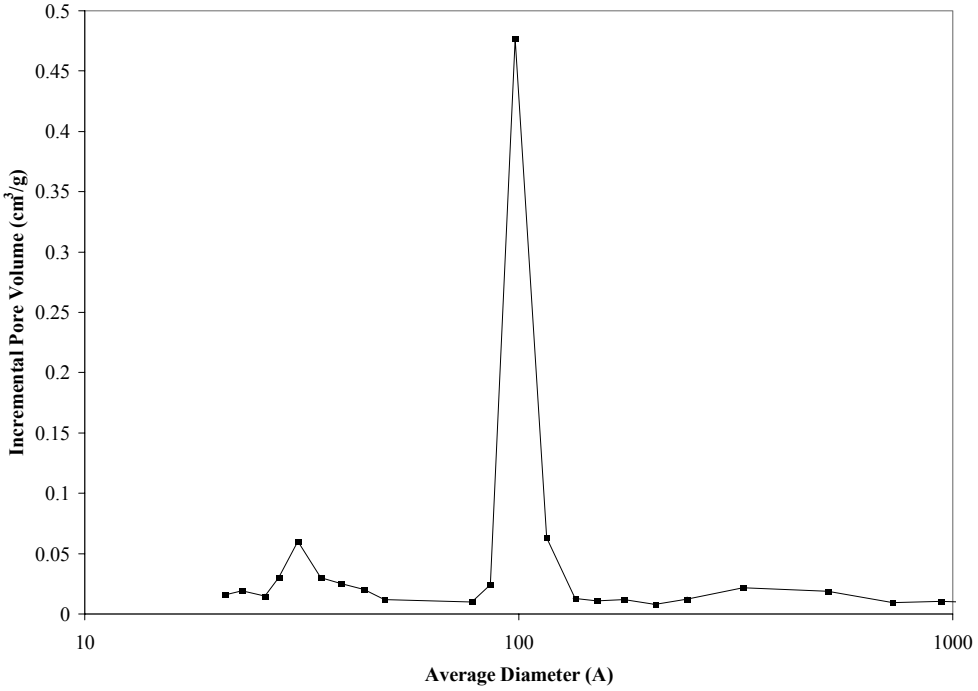

Figure 6.10 Pore size distribution calculated from desorption isotherm for large pore SBA-15

6.3.2 Catalyst testing and polymerization results

One of the goals of this work is to begin to elucidate the structure-reactivity relationships for an immobilized CGC. As such, the catalysts synthesized above were tested in ethylene polymerizations. The catalysts were tested using two common co-catalysts, methylalumoxane (MAO) and a borane/trialkylaluminum system. Polymerizations were performed as discussed previously.

The ethylene polymerization results of the various metallated Cp'-silane materials are shown in Table 6.9. The patterned titanium complexes are the most active materials, followed closely by the zirconium. Patterned hafnium catalysts show approximately half the productivity of the other two metals when MAO is used. Using a borane/alkylaluminum cocatalyst, the same trend is observed. As previously discussed, the borane/alkylaluminum co-catalyst systems do not leach metal complex and therefore they provide a better insight into the performance of immobilized species. The polymerization procedure was optimized (i.e. solvent volume, activation time, co-catalyst

Table 6.9 Ethylene Polymerization Results for Cp'-silane CGC solids

	Titanium		Zirconium		Hafnium	
Material Description	Patterned Silica	Densely Functionalized	Patterned Silica	Densely Functionalized	Patterned Silica	Densely Functionalized
Metal Loading (mmol/g)	0.39[a]	0.52[a]	0.37[a]	0.41[a]	0.40[a]	0.37[a]
Productivity (kg PE/mol M hr) MAO[b]	19.4	6.2	18.7	1.2	8.5	Trace
Productivity (kg PE/mol M hr) borane[c]	23.7	1.8	15.1	3.8	4.0	1.6

a: Loading determined by Elemental Analysis; b: conditions: T = 25 ºC; co-catalyst: MAO; Al/Ti = 800; solvent: toulene; ethylene pressure: 60 psi; reaction time: 10 min.; c: conditions: T = 25 ºC; co-catalyst: borane/triisobutylaluminum; Al/Ti = 400; solvent: toulene; ethylene pressure: 60 psi; reaction time: 10 min.

ratios) using the titanium catalyst systems. Therefore, it is possible the zirconium catalysts require slightly longer activation time or more solvent must be used to reach its maximum productivity. It is also possible there is more inactive complex formation of the immobilized zirconium CGCs. More in-depth studies will be required to compare these catalysts under a variety of polymerization conditions to further develop structure-reactivity relationships.

The polymerization results using the various immobilized catalysts with a Cp-silane ligand are shown in Table 6.10. In general, these catalysts are less active than the respective Cp'-silane materials, which is consistent with trends seen in the homogeneous literature. The only exception to this is the hafnium/borane system where the Cp material is more active than the Cp' materials. The trends between the metals are similar to that seen in the Cp'-silane materials. The patterned titanium catalysts have the highest productivity, regardless of the co-catalyst used. However, with this ligand system,

Table 6.10 Ethylene polymerization results with Cp-silane CGC solids

	Titanium		Zirconium		Hafnium	
Material Description	Patterned Silica	Densely Functionalized	Patterned Silica	Densely Functionalized	Patterned Silica	Densely Functionalized
Metal Loading (mmol/g)	0.30[b]	0.43[b]	0.31[b]	0.51[b]	0.26[b]	0.36[b]
Productivity (kg PE/mol M hr) MAO[b]	22.7	11.0	14.9	1.1	9.2	2.0
Productivity (kg PE/mol M hr) borane[c]	23.0	Trace	11.9	3.1	12.3	1.1

a: Loading determined by Elemental Analysis; b: conditions: T = 25 ºC; co-catalyst: MAO; Al/Ti = 800; solvent: toulene; ethylene pressure: 60 psi; reaction time: 10 min.; c: conditions: T = 25 ºC; co-catalyst: borane/triisobutylaluminum; Al/Ti = 400; solvent: toulene; ethylene pressure: 60 psi; reaction time: 10 min.

the zirconium and hafnium catalysts showed essentially the same productivity when activated by the borane system, a very different result than in the Cp'-silane materials. Also of note is the similarity between activities of the MAO and borane co-catalysts. This suggests that these materials may be less susceptible to leaching from contact with MAO.

The ethylene polymerization results for the Ti and Zr metallated Cp'-silane materials synthesized on 100 Å SBA-15 are shown in Table 6.11. The reactivity of the titanium catalysts is higher compared to the reactivity of the zirconium catalysts, mirroring the trends discussed above. In general, the complexes assembled on the smaller pore material are higher in activity than those assembled on the larger pore material. The lone exception to this generalization is when Ti materials activated by MAO are considered, which is skewed by leaching results as discussed previously. The Ti metallated Cp'-silane complex on large pore SBA can attribute nearly half of its

Table 6.11 Ethylene polymerization results with large pore CGC solids

Support Pore Size (Å)	Metal	Co-catalyst	Productivity (kg PE/mol M hr)
50	Ti	MAO[a]	19.4
50	Ti	Borane/TIBA[b]	23.7
50	Ti	Borane/TMA[b]	27.7
100	Ti	MAO[a]	22.1
100	Ti	Borane/TIBA[b]	19.0
100	Ti	Borane/TMA[b]	19.6
50	Zr	MAO[a]	18.7
50	Zr	Borane/TIBA[b]	15.1
50	Zr	Borane/TMA[b]	14.3
100	Zr	MAO[a]	12.3
100	Zr	Borane/TIBA[b]	11.5
100	Zr	Borane/TMA[b]	13.0

conditions: T = 25 ºC; solvent: toulene; ethylene pressure: 60 psi; reaction time: 10 min.; a: co-catalyst: MAO; Al/Ti = 800 b: co-catalyst: borane/trialkylaluminum; Al/Ti = 400.

activity to leached species (reported in Chapter 4), whereas leaching accounts for approximately 15% of the activity of the small pore system (reported in Chapter 3).

It might be expected that having a larger pore structure would increase mass transfer to the metal sites that are immobilized within a pore. This would ideally enable a higher efficiency of activation by the co-catalysts and increased diffusion of monomer to the catalytic sites. However, these results suggest neither of these benefits occur. One possible explanation is that in a larger pore material, a larger number of the active sites are located within the pores. As the polymerization occurs very quickly, the pore could quickly become clogged, blocking monomer from reaching any of the sites within the pore. With smaller pores, it is less likely to have immobilized a large number of metal sites on the interior pore wall, and this may make pore blockage less important during polymerization. It has been shown in the literature, in a polymerization catalyzed by a silica supported metallocene, enough polymer can form to fracture the silica particle, thereby exposing previously inaccessible metallocenes to monomer[15-17]. However, as these supported metallocenes are several orders of magnitude more active than the systems being studied in this work, it is unlikely enough polymer is being produced to fracture the SBA-15 support. To facilitate fracture studies, the commercial silica used is designed to fracture from 50 micron spherical particles to fragments of approximately 10 nm grain size, a phenomenon unlikely in SBA-15[17]. Aida and coworkers have reported the use of fibrous silica scaffold for supporting metallocenes[18]. These materials allow for an extrusion type polymerization to occur. Future work could entail using microscopy to examine the produced polymer, specifically to determine the effect (if any) the polymerization has on the silica support.

In general, the structure-reactivity relationships seen in the patterned catalysts are similar to those reported in homogeneous CGC studies. On a molar basis, titanium and zirconium catalysts have similar activities, while hafnium catalysts are less productive. On a mass basis, the titanium materials are much more active than any of the other materials. The results seen here are very different than the structure-reactivity relationships seen in previous work done on immobilized CGCs, likely due to the fact that the literature materials were shown to have multiple types of active sites.

6.4 Summary

A number of structural variations of immobilized CGC-type complexes were synthesized by modifying the patterning protocol previously developed. The synthesis of the patterned catalysts, regardless of the ligands or metals chosen, proceeded at a higher conversion than the densely loaded materials, which is consistent with the results seen in the initial titanium-Cp' catalysts synthesized. Preliminary structure-reactivity relationships developed for the patterned systems suggest among Group IV metals, titanium is the most productive, although the zirconium system is only slight less active. It was also shown the effect of changing cyclopentadienyl ligands mirrors the effect seen in analogous homogeneous systems. This continuity between the homogeneous structure-reactivity relationships and the patterned structure-reactivity relationships provides further evidence for the formation of perhaps a single-type of immobilized complex when the patterning protocol is followed. In comparison to literature materials, which have been shown to be multi-sited, there is no agreement between homogeneous and supported catalysts, suggesting it is in fact the formation of the multiple types of sites

which plays a large role in the behavior of the traditionally synthesized immobilized CGCs.

6.5 References

1. McKnight, A. L.; Waymouth, R. M., *Chem. Rev.* **1998,** *98*, 2587-2598.

2. Stevens, J. C., *Stud. Surf. Sci. Catal.* **1994**, 277-284.

3. Stevens, J. C.; Timmers, F. J.; Wilson, D. R.; Schmidt, G. F.; Nickias, P. N.; Rosen, R. K.; Knight, G. W.; Lai, S. Y. Eur Pat. Appl. 0 416 815 A2, 1991.

4. Juvaste, H.; Pakkanen, T. T.; Iiskola, E. I., *Organometallics* **2000,** *19*, 1729-1733.

5. Juvaste, H.; Pakkanen, T. T.; Iiskola, E. I., *Organometallics* **2000,** *19*, 4834-4839.

6. Galan-Fereres, M.; Koch, T.; Hey-Hawkins, E.; Eisen, M. S., *J. Organomet. Chem.* **1999,** *580*, 145-155.

7. Timonen, S.; Pakkanen, T. T.; Iiskola, E. I., *J. Organomet. Chem.* **1999,** *582*, 273-278.

8. McKittrick, M. W.; Jones, C. W., *Chem. Mater.* **2003,** *15*, 1132-1139.

9. McKittrick, M. W.; Jones, C. W., *J. Am. Chem. Soc.* **2004,** *126*, 3052.

10. Calleja, G.; van Grieken, R.; Garcia, R.; Melero, J. A.; Iglesias, J., *J. Mo.l Cata.l A* **2002,** *182*, 215-225.

11. Engelhardt, G.; Michel, D., *High Resolution Solid-State NMR of Silicates and Zeolites*. ed.; John Wiley and Sons: New York, 1988.

12. Sindorf, D. W.; Maciel, G. E., *J. Am. Chem. Soc.* **1983,** *105*, 3767-3776.

13. Alt, H. G.; Fottinger, K.; Milius, W., *J. Organomet. Chem.* **1998,** *564*, 109-114.

14. Dr. Johannes Leisen, Research Scientist Georgia Institute of Technology, Personal communications

15. Goretzki, R.; Fink, G.; Tesche, B.; Steinmetz, B.; Rieger, R.; Uzick, W., *J. Polym. Sci. Pol. Chem.* **1999,** *37*, 677-682.

16. Steinmetz, B.; Tesche, B.; Przybyla, C.; Zechlin, J.; Fink, G., *Acta Polym.* **1997,** *48*, 392-399.

17. Knoke, S.; Korber, F.; Fink, G.; Tesche, B., *Macromol. Chem. Phys.* **2003,** *204*, 607-617.

18. Kageyama, K.; Tamazawa, J.; Aida, T., *Science* **1999,** *285*, 2113-2115.

CHAPTER 7

SUMMARY AND FUTURE WORK

7.1 Summary

The major goals of this thesis work were to:

1. Develop a new methodology for the preparation of site-isolated catalytic sites on a silica surface.
2. Prepare the first truly single-site supported metallocene/CGC polymerization catalyst.
3. Develop structure-reactivity relationships for these new systems.

To synthesize these novel catalysts, the approach taken was to develop a protocol which allows for the synthesis of an aminosilica material with isolated, uniform amine sites. This patterning protocol was based on using a trityl-imine patterning agent to prevent unwanted interactions between the resulting amines and the surface. These patterned amine sites were shown to react uniformly[1]. Probe reactions showed they were separated by at least 8-10 Å. In comparison, traditionally grafted aminosilica materials show evidence of having multiple types of reactive amine sites.

This patterned aminosilica was then used as a scaffold to support a constrained geometry catalyst. The protocol developed involved reacting a tetramethyl-cyclopentadienyl silane with the immobilized amine sites. Metallation with tetrakis(diethylamino)titanium was performed using an amine elimination route. These functionalizations occurred at essentially a quantitative level, in stark contrast to previous literature reports[2-7]. The materials were characterized by a battery of techniques, including nitrogen physisorption, thermogravimetric analysis, elemental analysis, ^{13}C and

^{29}Si CP-MAS NMR, FT-Raman spectroscopy, and diffuse reflectance UV-Vis spectroscopy. UV-Vis was used to attempt to elucidate the speciation of the metal center, the first such report for immobilized CGC materials. These patterned catalysts were evaluated in the polymerization of ethylene and compared to densely loaded literature materials. Overall, it was found the patterned materials were 5-10 times more active than traditional immobilized CGC catalysts.

The patterned catalysts were also found to be effective catalysts for the copolymerization of norbornenes and ethylene, which was the first reported use of a tethered CGC for the production of ethylene-norbornene copolymers. Similar to results seen in literature for homogeneous systems, the copolymerization occurred with a higher productivity than the respective homopolymerizations. Functionalized norbornenes, including a polar monomer, were also able to be polymerized. The control materials were inactive in these polymerizations, providing further evidence that the patterning protocol allows for the synthesis of unique highly active, isolated catalytic sites.

Additional work was done in comparing two metallation strategies commonly used in the synthesis of CGCs. Using the same aminosilica scaffolds, the Royo and Jordan methods for metallation were compared using various characterization techniques and polymerization studies[8-11]. This was the first report of a direct comparison of using these metallation protocols for the synthesis of immobilized CGCs. These studies showed that the Royo metallation yielded a more active titanium site than the amine elimination metallation. However, this method also yielded materials with significantly lower metal loadings than the amine elimination route. Both metallation routes showed improved performance of the immobilized complexes when the patterned aminosilica

scaffold was used compared to the densely loaded aminosilica scaffold. In fact, the formation of an entirely different type of immobilized complex structure was created for the densely functionalized materials using the Royo protocol.

Various structural components of the immobilized CGC developed in this work were then tested for their impact on the catalyst synthesis and reactivity in ethylene polymerizations. The metal was varied with hafnium and zirconium materials added to the titanium system previously studied. The ligand was varied to include a tetramethylcyclopentadienyl ring or a cyclopentadienyl ring. The effect of changing the pore diameter of the mesoporous silica scaffold used was also studied. The results showed the patterned materials in general behaved according to the trends seen in homogeneous CGC polymerizations. Titanium and zirconium were found to have activities of roughly similar values, with hafnium materials slightly less active. The use of a tetramethylcyclopentadienyl ring as a ligand led to a more active catalyst than a cyclopentadienyl ring. These results, while congruent with similar homogeneous CGC studies, are in direct conflict with previous work on supported CGCs reported in the literature. This discrepancy is likely the result of the difference between the isolated, possibly single-site patterned catalysts developed in the course of this work and the multi-sited catalysts prepared by traditional supporting protocols. This also further illustrates the difficulty in developing structure-reactivity relationships when ill-defined solid catalysts are used.

The goal of this thesis work was to develop a single-site olefin polymerization catalyst supported on a mesoporous silica material, and to begin the development of structure-activity relationships for these supported systems. This was accomplished by

combining a patterning protocol allowing for the synthesis of a novel aminosilica and adaptation of literature metallation protocols for functionalization of the aminosilica to produce solid CGC materials. These catalysts were studied in the polymerization of ethylene, showing a significant increase in activity over traditional materials. Additional chemistries explored in this system were the copolymerization of ethylene and norbornenes, including polar norbornenes, and the effect of metallation route on complex formation. Preliminary development of structure-reactivity relationships was also studied, which confirmed the importance of using a well-defined immobilized catalyst for further elucidation of these relationships.

7.2 Recommendations for Future Work

7.2.1 Potential Applications for Patterned Aminosilica

The development of the patterned aminosilica was a smaller objective towards the larger goal of synthesizing a well-defined, isolated, single-site organometallic catalyst for olefin polymerization. However, this aminosilica has potential uses in a variety of field which could present benefits over traditionally prepared materials. Some of the areas for future work with the patterned aminosilica include:

1. Supporting various organometallic complexes
2. Adsorption/Separation applications
3. Supporting co-catalysts for olefin polymerizations

Possible future work would involve using the aminosilica scaffold as a support for other organometallic complexes. One such class of complexes are the FI catalysts developed by Fujita and coworkers[12]. The complexes developed are extremely active catalysts for olefin polymerization, with the potential to have a larger impact on the field than metallocenes and CGCs. It was been reported these catalysts allow for living polymerizations of ethylene and propylene[13, 14]. In ethylene polymerizations, the FI catalysts showed a linear relationship between number-average molecular weight (M_n) and polymerization time. Polydispersity indices were between 1.05 and 1.13. Block copolymers were also able to be produced using these complexes. These catalysts have been immobilized on $MgCl_2$ by contacting the FI complex, alkyl aluminum, and the solid[15]. As discussed previously, this co-catalyst immobilization technique can create a multi-sited material, evidenced by the polydispersities exceeding 13 in some cases. Additionally, it is difficult to characterize the metal center on a molecular level due to the large excess of co-catalyst. Immobilization of an FI catalyst system via the patterned aminosilica would potentially create a highly active supported catalyst for olefin polymerization. Of particular interest would be whether the supporting protocol would have an effect on the catalysts ability for "controlled" polymerizations.

Tatsumi and co-workers have shown traditionally synthesized aminosilicas are effective agents for adsorption of heavy metals anions, such as chromate and arsenate[16]. As shown in this thesis work, the patterned amine sites developed exhibit a higher reactivity and uniformity than traditional aminosilicas. This may also allow for a more efficient adsorption behavior. The use of the patterned aminosilica would probe whether the adsorption is occurring at single or dual amine sites. One difficulty that would likely

have to be addressed would be the patterned amine loading on the silica surface. The benefit achieved due to the increased reactivity of the isolated amine sites may be muted because of the decrease in quantity of amine sites per gram of solid.

A project currently underway in the Jones group, being studied by Jason Hicks, is the use of a supported borane as a co-catalyst for olefin polymerizations. A method to immobilize boranes on patterned aminosilica will be developed. These immobilized co-catalysts can be tested with homogeneous metallocenes, CGCs, FI catalysts, etc., to test the effectiveness of the supported borane in activatation of the various metal centers for olefin polymerization (i.e. ethylene, propylene, styrene). The major advantage of this system will be the removal of MAO from the system. The cost of MAO co-catalysts is several orders of magnitude more expensive than the homogeneous catalysts, and can cause significant leaching in supported systems used in solution polymerizations. The site density and structure of the catalyst and boron activator can be altered, allowing their impact on the catalyst's polymerization activity to be determined.

7.2.2 Recommendations for continuing CGC work

There are numerous studies which can be continued from the supported CGC work presented in this thesis. The polymerizations here were performed in a small glass pressure vessel. It would be beneficial to perform more detailed kinetic studies in the performance of these catalysts. Such experiments would allow for investigations into activation efficiencies of the various catalysts, maximum polymerization activities, deactivation rates, and catalyst lifetimes. As the elucidation of the in-situ behavior of the catalysts would provide insight into the active species, this is an important area for

continued work. These studies were attempted in the course of this work, however reproducible results could not be achieved with the catalysts developed in this work. Using homogeneous polymerization catalysts (such as titanocene or zirconocene) yielded the desired data, but using the less active supported catalysts caused difficulties. It is likely the reactor system used will need to be modified to work with supported CGCs.

There is also potential benefit in performing more detailed characterization of the polymers produced from supported CGCs. In depth polymer characterization will allow for the development of structure-property relationships for the patterned catalyst. Additionally, ^{13}C NMR was used to study the norbornene-ethylene polymerizations. The use of this analytical tool on polyethylenes can lead to studies determining the effect of the catalyst used on polymer branching and microstructure. Microscopy studies would allow for morphological determinations of the polymers synthesized, as well as determining the fate of the SBA-15 support used for all of the immobilized materials.

In this work, diffuse reflectance UV-Vis was used to help characterize the metal center of the immobilized complexes. However, as discussed, it was difficult to draw conclusions from those studies. Further characterization of the metal center using Extended X-ray Absorption Fine Structure (EXAFS) and/or Electron Paramagnetic Resonance (EPR) would help determine the type and number of metal sites present in the materials. The data is necessary to conclude whether the patterning protocol produces a truly single-site material, and is likely the most important studies to be continued.

7.2.3 Potential Application of CGC Immobilization Protocol

An interesting application for metallocenes and constrained geometry catalysts is their use as anti-tumor agents[17-20]. In recent years, there has been an increasing emphasis on replacing cis-platin in chemotherapy treatments with a therapy which more efficiently attacks the cancerous cells without harming normal, healthy cells. An issue in any sort of chemotherapy is the large amount of drugs which must be placed into the body. Localized drug delivery would maximize benefits while reducing adverse side effects. One such method for drug delivery would be polymeric supported metallocenenes. The study of the anti-tumor activity of polymer-supported ferrocene was reported with non-uniform results (anti-tumor activity followed by sudden decline), likely resulting from deactivation of the metal active site[21]. The inefficiency of the supported ferrocene would require a higher dosing, minimizing the advantages of using a highly active anti-tumor agent. A possible, far-reaching area for future work would be the development of an analogous patterned polymeric material which could be used to support metallocene type complexes. One difficulty which have to be addressed is the flexible nature of typical polymeric supports. On a rigid surface (Figure 7.1A), the patterning functionalities would remain isolated. However, on a flexible surface (Figure 7.1B), it is more difficult to retain the spacing induced by the patterning protocol. Using cross-linking may limit this flexibility and retain the isolation, however special care must also be to taken to retain biocompatibility of the polymer. If able to be produced, these patterned polymer supported complexes should retain high activity, allowing for an efficient anti-tumor material.

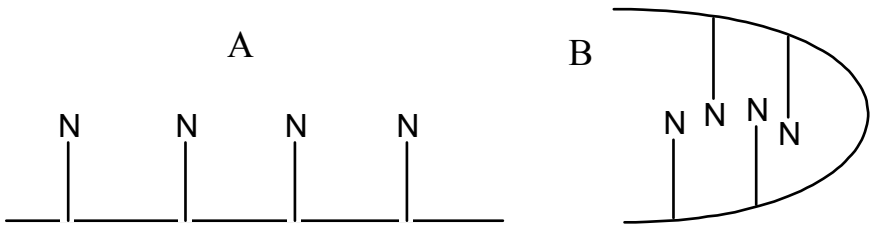

Figure 7.1 Comparison of patterning on (A) rigid and (B) flexible surfaces

In conclusion, the immobilization of olefin polymerization catalysts on a mesoporous silica scaffold and the polymerization activity of these complexes has been examined. Significant progress has been made towards developing a well-defined, single-site immobilized CGC, which will allow for the development of structure-reactivity relationships for these important materials.

7.3 References

1. McKittrick, M. W.; Jones, C. W., *Chem. Mater.* **2003,** *15*, 1132-1139.

2. McKittrick, M. W.; Jones, C. W., *J. Am. Chem. Soc.* **2004,** *126*, 3052.

3. McKittrick, M. W.; Jones, C. W., *J. Catal.* **2004,** *227*, 186-201.

4. Iiskola, E. I.; Timonen, S.; Pakkanen, T. T.; Harkki, O.; Lehmus, P.; Seppala, J. V., *Macromolecules* **1997,** *30*, 2853-2859.

5. Iiskola, E. I.; Timonen, S.; Pakkanen, T. T.; Harkki, O.; Seppala, J. V., *Appl. Surf. Sci.* **1997,** *121*, 372-377.

6. Juvaste, H.; Iiskola, E. I.; Pakkanen, T. T., *J. Organomet. Chem.* **1999,** *587*, 38-45.

7. Juvaste, H.; Iiskola, E. I.; Pakkanen, T. T., *J. Mol. Catal. A* **1999,** *150*, 1-9.

8. Ciruelos, S.; Cuenca, T.; Gomez, R.; GomezSal, P.; Manzanero, A.; Royo, P., *Organometallics* **1996,** *15*, 5577-5585.

9. Royo, B.; Royo, P.; Cadenas, L. M., *J. Organomet. Chem.* **1998,** *551*, 293-297.

10. Diamond, G. M.; Jordan, R. F.; Petersen, J. L., *J. Am. Chem. Soc.* **1996,** *118*, 8024-8033.

11. Diamond, G. M.; Rodewald, S. R.; Jordan, R. F., *Organometallics* **1995,** *14*, 5-7.

12. Kojoh, S.; Matsugi, T.; Saito, J.; Mitani, M.; Fujita, T.; Kashiwa, N., *Chem. Lett.* **2001**, 822-823.

13. Saito, J.; Mitani, M.; Mohri, J.; Yoshida, Y.; Matsui, S.; Ishii, S.; Kojoh, S.; Kashiwa, N.; Fujita, T., *Angew. Chem. Int. Edit.* **2001,** *40*, 2918-2920.

14. Saito, J.; Mitani, M.; Mohri, J.; Ishii, S.; Yoshida, Y.; Matsugi, T.; Kojoh, S.; Kashiwa, N.; Fujita, T., *Chem. Lett.* **2001**, 576-577.

15. Nakayama, Y.; Bando, H.; Sonobe, Y.; Fujita, T., *J. Mol. Catal. A* **2004,** *213*, 141-150.

16. Yoshitake, H.; Yokoi, T.; Tatsumi, T., *Chem. Mater.* **2002,** *14*, 4603-4610.

17. Kopfmaier, P.; Hesse, B.; Kopf, H., *J. Cancer Res. Clin.* **1980,** *96*, 43-51.

18. Harding, M. M.; Mokdsi, G., *Curr. Med. Chem.* **2000,** *7*, 1289-1303.

19. Melendez, E., *Crit. Rev. Oncol. Hemat.* **2002,** *42*, 309-315.

20. Meyer, R.; Brink, S.; van Rensburg, C. E. J.; Joone, G. K.; Gorls, H.; Lotz, S., *J. Organomet. Chem.* **2005,** *690*, 117-125.

21. Neuse, E. W., *Macromol. Symp.* **2001,** *172*, 127-138.

VITA

Michael W. McKittrick was born April 19, 1977 in Richmond, VA to Tom and Linda McKittrick. After graduating from Lee-Davis High School (Mechanicsville, VA) in 1995, he spent a year at the University of Richmond before transferring to Virginia Commonwealth University. At VCU, he earned a Bachelor of Science in Chemical Engineering while receiving a double major in Chemistry, graduating in May 2000 as part of the Founding Engineering School class. Michael began his graduate studies at the Georgia Institute of Technology the following fall. After receiving his Ph.D., he will begin a post-doctoral research appointment at the University of Colorado-Boulder.